國　立　交　通　大　學

機 械 工 程 學 系

博 士 論 文

振動狀態下摩擦力降低效應之研究

A Study on the Effect of Friction Reduction in the Presence of Vibrations

研 究 生：蔡 鎮 竹

指導教授：曾 錦 煥

中華民國九十三年六月

振動狀態下摩擦力降低效應之研究

A Study on the Effect of Friction Reduction in the Presence of Vibrations

研 究 生：蔡 鎮 竹　　Student: Chen-Chu Tsai
指導教授：曾 錦 煥　　Advisor: Ching-Huan Tseng

國立交通大學
機械工程學系
博士論文

A Dissertation
Submitted to Department of Mechanical Engineering
College of Engineering
National Chiao Tung University
in Partial Fulfillment of the Requirements
for the Degree of
Doctor of Philosophy
in
Mechanical Engineering

2004
Hsinchu, Taiwan, Republic of China

中華民國九十三年六月

振動狀態下摩擦力降低效應之研究

研究生：蔡鎮竹　　　　　　　　　指導教授：曾錦煥

國立交通大學機械工程學系

摘要

本文針對振動狀態下的摩擦力降低現象提出理論研究，其中包含垂直及平行於接觸面的振動，除了無潤滑狀態下之接觸外，亦考慮在潤滑接觸下的影響。研究顯示接觸面的切線彈性對摩擦力降低效應的影響很大，本文提出以振動的位移振幅與表面突起的穩態撓曲的位移比來描述切線彈性對摩擦力降低效應的影響，對於平行於接觸面的振動，切線彈性會降低摩擦力降低效應，然而對於垂直於接觸面的振動，切線彈性會提昇摩擦力降低效應，對於任何型態的振動，當滑行速度小於振動速度時，摩擦力降低效應較顯著。對於潤滑接觸，表面突起的線性阻尼對摩擦力降低不起作用，而接觸面的黏滯性會降低摩擦力降低效應，Stribeck 效應對摩擦力降低亦有影響。本文亦提出其他對摩擦力降低有影響的因子並分別加以分析，其中包括振動波形、非對稱摩擦及自伺服效應，藉由振動波形、非對稱摩擦的方向及伺服結構的選擇，可增強或抑制摩擦力降低效應來符合實際應用的需求。藉由本文提出的方法所計算出的摩擦力降低量與文獻中實驗結果相當符合。

A Study on the Effect of Friction Reduction in the Presence of Vibrations

Student: Chen-Chu Tsai Advisor: Ching-Huan Tseng

Department of Mechanical Engineering
National Chiao Tung University

ABSTRACT

Theoretical approaches are presented that describe the friction reduction observed in the presence of the vibrations. The direction of vibrations can be either normal or tangential to the contact surfaces, and the contact surfaces can be either dry or lubricated. It is showed that the tangential compliance of the contacts should be taken into consideration in the analysis of the friction reduction by vibrations. A displacement ratio of the displacement amplitude of the vibrations to the steady-state deflection of the asperity is proposed to describe the influence of the tangential compliance. For tangential vibrations, the tangential compliance degrades the effect of friction reduction. However, for normal vibrations, the tangential compliance enhances the effect of friction reduction. For any type of vibrations, the friction reduction effect is more significant when the magnitude of macroscopic velocity is smaller than the velocity amplitude of vibration. In the lubricated contacts, the linear damping of the asperities has no effect on the friction reduction, and the linear viscosity of the contacts degrades the effect of friction reduction. The influence of Stribeck effect on the friction reduction effect is also presented. Other factors that also have influences on the friction reduction are proposed and investigated individually, including the waveform of the oscillation, asymmetric Coulomb friction and self-servo effect. By choosing a suitable waveform of the oscillation, direction of the asymmetric Coulomb friction or self-servo

structure, the friction reduction can be enhanced or suppressed depends on the applications. The amount of the friction force reduction calculated by the proposed approach is quite consistent with the experimental results in the literatures.

ACKNOWLEDGEMENT

博士學業的完成，首先要感謝我的指導教授　曾錦煥博士，提供了穩定無虞的求學環境，除了課業上的指導外，在待人處事方面的經驗分享與生活上的關心，更讓學生滿心感動。

感謝我的論文口試委員：中央大學王教授國雄、國科會蔡處長忠杓、臺灣科技大學黃教授世欽、中山大學邱教授源成、中正大學馮教授展華，與交通大學洪教授景華，不辭辛勞，撥冗前來擔任學生的論文口試，並對學生的論文提供許多寶貴的建議與修正，使論文的內容更加完整與充實。其中特別感謝國科會蔡處長忠杓在百忙之中特別撥出時間擔任學生口試委員，並對學生論文逐頁逐字仔細的修正，另外，感謝交通大學洪教授景華提供相關的研究經驗，與求學路上的鼓勵。

在應用最佳化實驗室的日子裡，感謝學長、同學與學弟們在研究上的協助與勉勵，並一起分享生活的樂趣。特別感謝大師在我沒日沒夜趕論文時的雪中送炭，王維漢學長及劉俊賢學長對於論文口試的寶貴建議。在這些日子中，還要感謝我女朋友的照顧、包容與鼓勵，多少的假日與深夜，她陪我在沒人的實驗室中度過，沒能好好睡，也沒能享受該有的休閒時間。

在這漫長的求學過程中，父母親是最溫暖的支持，我想若不是父親在我小時後引導我上軌道，及母親一路的鼓勵，我應該沒能攻讀博士，博士求學期間的不順利，讓父母親擔心的到處為我祈求論文順利，如今完成博士學業，若有丁點成就，應該歸功於我的父母親，同時也該謝天謝地。

TABLE OF CONTENTS

LIST OF TABLES

LIST OF FIGURES

NOMENCLATURE

C_v	empirical parameter for Stribeck curve
d	ratio of the time interval of the positive velocity to one period
F	friction force without vibration
$\tilde{F}$	instantaneous friction force
$\overline{F}$	time-averaged friction force
$\tilde{F}_0$	friction force without the self-servo effect
F_{ba}	breakaway force (static friction)
F_c	Coulomb friction force
F_{cn}	normalized Coulomb friction
F_{ss}	steady state friction force for lubricated contacts
$\overline{F}_{\sigma_1}$	time average of the damping term of the LuGre model
$\overline{F}_{\sigma_2}$	average of the viscous term of the LuGre model
h	height of the hinge pin
i	parameter of Dahl model
l	length
m	mass
M_A	moment about the hinge pin
N	normal force

P_s	average dissipated power in the absence of vibrations
P_v	average dissipated power in the presence of vibrations
$P_{v,Coulomb}$	average dissipated power based on Coulomb friction
$P_{v,Dahl}$	average dissipated power based on Dahl model
r	friction ratio
r_{disp}	displacement ratio
r_f	parameter for asymmetric Coulomb friction
r_{sf}	friction ratio, F_{ba}/F_c
r_{sv}	velocity ratio, v_v/v_s
r_{σ_0}	friction ratio for the stiffness term of the LuGre model
t	time
t_0, t_1, t_2	time when the relative velocity is zero
T	period
v	velocity
v_b	macroscopic velocity
v_{rel}	relative sliding velocity
v_s	characteristic velocity of the Stribeck curve
v_v	velocity amplitude of the vibration component
w	sliding distance of the asperity

σ_{0n}

$\dot{w}$	derivative of w
W	actuating force
W_v	energy dissipated during one steady state period of vibrations
x	displacement
$\dot{x}$	derivative of x
z	average deflection of the asperities
$\dot{z}$	derivative of z
z_{ss}	average steady state deflection of the asperities
z_0	initial deflection of the asperities
α	parameter of the Stribeck curve
ζ	velocity ratio, v_b / v_v
η	viscosity
θ	angle of the harmonic velocity with the constant velocity
μ	friction coefficient
μ_{ba}	normalized static friction
μ_c	normalized Coulomb friction
μ_{ss}	normalized friction force for lubricated contacts
σ_{0n}	normalized tangential stiffness of the asperities
σ_0	tangential stiffness of the asperities

σ_1	damping coefficient
σ_2	viscous coefficient
ω	angular velocity

CHAPTER 1 INTRODUCTION

1.1 Introduction

A reduction of friction by vibrations has been observed in various experiments. This phenomenon is a common occurrence in many machine elements, for instance, nuts loosed from vibrating screws. When surfaces are in contact, they are often subjected to combinations of steady and dynamic loads. The dynamic loads can cause vibrations. The dynamic loads may be generated either external to the contact region, as in the case of unbalanced moving machinery components, or within the contact region, as in the case of surface roughness or waviness-induced vibrations. For the external loading, the dynamic loads can be easily modulated; thus the frictional forces can be actively controlled.

The performance of many sensitive devices such, for example, as floated gyros and the like is harmfully affected by the presence of friction in the bearings that support the sensitive element of the devices. Introducing the vibrations into these devices can improve the performance because the friction forces are reduced. On the other hand, there are various devices utilizing dynamic friction, for instance, brakes and clutches. Introducing the vibrations can also reduce the dynamic frictional forces of these devices when the dynamic frictional forces exceed the suitable values. In the case of the friction clutches, when the undesired conditions such as overloading or over speed are detected, the application of vibrations to one of the clutch elements allows the clutch to slip during such times as the adverse conditions are maintained. Moreover, this effect can also be used for reduction of process force in manufacturing processes, such as ultrasonic machining and ultrasonic-vibrations drawing (Hayashi *et al.*, 2003), or solving the problem of position control in high vacuum environments, such as electron microscopes, where friction can be controlled through the variation of the vibration amplitude only. Some applications can be found in the patents (Broeze and Laubendorfer, 1966; Argentieri and Andresen, 1974; Armour, 1982; Armour and Watson, 1982; Saito and Mohri, 1992; Kramer, 2000).

The reasons for the friction reduction in the presence of vibrations can be divided into two categories (Zeng *et al*., 1998). One is the mechanics. The vibrations can change the direction or magnitude of the friction force. The other is the physical property. The vibrations can reduce the surface roughness. The heat resulted from the vibrations can soften the sliding surfaces. For lubricated contacts, the vibrations can enhance the formation of the fluid lubrication.

It is widely agreed that dynamic frictional forces in complex mechanisms are not being adequately modeled at the present time. Therefore, most investigations about the friction reduction by vibrations gave only the qualitative descriptions of its behavior. Few analytical models have been proposed, but they can't estimate the reduction of friction under a wide variety of conditions.

1.2 Literature Review

According to the direction of vibrations with respect to the contact surface, the vibrations can be divided into two categories. One is the tangential (in plane) vibration and the other is the normal (out of plane) vibration.

1.2.1 Tangential Vibrations

The practical importance of this type of friction led some researchers to undertake experimental analysis. To explore the origin of ultrasound-induced friction reduction, Hesjedal and Behme (2002) experimentally studied the friction reduction phenomena in microscopic mechanical contacts using a scanning force microscope in the lateral force mode

(LFM) and a scanning acoustic force microscope (SAFM). The data suggest that the lateral oscillation component has no influence on the reduction of friction. They concluded that the friction reduction effect results entirely from the vertical oscillation component. However, previous experimental investigations on tangential vibration showed friction reduction (Matunaga and Onoda, 1992; Littmann *et al*., 2001a, 2001b, 2002). This discrepancy is thought to be lack of quantitative analysis.

Matunaga and Onoda (1992) and Littmann *et al*. (2001a, 2001b, 2002) also proposed quantitative analytical models based on the rigid Coulomb friction. The ratios of the friction with and without vibrations obtained in the experiments showed the same tendency as the experimental data, but have higher values. The main reason of the discrepancy is thought to be that the rigid Coulomb friction does not provide a very good description of the friction phenomena under vibrations. For these types of contacts, with small amplitude of sliding displacement, Tani (1996) showed that the rigid Coulomb friction model was insufficient to describe the friction behavior. He built a small mobile machine which has two legs made of bimorph piezoelectric actuators. Simulations were made to investigate the dynamics of its mobility using different friction models. The comparison of the simulation results with the measured speed and acceleration suggests that the viscous friction model explains the movement better than the Coulomb friction model. The viscous friction model is adapted such that the friction coefficient is proportional to the relative velocity up to a certain limit and is saturated at the limit value.

1.2.2 Normal Vibrations

A reduction in friction due to normal contact motions during sliding has been observed by many researchers. In the first works related to this subject, Tolstoi *et al*. (1973) modeled the contact region between two surfaces as a non-linear spring without damping, using an empirical stiffness relation which are based on the experiment data given by static loading. When the normal vibration is applied in the contact region, the average compression of the non-linear spring is reduced. The reduced average compression can be calculated by his empirical stiffness relation from energy considerations. Then the effective value of normal load can be calculated by substituting the reduced average distance into the empirical stiffness relation. Finally, the friction reduction by normal vibration was calculated by the reduction of the effective normal load. Both the model and measurement showed that the friction reduction due to normal vibration could be as large as 30% for various steel surfaces. No attempt was made to analyze the system dynamics.

In the case of the kinetic friction between plastics and ice or snow, Lehtovaara (1987) presented experimental results. In his apparatus, vibrations were induced in the test specimen by an exciter while the test specimen was sliding on smooth ice. The results showed that the frictional force reduction was greatest at the first natural frequency of the test specimen where the vibration amplitude was large compared with the amplitudes of the antiresonance frequencies. At temperature below –1 ºC, where dry friction is dominant, the kinetic friction was reduced even when the acceleration of the vibrating body was much lower than the acceleration of gravity (no loss of contact). The reduction in kinetic friction is almost linearly dependent on the normal acceleration. At air temperatures above zero, where wet friction (viscous shear of water) dominates, vibration has no effect on friction.

Tworzydlo and Becker (1991) investigated the influence of forced vibration on the static coefficient of friction. They applied a model of frictional interface, assuming the existence of non-linear normal compliance of the interface, to the transient analysis of vibration of the system. Their analysis revealed that in the presence of normal vibrations the tangential motion of the slider consisted of microscopic sticks and slips, which in the macroscopic scale are perceived as a "creep"-type motion. The experimental results showed that the rate of decrease of the friction was very sensitive to the amount of damping applied on the interface. The maximum reduction of the static friction for steels is about 84% for clean surfaces (lower damping) and is about 30% for contaminated surfaces (higher damping). The presence of interface damping weakens the effect of friction reduction, especially in the vicinity of a resonance zone.

Hess and Soom (1991a, 1991b, 1993) analyzed resonant non-linear normal vibrations as well as the associated instantaneous contact area and friction force under harmonic loads applied to both Hertzian contacts and rough planar contacts using a non-linear mass-spring-damper model. A decrease in the average contact deflection under dynamic loading was predicted in each case. This resulted in an 11% reduction in the average friction force for Hertzian contacts when the normal vibration amplitude was just below that required to produce momentary loss of contact. However, the average contact area and friction force for the rough planar contacts were hardly affected. Further, the normal vibrations and friction at Hertzian contact under random excitation were analyzed. Both external excitation and internal excitation that arose from surface roughness were considered. It was found that for a 5% probability of contact loss, a reduction in the mean friction force of approximately 9% is expected for both cases. The reduction in average friction arose due to the non-linear relationship between the normal contact load and the area of contact, under the assumption that the instantaneous friction force was proportional to the instantaneous area of contact. Average friction measurements taken during continuous sliding were in agreement with the analysis. However, their analysis was restricted to the conditions without loss of contact, and the tangential compliance was not considered.

To analyze the mechanism of friction drive with ultrasonic wave, Adachi *et al.* (1996) developed an apparatus that can measure the friction force at the interface between a rotational disk and an oscillatory pin induced by ultrasonic wave. The experimental results showed that the friction force decreased with the decrease of the rotational speed of disk and the increase of the amplitude of pin motion (the pin-disk contact is broken for part of the vibration cycle). They introduced a simple relationship between tangential coefficient and micro-displacement at the contact region to explain the friction reduction phenomenon.

The friction force microscope (FFM) has opened a way for the study of the friction in micro-/nanoscopic mechanical contacts. Dinelli *et al*. (1997) studied the dynamic friction dependence on out-of-plane ultrasonic vibration, using friction force microscopy and a scanning probe technique, the ultrasonic force microscope (UFM), which can probe the dynamics of the tip-sample elastic contact as a submicrosecond scale. The results showed that friction fell sharply when the tip-surface contact broke for part of the out-of-plane vibration cycle. Moreover, the friction force reduced well before such a break, and this reduction does not depend on the normal load. They suggested that the contact was solid-liquid-solid. However, the mechanism of the friction reduction was not studied in detail.

Similarly, Hesjedal and Behme (2000, 2002) experimentally studied the friction reduction phenomena in microscopic mechanical contacts using a scanning force microscope in the lateral force mode (LFM) and a scanning acoustic force microscope (SAFM). The data suggested that the lateral oscillation component has no influence on the reduction of friction. They concluded that friction reduction effect is only due to the vertical oscillation component that leads to an effective shift of the cantilever away from the surface.

The general conclusion of these researches is that average friction falls sharply when the contact broke for part of the out-of-plane vibration cycle and the presence of interface damping weakens the effect of friction reduction. Analytical models that assumed the non-linear normal compliance of the interface showed that without loss of contact the vibration has little effect on the average friction. However, these analytical models were restricted to the conditions without lost of contact, and the tangential compliance was not considered.

1.2.3 Friction Model

Experiments have observed that when two contacting surfaces slide against each other, a motion of one surface over the other occurs before actual body sliding begins. This effect occurs with the tangential compliance. The movement caused by the applied force below the breakaway force is called the presliding displacement or micro-slip (Olofsson, 1995, 1998, 1999).

Dahl (1976) formulated a mathematical model of the presliding displacement by incorporating tangential compliance. The model acts as a nonlinear spring with a nearly linear elastic response for small deflections, which yields and approaches an asymptotic value for large deflections. The asymptotic value is the Coulomb friction force. When the rest stiffness tends to infinity, the response of the Dahl model converges to that of the rigid Coulomb friction model. Bliman (1992) studied the existence and uniqueness of solutions and hysteresis effects of the model.

In order to capture more frictional phenomena observed in the experiments, Canudas de Wit *et al.* (1995) proposed a new model, LuGre friction model, which is an extension of the Dahl model. They were inspired by the bristle model proposed by Haessig and Friedland (1991). The surfaces in contact are visualized as two rigid bodies that make contact through elastic bristles. When a tangential force is applied, the bristles will deflect like springs which gives rise to the friction force. If the deflection is sufficiently large, the bristles start to slip. The average bristle deflection for a steady state motion is determined by the velocity. It is lower at low velocities, which implies that the steady state deflection decreases with increasing velocity. This models the Stribeck effect that is the steady-state relationship between friction force and slip velocity. In addition, the damping effect of the bristles and viscous friction between the surfaces are also included. This dynamic model can capture most of the friction behavior. This includes the presliding displacement, Stribeck effect, hysteresis, and varying breakaway force. Further analysis of the model and its application can be found (Dupont *et al.*, 1997; Olsson *et al.*, 1998; Altpeter, 1999; Canudas de Wit and Tsiotras, 1999; Barabanov and Ortega, 2000).

A significant limitation of the Dahl and LuGre models, however, is that they exhibit drift when systems subjected to a small bias force and small vibrations. To minimize the drift, Dupont *et al.* (2000, 2002) proposed a elasto-plastic model in which presliding is elasto-plastic, *i.e.*, under loading the displacement is first purely elastic (reversible) before transitioning to plastic (irreversible).

1.3 Objectives

The objective of this study is to provide the theoretical approaches that can estimate the reduction of friction under a wide variety of conditions, including the dry and the lubricated contacts, the tangential and the normal vibrations.

1.4 Thesis Outlines

Chapter 2 is devoted to investigate the phenomenon of the friction reduction by the tangential vibrations by incorporating the Dahl friction model. The comparison between the friction reduction based on the Dahl model and that based on the rigid Coulomb friction model are presented. A displacement ratio of the displacement amplitude of the vibrations to the steady-state compliance is given to describe the influence of tangential compliance on the friction reduction effect. Other factors that affect the effect of the friction reduction are proposed and investigated individually. Finally, the energy dissipated with the oscillation is computed and compared to that without the oscillation.

Chapter 3 applies the LuGre model to investigate the friction reduction observed in the lubricated contacts with the parallel vibrations. Stribeck effect is an important characteristic of lubricated contacts. Its influence on the friction reduction effect is also investigated.

Chapter 4 investigates the influence of the direction of tangential vibrations on the friction reduction. An approach based on the deflection of the asperities is proposed to model the instantaneous friction in the presence of the non-parallel tangential vibrations. A comparison between the calculated results and the experimental data in the literatures is presented.

Chapter 5 focuses on the analysis of the friction reduction phenomenon in the presence of the normal vibrations. The friction reduction when the contact is broken for part of the normal vibration cycle is also studied. First, a simple analysis is performed for a contact that is modeled simply as a nonlinear spring without the tangential compliance. Then the Dahl model is applied to investigate influence of the tangential compliance on the friction reduction in the presence of the normal vibrations.

Chapter 6 gives conclusions and discusses further works of this study.

CHAPTER 2 FRICTION REDUCTION BY PARALLEL VIBRATIONS

The phenomenon of the friction reduction by the parallel vibrations is investigated by incorporating the Dahl's friction model that is a mathematical model of micro-slip. The assumption in this study is that the friction force is not influenced by the wear and heat of the contact surfaces.

2.1 Theoretical model

In order to investigate the mechanism of friction reduction by tangential vibrations, a simple model shown in Fig. 2.1 is adopted. The model consists of a flat plane with a macroscopic velocity v_b and a vibrating body that is pressed against the flat plane by constant normal force. The velocity of the vibrating body is defined as

$$v(t) = v_v \cos(\omega t) . \tag{2.1}$$

Thus the relative sliding velocity is

$$v_{rel}(t) = v_b - v(t) = v_v(\zeta - \cos(\omega t)) , \tag{2.2}$$

where $\zeta = v_b / v_v$ is the ratio of the macroscopic velocity and the velocity amplitude of the vibration component. The effective friction force, which is observed macroscopically, is the time-averaged mean friction force over one period of vibration $T = 2\pi / \omega$:

$$\overline{F} = \frac{1}{T}\int_0^T \widetilde{F}(t)dt . \tag{2.3}$$

The effect of friction reduction by superposed tangential vibrations can be described quantitatively by the ratio

$$r = \frac{\overline{F}}{F}, \tag{2.4}$$

of the reduced friction force $\overline{F}$ and the friction force F observed in the absence of vibrations. For demonstration, the friction is assumed to be the Coulomb friction first which is described by

$$\tilde{F}(t) = F_c \operatorname{sgn}(v_{rel}(t)) = \mu F_N \operatorname{sgn}(v_{rel}(t)), \tag{2.5}$$

Where F_c is the amplitude of Coulomb friction force, F_N the normal load and μ the friction coefficient. The amplitude of the Coulomb friction force is constant because the normal force and friction coefficient are assumed to be constant, but the direction is opposite to the relative sliding velocity. After some calculations, the friction ratio in this case is

$$r = \begin{cases} \frac{2}{\pi}\sin^{-1}(\zeta) & |\zeta| \le 1 \\ 1 & |\zeta| > 1 \end{cases}. \tag{2.6}$$

It only depends on the dimensionless velocity ratio ζ. A significant reduction of friction force can be observed if the macroscopic velocity is small compared to that of the vibrations, as shown in Fig. 2.2. However, the values of the results of the experiments by Matunaga and Onoda (1992) or Littmann *et al*. (2001a, 2001b, 2002) are larger than that of the model based on the Coulomb friction. In other words, the amount of the friction reduction by vibrations is over estimated. One important characteristic of the sliding pair is that the superimposed vibrations may periodically change the direction of the relative sliding and the displacement amplitude of the harmonic component is usually in the range of some micrometers (e.g. amplitude of 0.7 μm at 60 kHz in the experiment by Littmann *et al*.) that is in the same order with the presliding displacement. In the condition with vibrations, the rigid Coulomb friction model can't properly describe the friction behavior (Tani, 1996).

2.2 Dahl's Friction Model

On the microscopic level, apparently smooth surfaces are still 'rough'. When these surfaces are press against each other, the true contact area usually is from 1/400 to 1/10000 of the apparent area observed by the naked eye, as shown in Fig. 2.3. The protuberant features are called asperities.

When a tangential force is applied, the asperities will deform like springs which gives rise to the friction force. When the strain of any particular asperity exceeds a certain level, the bond is broken and a new bond having a smaller strain is established. Dahl modeled the average stress-strain curve by a differential equation. Let x be the deflection, $\widetilde{F}$ the friction force, and F_c the Coulomb friction force. Then Dahl model has the form

$$\frac{d\widetilde{F}}{dx} = \sigma_0 (1 - \frac{\widetilde{F}}{F_c} \operatorname{sgn} \dot{x})^i , \tag{2.7}$$

where σ_0 is the contact stiffness or slop of the force-deflection curve at $\widetilde{F} = 0$, and i is a parameter that determines the shape of the stress-strain curve, which describe ductile materials if $i \geq 1$ and brittle type materials if $i < 1$. Applications of this model commonly employ the value i=1. It is remarkable that the friction force of the Dahl model is only a function of displacement and the sign of the velocity when σ_0 and F_c are constant. With sufficient unidirectional sliding, the friction force saturates at the Coulomb level F_c, as shown in Fig. 2.4(a). This figure also shows that the reverse of the speed is not sufficient to reverse the friction immediately: a memory does exit. Due to the memory effect, the instantaneous power of the friction force ($-\widetilde{F}v$) is not always negative (dissipative). The friction can store energy and give it back to the system (Bliman, 1992).

The time rate of change of the friction could be expressed as

$$\frac{d\tilde{F}}{dt} = \frac{d\tilde{F}}{dx}\frac{dx}{dt} = \frac{d\tilde{F}}{dx}v_{rel} = \sigma_0\left(1 - \frac{\tilde{F}}{F_c}\operatorname{sgn} v_{rel}\right)^i v_{rel} . \tag{2.8}$$

Introducing $\tilde{F} = \sigma_0 z$ and assuming i=1, the Dahl model can be written as

$$\frac{dz}{dt} = v_{rel}\left(1 - \frac{\sigma_0}{F_c}\operatorname{sgn}(v_{rel})z\right), \tag{2.9}$$

and $\tilde{F} = \sigma_0 z$, (2.10)

where z is the average deflection of the asperities. Equation (2.9) gives the steady state deflection

$$z_{ss} = \frac{F_c}{\sigma_0} . \tag{2.11}$$

Using the initial condition $\tilde{F}(x) = 0$ at $x = 0$ and assuming i=1 and $v_{rel} > 0$, Eq. (2.7) gives the result

$$\frac{\tilde{F}}{F_c} = 1 - e^{-(\frac{x}{z_{ss}})} . \tag{2.12}$$

The dimensionless friction and the dimensionless displacement given by Eq. (2.12) are shown in Fig. 2.4(b).

Unlike the Coulomb friction which is described by static maps between velocity and friction force, the Dahl model is a dynamic model that is relative to the sliding history. When the direction of motion is changed, it has a lag in the change of friction force. Hence, in the case of the sliding with harmonic vibrations imposed, the initial responses of the friction force are transient, which depend on the initial conditions. After sufficient cycles of the vibrations, the responses of the friction force reach the steady state, which can be constant or periodic. Due to the fact that the transient responses disappear quickly under the high frequency vibrations, this paper focused on the steady-state behavior of the sliding with vibrations.

Equation (2.9) can be separated into two equations, one for positive and the other one for negative velocity. When the velocity is positive, $dz/dt \geq 0$, the friction force $\widetilde{F}$ increases and approaches F_c; when the velocity is negative, $dz/dt \leq 0$, the friction force $\widetilde{F}$ decreases and approaches $-F_c$.

For velocity ratio $\zeta > 1$, the relative velocity, Eq. (2.2), is always positive. According to Eqs. (2.9) and (2.10), the friction of Dahl model will increase and saturate at F_c. Thus friction ratio is $r = 1$. In other words, the imposed vibrations do not reduce the time-average frictions.

For the velocity ratio $0 \leq \zeta \leq 1$, let the velocity increase from zero at the beginning of one period ($v_{rel}(t_0) = 0$), one period can be divided into two time intervals, one for positive and the other one for negative velocity. The instantaneous friction force and the relative sliding velocity are plotted in Fig. 2.5 for one period of the steady state. The curve of the relative sliding velocity intersects the time axis at t_o, t_1 and t_2 that have the relations:

$$t_1 - t_o = \frac{2\pi - 2\cos^{-1}(\zeta)}{\omega}, \tag{2.13}$$

and $t_2 - t_1 = \dfrac{2\cos^{-1}(\zeta)}{\omega}$. (2.14)

To calculate the deflection of the steady state at t_0, let

$$z(t_0) = z_0 . \tag{2.15}$$

In the first time interval, the relative velocity is positive, thus $\mathrm{sgn}(v) = 1$. The relative sliding velocity in this time interval is

$$v_{rel}(t) = v_v(\zeta - \cos(\omega t + \cos^{-1}(\zeta))) . \tag{2.16}$$

The deflection $z(t_1)$ can be obtained by solving Eqs. (2.9) and (2.16) with the initial condition (2.15):

$$z(t_1) = -\frac{F_c + (z_0\sigma_0 - F_c)e^{\frac{2v_v\sigma_0\left(\sqrt{1-\zeta^2}+\zeta(\pi-\cos^{-1}(\zeta))\right)}{\omega F_c}}}{\sigma_0}. \tag{2.17}$$

In the second time interval, the relative velocity is negative, thus $\operatorname{sgn}(v) = -1$. The relative sliding velocity in this time interval can be written as

$$v_{rel}(t) = v_v(\zeta - \cos(\omega t + 2\pi - \cos^{-1}(\zeta))). \tag{2.18}$$

The deflection $z(t_2)$ can be obtained by solving Eqs. (2.9) and (2.18) with the initial condition (2.17):

$$z(t_2) = e^{-\frac{4v_v\sigma_0\left(\sqrt{1-\zeta^2}+\zeta\sin^{-1}(\zeta)\right)}{\omega F_c}}\left(z_0 - \frac{F_c}{\sigma_0}\left(1 + e^{\frac{4v_v\sigma_0\left(\sqrt{1-\zeta^2}+\zeta\sin^{-1}(\zeta)\right)}{\omega F_c}} - 2e^{\frac{v_v\sigma_0\left(\pi\zeta+2\sqrt{1-\zeta^2}+2\zeta\sin^{-1}(\zeta)\right)}{\omega F_c}}\right)\right). \tag{2.19}$$

Due to the fact that the system is in steady state (periodic), the deflection $z(t_0)$ must be equal to $z(t_2)$. Hence the deflection z_0 can be obtained by solving Eqs. (2.15) and (2.19), which is

$$z(t_0) = z_0 = -\frac{(1 + e^{4ab} - 2e^{a(\pi\zeta+2b)})F_c}{(-1 + e^{4ab})\sigma_0}, \tag{2.20}$$

where

$$a = \frac{v_v\sigma_0}{\omega F_c}, \tag{2.21}$$

and $b = \sqrt{1-\zeta^2} + \zeta\sin^{-1}(\zeta)$. (2.22)

The Dahl friction of one steady state period, as shown in Fig. 2.5, can be obtained by solving Eqs. (2.9), (2.10) and (2.16) with the initial condition (Eq. (2.20)). Then the friction ratio, Eq. (2.4), can be rewritten as

$$r = \frac{\overline{F}}{F} = \frac{\dfrac{\omega}{2\pi}\displaystyle\int_0^{\frac{2\pi}{\omega}} \sigma_0 z(t)dt}{F_c}. \tag{2.23}$$

The friction ratio versus velocity ratio ζ is shown in Fig. 2.6. Only if the macroscopic velocity is smaller than that of the vibrations (i.e. $\zeta < 1$), the time-average friction force can be reduced. For $0 < \zeta < 1$, the friction ratio decreases as the velocity ratio ζ decreases. However, the friction ratio depends on not only the velocity ratio ζ but also v_v, ω, σ_0 and F_c. Introducing the displacement ratio

$$r_{disp} = \frac{v_v \sigma_0}{\omega F_c} = \frac{v_v/\omega}{F_c/\sigma_0} = \frac{x_v}{z_{ss}}, \tag{2.24}$$

which is same with Eq.(2.21), then Eq. (2.23) has the form

$$r = TAFR\left(r_{disp}, \zeta\right), \tag{2.25}$$

where x_v is the displacement amplitude of the vibrations, z_{ss} is the steady-state deflection, and TAFR is the function of the time-average friction ratio. For a specific velocity ratio ζ, the friction ratio decreases as the displacement ratio increases, as shown in Fig. 2.6. The instantaneous Dahl friction forces of the different displacement ratios and relative sliding velocity over one steady state period is plotted in Fig. 2.7. As the displacement ratio increasing, the friction force approaches to the Coulomb friction level F_c. Hence the friction ratio approaches to that of rigid Coulomb friction model, i.e. Eq. (2.6). On the contrary, as the displacement ratio decreasing, the friction force becomes insensitive to the change of the relative velocity and approaches to the initial condition of the steady state period, $\sigma_0 z_0$. So the friction ratio has an upper bound and a lower bound as follows

$$r_{max} = \lim_{r_{disp}\to 0} \frac{\sigma_0 z_0}{F_c} = \frac{\sigma_0}{F_c} \lim_{r_{disp}\to 0} z_0 = \frac{\pi\zeta}{2\left(\sqrt{1-\zeta^2} + \zeta \sin^{-1}(\zeta)\right)}, \qquad |\zeta| \le 1, \tag{2.26}$$

$$r_{min} = \tfrac{2}{\pi}\sin^{-1}(\zeta), \qquad |\zeta| \le 1. \tag{2.27}$$

The calculated friction ratio from the analysis based on the rigid Coulomb friction (Matunaga and Onoda, 1992; Littmann *et al.*, 2001a, 2001b, 2002) is equal to the lower bound. However, the tangential compliance of the sliding pair reduces the effect of the friction reduction by vibrations. Hence the friction ratios obtained from the experiments are higher than the lower bound, r_{min}.

A comparison between the experimental results and the calculated values is showed in Fig. 2.8. The values obtained from the experiment by Littmann *et al.* are higher than the lower bound, r_{min}, but are in very good agreement with the curve of $r_{disp} = 2$. The displacement amplitude of the vibrations is 0.7 μm in their experiment. Hence Eq. (2.24) gives the steady-state deflection $z_{ss} = 0.7/2 = 0.35$ μm. This value cannot be measured directly because it is an average behavior of the asperities during sliding. What can be measured directly is the presliding displacement. The presliding displacement of this case can be obtained from Eq. (2.12). Due to the reason that the friction of Dahl model only approaches but never reach the steady-state sliding friction Fc as displacement increases continuously, the presliding displacement can be defined as the displacement when the friction is 99.3 % of Fc, i.e. $F/F_c = 0.993$. Then Eq. (2.12) leads to the dimensionless displacement $x/z_{ss} \cong 5$. Thus the presliding displacement of this case is $x_{presliding} = 5z_{ss} = 5 \times 0.35 = 1.75$ μm. The presliding displacements of the metals measured in the experiments (Armstrong, B., 1991; Olofsson, U., 1995; Hagman, L. A.; Olofsson, U., 1998) are about 0.3~10 μm which is near the typical asperity dimension of finished hard metals. Hence the calculated presliding displacement of 1.75 μm is reasonable. According to Fig. 2.6 and the analysis above, it is obvious that the tangential compliance should be taken into consideration in modeling the effect of friction reduction by vibrations when the presliding displacement is comparable to the displacement amplitude of the vibrations. Although the tangential compliance of Dahl model results from the small-scale asperities, the tangential compliance of the bulk material has the similar influence on the friction reduction that can be included in the model with a modified stiffness σ_0.

From the viewpoint of friction control, the vibration frequency is an important control parameter. If the vibration amplitude (v_v/ω) is constant (*i.e.* a constant displacement ratio), a higher vibration frequency will lead to a larger vibration velocity (*i.e.* a lower velocity ratio). According to Fig. 2.6, a lower velocity ratio leads to a smaller friction ratio. Hence, increasing the vibration frequency can enhance the effect of the friction reduction. However, for typical vibrators the vibration amplitude decreases with the vibration frequency. If this dependence is assumed that the vibration amplitude is proportional to $1/\omega$ (namely the vibration velocity is constant), then a higher frequency leads to a lower displacement ratio that results in a higher friction ratio. In one word, increasing the vibration frequency degrades the effect of the friction reduction.

Sometimes, the reduction in friction is not advantageous, particularly in various machine joints or friction driven actuators such as ultrasonic motors. This may lead to loosening of joints or decreasing of efficiency. Hence the selection of the parameters depends on the applications.

2.3 Factors to Affect the Effect of Friction Reduction by Vibrations

According to the analysis above, the important factors that affect the effect of friction reduction by vibrations is the velocity ratio ζ and displacement ratio r_{disp}. However, there are still other factors that affect this effect. They are studied in this section.

2.3.1 Waveform

In the situation that the vibrator has large inertia, the sinusoidal oscillation may be the best waveform for the friction reduction method. However, if the inertia is small, other waveform of oscillation is possible. In addition, the oscillations from machines are not necessarily sinusoidal waveform. Hence it is worth evaluating the friction under oscillations with other waveforms.

2.3.1.1 Triangular Wave

The system to be investigated is same as Fig. 2.1 but the velocity of the vibrating body is defined as Fig. 2.9, the triangular-wave oscillation. Applying the procedures as Eqs. (2.13)-(2.20), the initial deflection of one steady state period (the relative velocity increases from zero at the beginning) is

$$z_0 = -\frac{(1+e^{\pi(1+\zeta^2)a} - 2e^{\frac{\pi}{2}(1+\zeta)^2 a})F_c}{(-1+e^{\pi(1+\zeta^2)a})\sigma_0} = \left(-1 + \frac{2\left(-1+e^{\frac{\pi}{2}(1+\zeta)^2 a}\right)}{-1+e^{\pi(1+\zeta^2)a}} \right)\frac{F_c}{\sigma_0}, \tag{2.28}$$

where

$$a = \frac{v_v \sigma_0}{\omega F_c} = r_{disp} .$$

The instantaneous friction forces of different displacement ratios and relative sliding velocity over one steady state period for the triangular wave oscillation is plotted in Fig. 2.10. The friction ratio can be obtained from Eqs. (2.9), (2.10) and (2.23) with initial condition (2.28):

$$r = \zeta + \frac{1}{2\sqrt{a}(B_1 - 1)}\left((A_1 - B_1)\mathrm{erf}(C_1) + (A_2 - B_1)\mathrm{erf}(C_2) - (A_2 - 1)\mathrm{erfi}(C_1) - (A_1 - 1)\mathrm{erfi}(C_2)\right), \quad (2.29)$$

where

$$a = \frac{v_v \sigma_0}{\omega F_c} = r_{disp},$$

$$A_1 = e^{\frac{1}{2}\pi a(1+\zeta)^2}, \quad A_2 = e^{\frac{1}{2}\pi a(-1+\zeta)^2}, \quad B_1 = e^{\pi a(1+\zeta^2)}, \quad C_1 = \frac{\sqrt{\pi a}(1+\zeta)}{2}, \text{ and } C_2 = \frac{\sqrt{\pi a}(-1+\zeta)}{2}.$$

The friction ratios of different displacement ratios are plotted in Fig. 2.11. As the case of the sinusoidal oscillation, the upper bound and lower bound of the friction ratio in this case are

$$r_{\max} = \lim_{r_{disp}\to 0} \frac{\sigma_0 z_0}{F_c} = \frac{\sigma_0}{F_c} \lim_{r_{disp}\to 0} z_0 = \frac{2\zeta}{1+\zeta^2}, \qquad |\zeta| \le 1, \tag{2.30}$$

and $$r_{\min} = \frac{\overline{F}}{F} = \frac{\left(\int_0^{\frac{\pi(1+\zeta)}{\omega}} F_c dt + \int_{\frac{\pi(1+\zeta)}{\omega}}^{\frac{2\pi}{\omega}} -F_c dt\right)\frac{\omega}{2\pi}}{F_c} = \zeta, \qquad |\zeta| \le 1. \tag{2.31}$$

Both of them are larger than that of sinusoidal oscillation. Hence the triangular wave is not a good waveform for the friction reduction. It is noticeable that the lower bound is a linear function of ζ.

2.3.1.2 Square Wave

For the square-wave oscillation, the velocity of the vibrating body is defined as Fig. 2.12. Thus the relative velocity can be defined as

$$v_{rel}(t) = v_v\left(\zeta - \mathrm{sgn}(-\sin(\omega t))\right). \tag{2.32}$$

The initial deflection of one steady state period is

$$z_0 = -\frac{(1 + e^{2\pi a} - 2e^{\pi(1+\zeta)a})F_c}{(-1 + e^{2\pi a})\sigma_0}, \tag{2.33}$$

where

$$a = \frac{v_v \sigma_0}{\omega F_c} = r_{disp} .$$

The instantaneous friction forces of different displacement ratios and relative sliding velocity over one steady state period for the square wave oscillation is plotted in Fig. 2.13. The friction ratio can be obtained from Eqs. (2.9), (2.10) and (2.23) with initial condition (2.33):

$$r = \frac{2\zeta\left(\coth(\pi a) - \cosh(\pi\zeta a)\operatorname{csch}(\pi a)\right)}{\pi a(1-\zeta^2)} . \tag{2.34}$$

The friction ratios of different displacement ratios are plotted in Fig. 2.14. The upper bound and lower bound of the friction ratio are

$$r_{\max} = \lim_{r_{disp}\to 0} \frac{\sigma_0 z_0}{F_c} = \frac{\sigma_0}{F_c} \lim_{r_{disp}\to 0} z_0 = \zeta , \qquad |\zeta| \le 1 , \tag{2.35}$$

and $$r_{\min} = \frac{\overline{F}}{F} = \frac{\left(\int_0^{\frac{\pi}{\omega}} F_c dt + \int_{\frac{\pi}{\omega}}^{\frac{2\pi}{\omega}} - F_c dt\right)\frac{\omega}{2\pi}}{F_c} = 0 , \qquad |\zeta| \le 1 . \tag{2.36}$$

Both of them are lower than that of the sinusoidal oscillation. Especially, if the displacement ratio is large enough, the friction ratio is insensitive to the change of the velocity ratio ζ and approaches zero for $|\zeta| < 1$. It is due to the character of the square wave that the time interval of the positive velocity and the time interval of the negative velocity are not changed by the velocity ratio ζ for $|\zeta| < 1$ (refer to Eq. (2.32)). Hence the square wave is very suitable for the friction reduction. Comparing the friction ratio of the square wave oscillation to that of the triangular wave oscillation, it is found that the lower bound of the triangular wave oscillation is equal to the upper bound of the square wave oscillation.

2.3.1.3 Asymmetrical Square Wave

The friction ratio of square wave oscillation can be reduced further if the time interval of the negative velocity is larger than that of the positive velocity. For this reason, the velocity of the vibrating body can be defined as an asymmetrical square wave, as shown in Fig. 2.15, where d is the ratio of the time interval of the positive velocity to one period. It is assumed that the net displacement of the vibrating body is zero over one period, i.e. $v_1 d - v_2(1-d) = 0$. Letting $v_2 = v_v$, then the positive velocity v_1 is

$$v_1 = \frac{(1-d)}{d} v_v \qquad 0 < d < 1. \tag{2.37}$$

Following the procedure used in the previous section, the initial deflection of one steady state period can be obtained, namely

$$z_0 = -\frac{(1 + e^{2\pi a(2+2d(-1+\zeta)-\zeta)} - 2e^{2\pi a(1+d(-1+\zeta))})F_c}{(-1 + e^{2\pi a(2+2d(-1+\zeta)-\zeta)})\sigma_0}, \tag{2.38}$$

where

$$a = \frac{v_v \sigma_0}{\omega F_c} = r_{disp}.$$

The friction ratio can be obtained from Eqs. (2.9), (2.10) and (2.23) with initial condition (2.38):

$$r = \frac{2e^{-2a\pi\zeta}(e^D - 1)(e^{2a\pi\zeta} - e^D)(1 + 2d(\zeta - 1))}{D(e^{2D-2a\pi\zeta} - 1)(\zeta - 1)} + 2d - 1, \tag{2.39}$$

where

$$a = \frac{v_v \sigma_0}{\omega F_c} = r_{disp},$$

and $D = 2\pi a(1 + d(\zeta - 1))$.

The upper bound and the lower bound of the friction ratio are

$$r_{\max} = \lim_{r_{disp}\to 0} \frac{\sigma_0 z_0}{F_c} = \frac{\sigma_0}{F_c} \lim_{r_{disp}\to 0} z_0 = \frac{\zeta}{2 + 2d(-1+\zeta) - \zeta}, \qquad -\frac{1-d}{d} \le \zeta \le 1, \tag{2.40}$$

and $r_{\min} = \dfrac{\overline{F}}{F} = \dfrac{\left(\int_0^{\frac{2\pi d}{\omega}} F_c dt + \int_{\frac{2\pi d}{\omega}}^{\frac{2\pi}{\omega}} - F_c dt \right) \dfrac{\omega}{2\pi}}{F_c} = 2d - 1, \qquad -\dfrac{1-d}{d} \le \zeta \le 1.$ (2.41)

It is noted that both of the upper bound and the lower bound decrease as d decrease. Furthermore, for $d < 0.5$, the friction ratio can be negative which means that the time-average friction becomes a "driving" force rather than a resisting force. The friction ratios of different displacement ratios are plotted in Fig. 2.16 (d = 0.2) and Fig. 2.17 (d = 0.8).

Unlike the previous cases that the friction ratio is an odd function of ζ, the friction ratio of the asymmetrical square wave oscillation is not symmetric about the origin. The curve of the lower bound intersects that of the upper bound at

$$\zeta_i = \frac{2d-1}{2d}, \tag{2.42}$$

which can be obtained from Eqs. (2.40) and (2.41). In fact, the curves of different displacement ratios all pass trough this point $(\zeta, r) = (\frac{2d-1}{2d}, 2d-1)$. In other words, the friction ratio is independent of the displacement ratio when $\zeta = \zeta_i$. It is remarkable that the time-average friction decreases as the displacement ratio decreases when the velocity ratio falls in the range of $0 \sim \zeta_i$.

2.3.2 Asymmetric F_c

The Coulomb friction force F_c is usually chose to be equal (symmetrical) for positive and negative velocities. However, it may be asymmetrical due to the anisotropic property of the sliding surface, such as the machined lay orientations. If F_c for positive velocities is lower than that for negative velocities, the friction reduction effect will be enhanced. The asymmetrical Coulomb friction is defined as Fig. 2.18(a), where the friction for the negative velocity is $-r_f F_c$ for $r_f > 0$.

Applying the procedures as Eqs. (2.13)~(2.27), the initial deflection of one steady state period under the sinusoidal oscillation is

$$z(t_0) = z_0 = -\frac{\left(1 + r_f e^{\frac{2a\left((1+r_f)E-\pi\zeta\right)}{r_f}} - (1+r_f)e^{2aE}\right)F_c}{\left(-1 + e^{\frac{2a\left((1+r_f)E-\pi\zeta\right)}{r_f}}\right)\sigma_0}, \tag{2.43}$$

where

$$E = \pi\zeta + \sqrt{1-\zeta^2} - \zeta\cos^{-1}(\zeta). \tag{2.44}$$

The upper bound and the lower bound of the friction ratio are

$$r_{\max} = \lim_{r_{disp}\to 0}\frac{\sigma_0 z_0}{F_c} = \frac{\sigma_0}{F_c}\lim_{r_{disp}\to 0} z_0 = \frac{\pi\zeta r_f}{\pi\zeta r_f + \left(1+r_f\right)\left(\sqrt{1-\zeta^2} - \zeta\cos^{-1}(\zeta)\right)}, \qquad |\zeta| \le 1, \tag{2.45}$$

and

$$r_{\min} = \frac{\overline{F}}{F} = \frac{\left(\int_0^{\frac{2\pi-2\cos^{-1}(\zeta)}{\omega}} F_c dt + \int_{\frac{2\pi-2\cos^{-1}(\zeta)}{\omega}}^{\frac{2\pi}{\omega}} -r_f F_c dt\right)\frac{\omega}{2\pi}}{F_c} = 1 - \frac{(1+r_f)\cos^{-1}(\zeta)}{\pi}, \qquad |\zeta| \le 1. \tag{2.46}$$

The lower bounds of different r_f are plotted in Fig. 2.18(b). For $\zeta > 0$, the lower bound of the friction ratio decreases as r_f increases. For $r_f > 1$, the lower bound of the friction ratio can be negative that means the time-average friction force become a "driving" force. Hence, the friction reduction effect will be enhanced when $r_f > 1$. The friction ratios of different displacement ratios are plotted in Fig. 2.19(r_f = 1.5) and Fig. 2.20 (r_f = 0.5). They are also not symmetric about the origin .For $\zeta > 0$, if $r_f > 1$, the time-average friction decreases as the displacement ratio increases, however, if $r_f < 1$, the time-average friction increases as the displacement ratio increases for small velocity ratio ζ.

2.3.3 Self-servo Effect

The friction moment can increase or decrease the normal force which in turn changes the friction force. This effect is called self-servo. A simple system is used to illustrate the effect shown in Fig. 2.21(a). The figure shows a sliding element hinged at *A*, having an actuating force *W*, a normal force *N* pushing the surfaces together, and a friction force $\tilde{F}$. The conditions of static equilibrium are applied by taking a summation of moments about the hinge pin. This gives

$$\sum M_A = Nl - Wl - \tilde{F}h = 0\,. \tag{2.47}$$

Assuming that $\sigma_{0n}z$ is the normalized friction force (Dahl model), i.e. the friction force per unit normal force, thus the friction force $\tilde{F}$ is given by

$$\tilde{F} = N\sigma_{0n}z, \qquad \sigma_{0n} > 0, \tag{2.48}$$

where σ_{0n} is the normalized tangential stiffness and z is the average deflection of the asperities. The normal force can be obtained by substituting $N\sigma_{0n}z$ for $\tilde{F}$ and solving (2.47), namely

$$N = \frac{W}{\left(1 - \frac{h}{l}\sigma_{0n}z\right)}. \tag{2.49}$$

Thus the friction force $\tilde{F}$ can be written as

$$\tilde{F} = N\sigma_{0n}z = \frac{W\sigma_{0n}z}{\left(1 - \frac{h}{l}\sigma_{0n}z\right)}. \tag{2.50}$$

Let the friction force without the self-servo effect ($h = 0$ and $W = N$) is $\tilde{F}_0 = W\sigma_{0n}z$. For $\sigma_{0n}z > 0$, the friction force with the self-servo effect is always large than that without the self-servo effect, i.e. $\tilde{F} > \tilde{F}_0$, this is called self-energizing. Contrarily, for $\sigma_{0n} z < 0$, $|\tilde{F}| < |\tilde{F}_0|$, this is called self-deenergizing. Note that a certain critical value of the normalized friction force $\sigma_{0n} z$ will cause the term $(1 - (h/l)\sigma_{0n} z)$ to become zero. This is the condition for self-locking.

Assuming that W is constant, thus the friction ratio is

$$r = \frac{\bar{F}}{F} = \frac{\dfrac{\omega}{2\pi}\displaystyle\int_0^{\frac{2\pi}{\omega}} \frac{W\sigma_{0n} z(t)}{\left(1 - \dfrac{h}{l}\sigma_{0n} z(t)\right)} dt}{\dfrac{WF_{cn}}{\left(1 - \dfrac{h}{l}F_{cn}\right)}} = \frac{\dfrac{\omega}{2\pi}\displaystyle\int_0^{\frac{2\pi}{\omega}} \frac{\sigma_{0n} z(t)}{\left(1 - \dfrac{h}{l}\sigma_{0n} z(t)\right)} dt}{\dfrac{F_{cn}}{\left(1 - \dfrac{h}{l}F_{cn}\right)}}, \tag{2.51}$$

where F_{cn} is the normalized Coulomb friction, i.e. the coefficient of Coulomb friction. Following the procedure used in the section of the sinusoidal oscillation, the upper bound and the lower bound of the friction ratio are

$$r_{\max} = \lim_{r_{disp} \to 0} \frac{\dfrac{\sigma_{0n} z(t)}{\left(1 - \dfrac{h}{l}\sigma_{0n} z(t)\right)}}{\dfrac{F_{cn}}{\left(1 - \dfrac{h}{l}F_{cn}\right)}} = \frac{\left(1 - \dfrac{h}{l}F_{cn}\right)\pi\zeta}{2\sqrt{1-\zeta^2} + 2\zeta\sin^{-1}(\zeta) - \dfrac{h}{l}F_{cn}\pi\zeta}, \qquad |\zeta| \le 1, \tag{2.52}$$

and $$r_{\min} = \frac{\dfrac{\omega}{2\pi}\left(\displaystyle\int_0^{\frac{2\pi - 2\cos^{-1}(\zeta)}{\omega}} \frac{F_{cn}}{\left(1 - \dfrac{h}{l}F_{cn}\right)} dt + \int_{\frac{2\pi - 2\cos^{-1}(\zeta)}{\omega}}^{\frac{2\pi}{\omega}} \frac{-F_{cn}}{\left(1 + \dfrac{h}{l}F_{cn}\right)} dt\right)}{\dfrac{F_{cn}}{\left(1 - \dfrac{h}{l}F_{cn}\right)}}$$

$$= \frac{2\sin^{-1}(\zeta) + \dfrac{h}{l}F_{cn}\pi}{\pi\left(1 + \dfrac{h}{l}F_{cn}\right)}, \qquad |\zeta| \le 1. \tag{2.53}$$

The friction ratio of the lower bound is plotted in Fig. 2.21(b). For $(h/l)F_{cn} > 0$ (self-energizing as the relative velocity is positive), the friction ratio increases as the value of (h/l) or F_{cn} increases. For $(h/l)F_{cn} < 0$ (self-deenergizing as the relative velocity is positive), the friction ratio decreases as the value of (h/l) or F_{cn} increases, and even becomes negative that means that the time-average friction force is a "driving" force. The friction ratios for different displacement ratios are plotted in Fig. 2.22. The influence of self-servo effect on the time-average friction is similar to that of asymmetric F_c. The time-average friction decreases as the displacement ratio increases, except the condition for $(h/l)F_{cn} > 0$ and small velocity ratio ($\zeta > 0$). It is worth to mention that other structures, such as the wedges and screws, will also cause the similar self-energizing effect.

2.4 Energy Dissipated

The asperities are elastic, so they can store energy and give it back to the system (Bliman, 1992). They can be represented by the physical analogy plotted in Fig. 2.23. The sliding body displacement x can be decomposed into elastic and plastic (sliding) components, z and w:

$$x = z + w. \tag{2.54}$$

The governing rate equation, from Eq. (2.54), is given by

$$\dot{x} = \dot{z} + \dot{w}. \tag{2.55}$$

For the friction force in the case with vibrations, the energy dissipated during one steady state period can be expressed as

$$W_v = \int_0^T \widetilde{F}(t) v_{rel}(t) dt. \tag{2.56}$$

Hence the average dissipated power is

$$P_v = \frac{1}{T}\int_0^T \widetilde{F}(t)v_{rel}(t)dt = \frac{\omega}{2\pi}\int_0^T \widetilde{F}(t)v_{rel}(t)dt\,, \tag{2.57}$$

which has the units of power. Applying the Dahl model, Eq. (2.57) can be written as

$$P_{v,Dahl} = \frac{\omega}{2\pi}\int_0^T \sigma_0 z(t)\dot{x}(t)dt = \frac{\omega\sigma_0}{2\pi}\left(\int_0^T z(t)\dot{z}(t)dt + \int_0^T z(t)\dot{w}(t)dt\right). \tag{2.58}$$

The dissipated power is divided into two parts, the first term for the elastic part and the second term for the plastic part. In the steady state, the average deflection has the relation,

$$z(0) = z(T)\,. \tag{2.59}$$

Thus

$$\int_0^T \dot{z}(t)dt = 0\,, \tag{2.60}$$

and

$$\int_0^T z(t)\dot{z}(t)dt = 0\,. \tag{2.61}$$

Then Eq. (2.58) is reduced to

$$P_{v,Dahl} = \frac{\omega\sigma_0}{2\pi}\int_0^T z(t)\dot{w}(t)dt\,. \tag{2.62}$$

The elastic term does not dissipate energy, but just stores energy and gives it back to the system. Under the sinusoidal oscillation, the average dissipated power of Dahl model in steady state is

$$P_{v,Dahl} = \begin{cases} F_c v_v \zeta & \zeta \ge 1 \\ \dfrac{2F_c v_v}{a\pi\left(e^{4aE_1}-1\right)}\left(e^{a(2E_1-\pi\zeta)} + e^{a(2E_1+\pi\zeta)} + e^{4aE_1}\left(aE_1-1\right) - aE_1 - 1\right) & 0 \le \zeta < 1 \end{cases}, \tag{2.63}$$

where

$$a = \frac{v_v\sigma_0}{\omega F_c}\,,$$

and $E_1 = \sqrt{1-\zeta^2} + \zeta\sin^{-1}(\zeta)\,.$

If the friction is assumed to be a rigid Coulomb friction, the elastic component z is zero, i.e. $\dot{x} = \dot{w}$, and $\widetilde{F}(t) = F_c \operatorname{sgn}(v_{rel})$. Thus under the sinusoidal oscillation, the average dissipated power, Eq. (2.57), can be written as

$$P_{v,Coulomb} = \begin{cases} F_c v_v \zeta & \zeta \geq 1 \\ \dfrac{2F_c v_v}{\pi}\left(\zeta \sin^{-1}(\zeta) + \sqrt{1-\zeta^2}\right) & 0 \leq \zeta < 1 \end{cases}, \tag{2.64}$$

which is the limit of Eq. (2.63) when the displacement ratio *a* approaches infinity. In the case without vibrations, the dissipated power is calculated by

$$P_s = F_c v_b = F_c v_v \zeta \,. \tag{2.65}$$

For $\zeta \geq 1$, note that the dissipated power with vibrations is equal to the dissipated power without vibrations (refer to Eqs. (2.63)-(2.65)) because the vibrations do not affect the friction in this condition, *i.e.* the friction force is constant.

The normalized average dissipated power $P_{v,Dahl}/(F_c v_v)$ is plotted in Fig. 2.24. The normalized average dissipated power with vibrations decreases as the displacement ratio decreases because the tangential compliance reduces the sliding component *w*. The ratio of the dissipated energy with vibrations to that without vibrations, which can be obtained from Eq. (2.63) divided by Eq. (2.65), is plotted in Fig. 2.25. The average dissipated power with vibrations may be lower than that without vibrations, especially when the displacement ratio *a* is small. This can be explained by the friction-displacement curve in Fig. 2.26. The energy dissipated is equal to the area below the friction-displacement curve. Due to the tangential compliance, the friction with vibrations is smaller than that without vibrations. Thus the area below the curve with vibrations is smaller than the area below the curve without vibrations, i.e. $F_c x$. Note that the Dahl's friction model does not include the damping of the asperity. Hence, if the damping is included, the dissipated energy will be higher than the value calculated from Eq. (2.63) and increase with the frequency of the vibrations. However, the dissipated energy only approaches but does not exceed the value calculated from Eq. (2.64) because the damping of the asperity only increases the effective stiffness of the asperity but not the Coulomb friction F_c.

2.5 Concluding Remarks

A theoretical approach based on Dahl's friction model is presented that describes the time-average friction reduction by the parallel vibrations. The comparison between the friction reduction based on the rigid Coulomb friction model and the experimental data shows that the tangential compliance should be take into consideration in the analysis of the friction reduction by the tangential vibrations. A displacement ratio of the displacement amplitude of the vibrations to the steady-state compliance is proposed to describe the influence of the tangential compliance. The analysis shows that the time-averaged friction is reduced when the base velocity is smaller than the vibrating velocity, and it decreases as the displacement ratio increases. In addition to the tangential compliance, other factors that also have influences on the friction reduction are proposed and investigated individually, including the waveform of the oscillation, asymmetric Coulomb friction and self-servo effect. By choosing suitable waveform of the oscillation, direction of the asymmetric Coulomb friction or self-servo structure, the friction reduction can be enhanced or suppressed depending on the applications. The energy dissipated during sliding with vibrations is also studied. As the displacement ratio decreases, the average dissipated energy with vibrations decreases and may be lower than that without vibrations. Sensitivity studies and optimizations for specified applications are natural extension of this work.

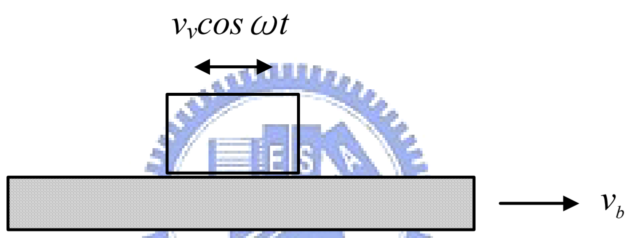

Fig. 2.1 An analytical model

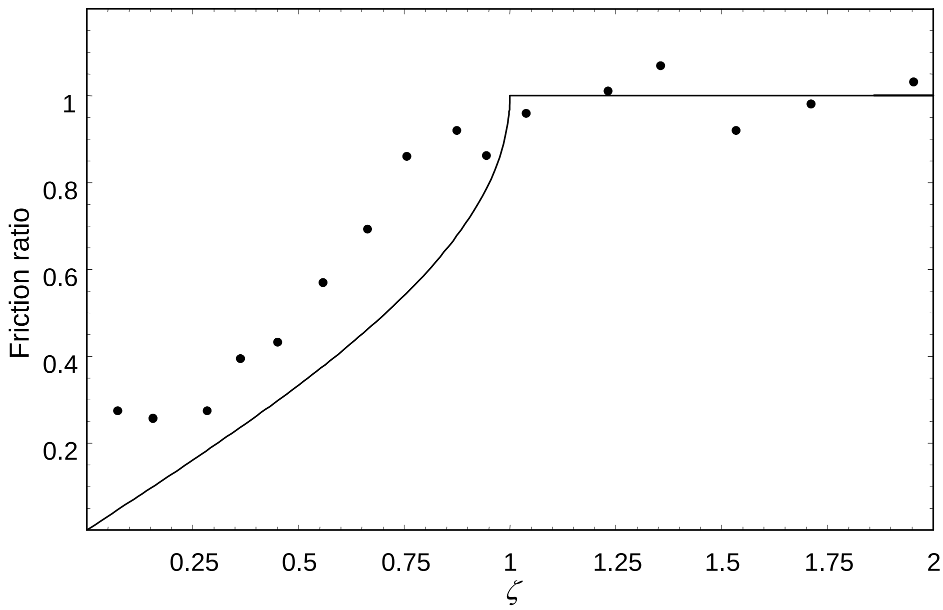

Fig. 2.2 Friction ratio for $\zeta > 0$ and experimentally obtained values (dot) by Littmann *et al.*

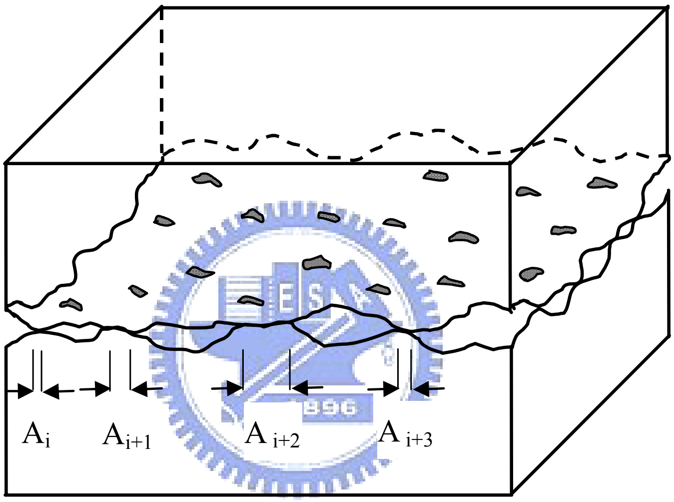

Fig. 2.3 True contact between surfaces

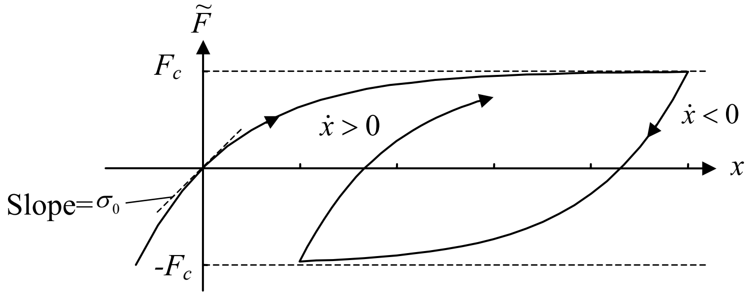

(a) Friction force and displacement

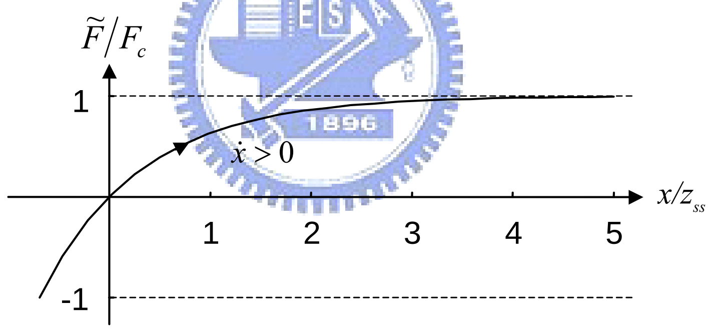

(b) Dimensionless

Fig. 2.4 Relation between the friction force and the displacement

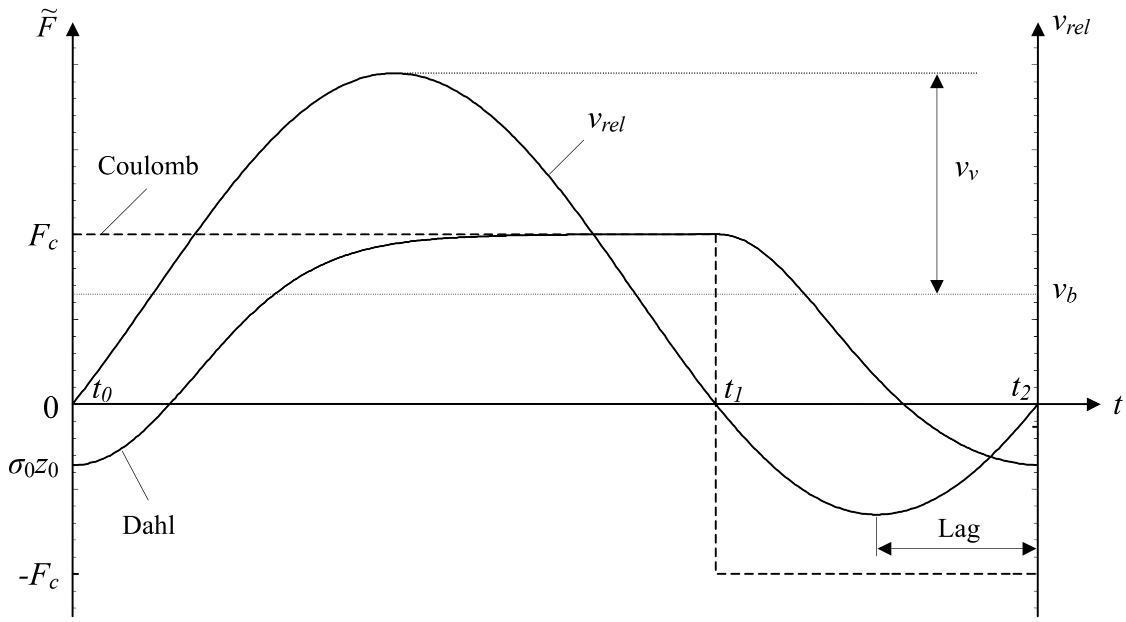

Fig. 2.5 Instantaneous friction force (Dahl and Coulomb) and relative sliding velocity over one steady state period

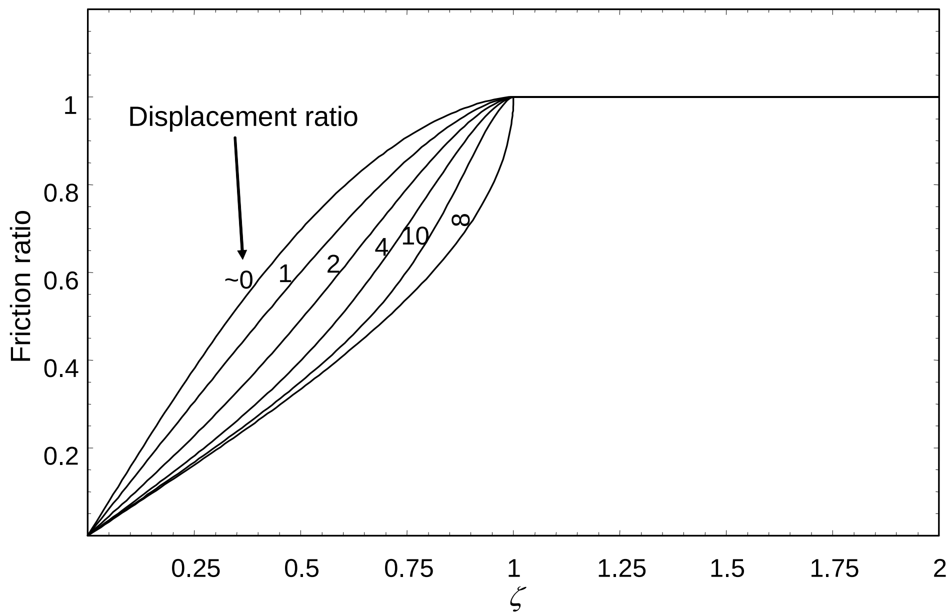

Fig. 2.6 Friction ratios based on Dahl model

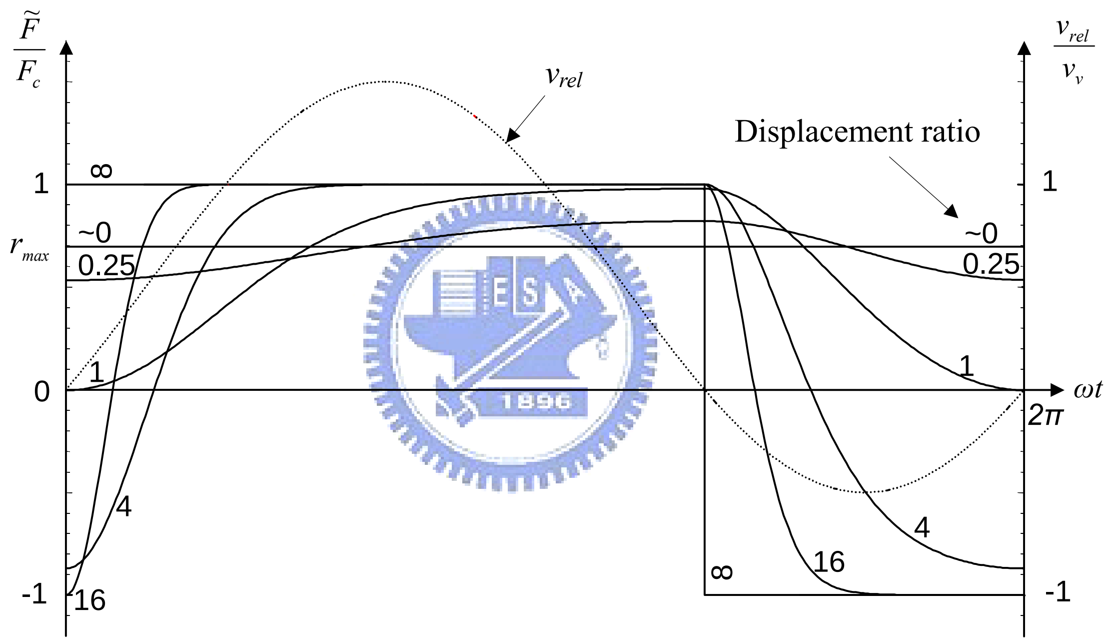

Fig. 2.7 Instantaneous Dahl friction forces of different displacement ratios and relative sliding velocity over one steady state period

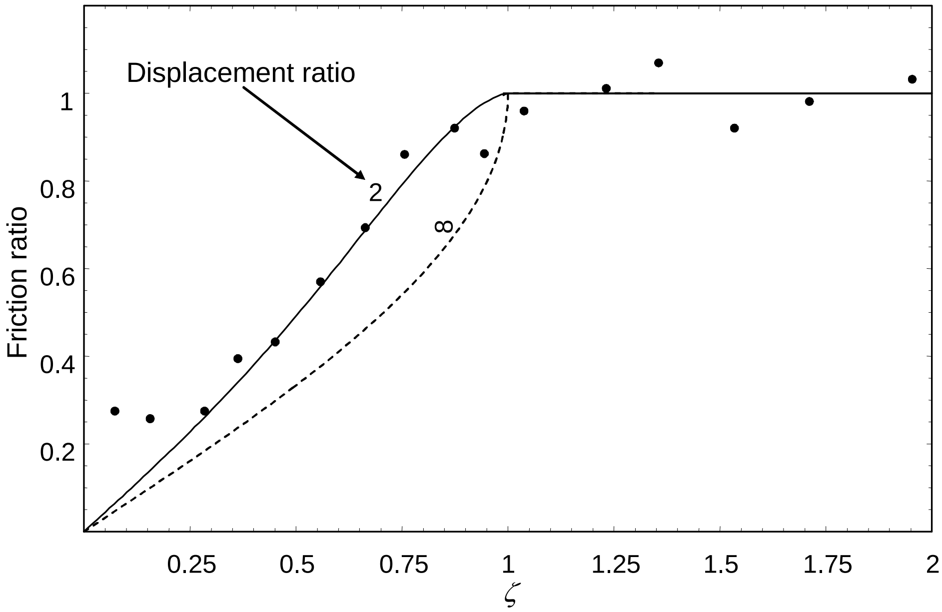

Fig. 2.8 Friction ratio based on Dahl model and experimentally obtained values (dot) by Littmann *et al.*

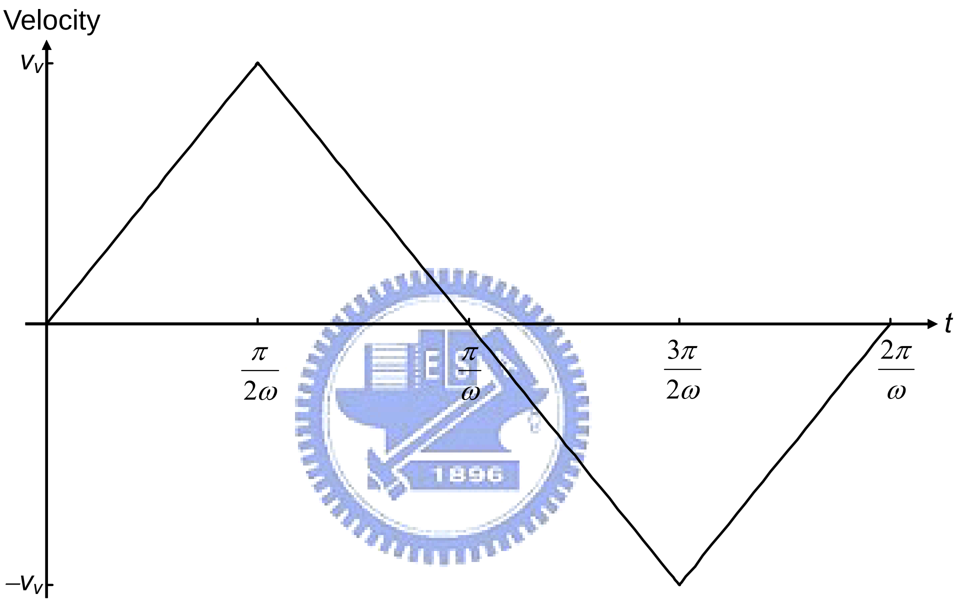

Fig. 2.9 Velocity of the vibrating body over one period – triangular wave

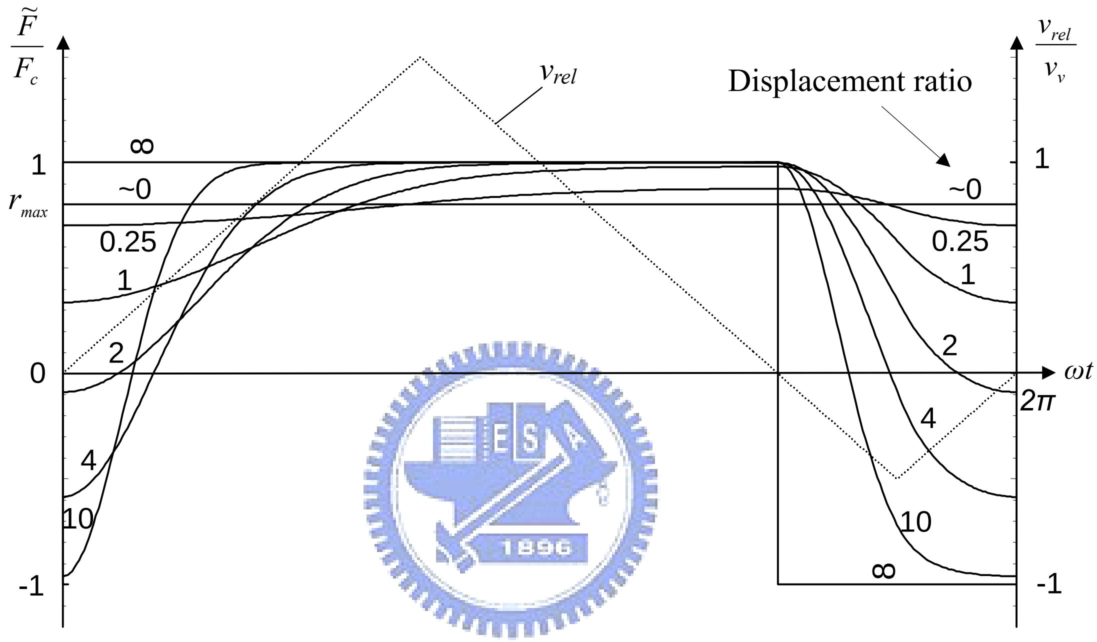

Fig. 2.10 Instantaneous Dahl friction forces of different displacement ratios and relative sliding velocity over one steady state period for the triangular wave oscillation

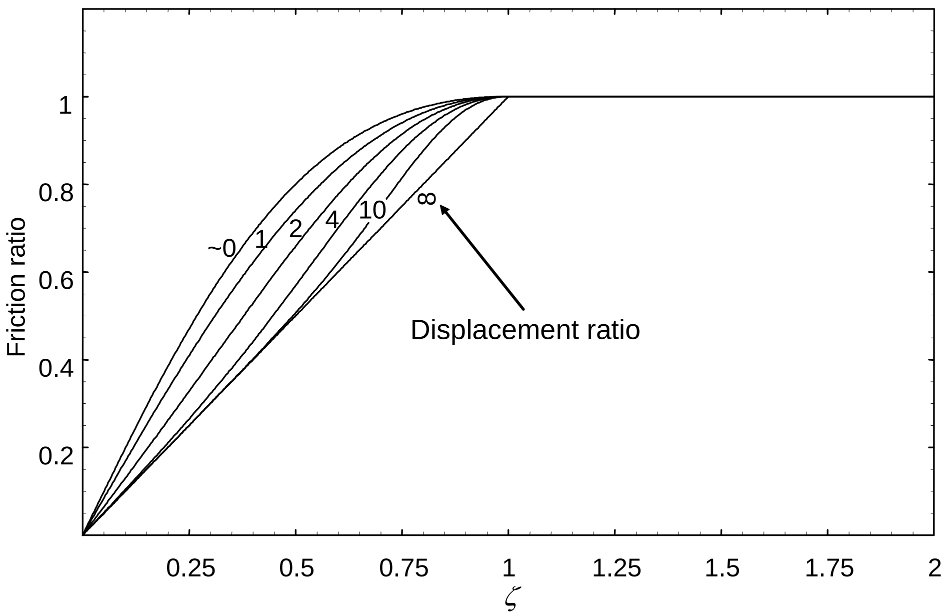

Fig. 2.11 Friction ratios for triangular wave oscillation

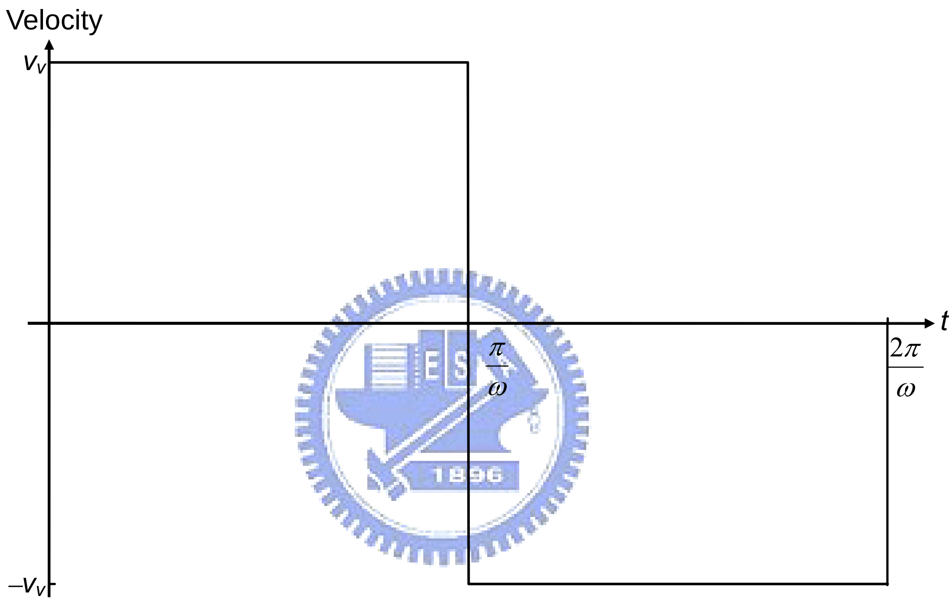

Fig. 2.12 Velocity of the vibrating body over one period – square wave

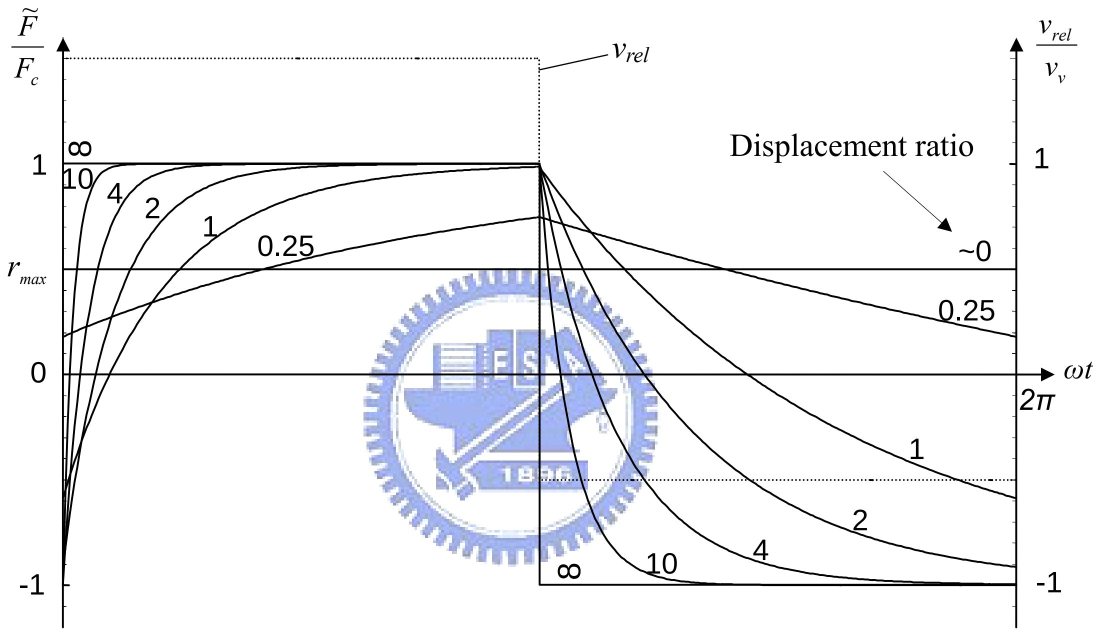

Fig. 2.13 Instantaneous Dahl friction forces of different displacement ratios and relative sliding velocity over one steady state period for the symmetrical square wave oscillation

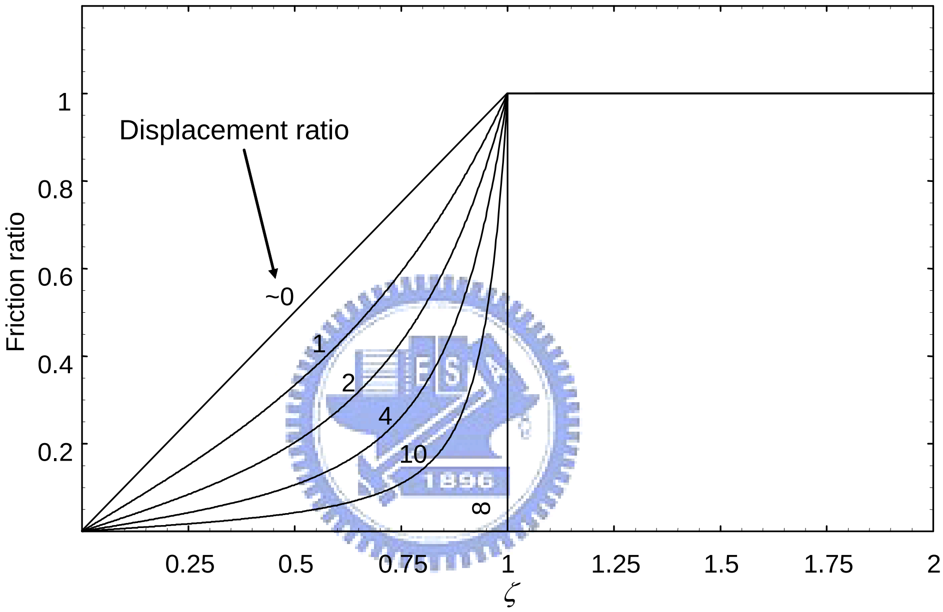

Fig. 2.14 Friction ratios for the symmetrical square wave oscillation

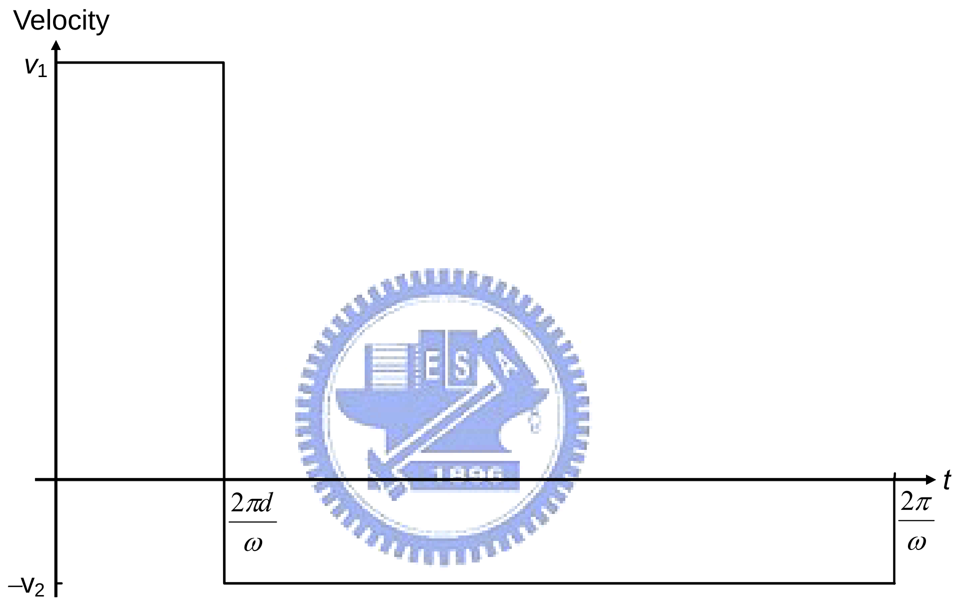

Fig. 2.15 Velocity of the vibrating body over one period – asymmetrical square wave

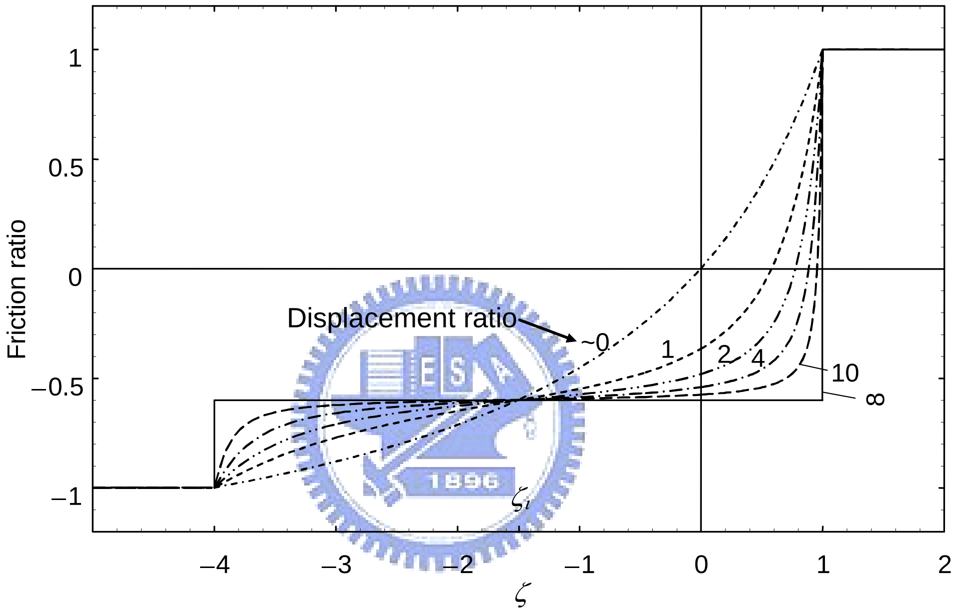

Fig. 2.16 Friction ratios for the asymmetrical square wave oscillation (d = 0.2)

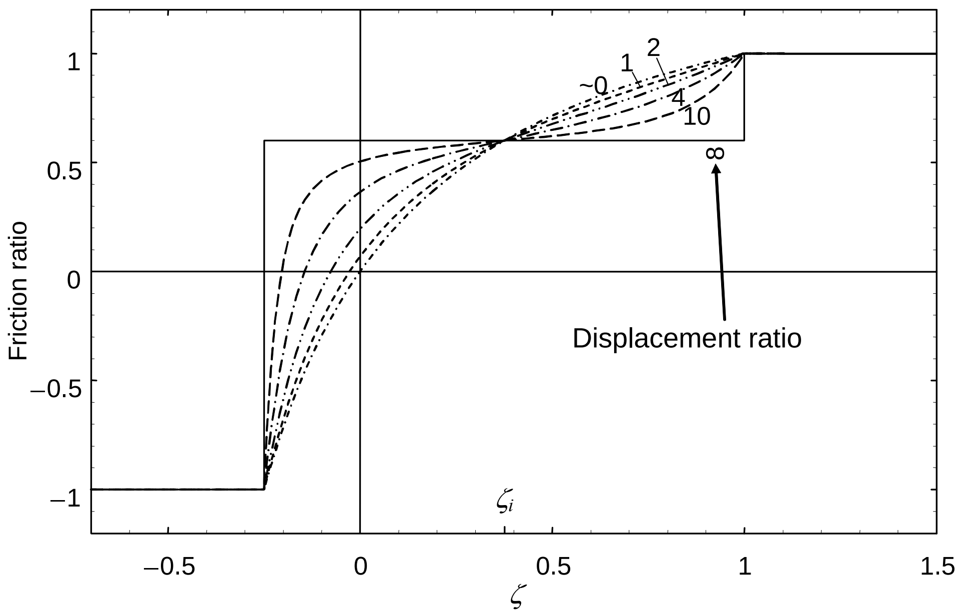

Fig. 2.17 Friction ratios for the asymmetrical square wave oscillation (d = 0.8)

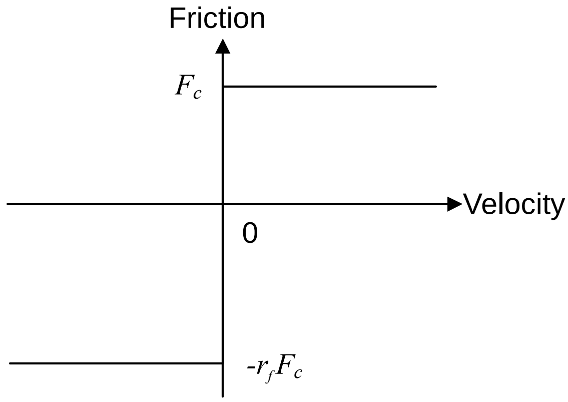

(a) Asymmetrical Coulomb friction

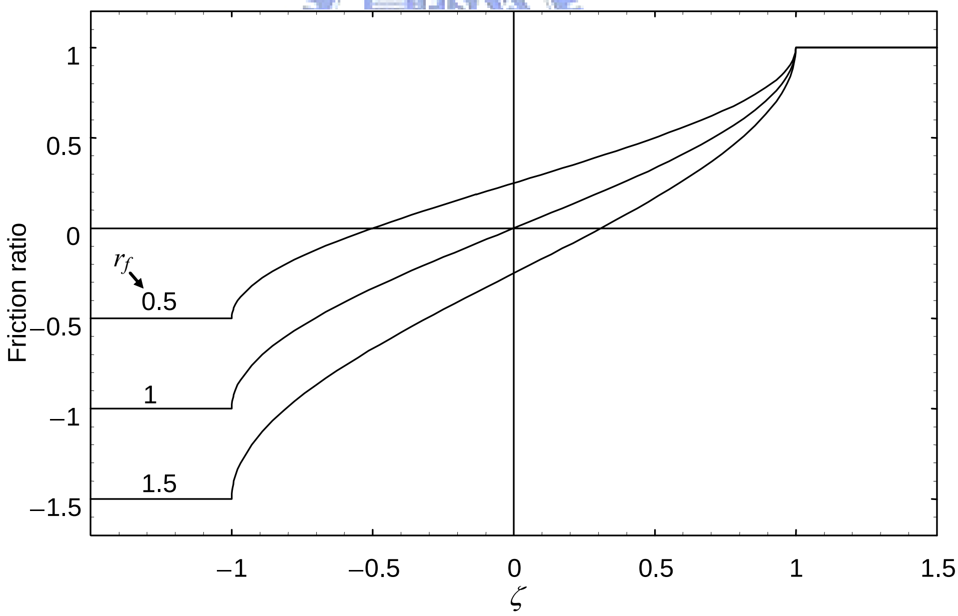

(b) Friction ratio r_{min}

Fig. 2.18 Asymmetrical Coulomb friction and its influence on the friction ratio

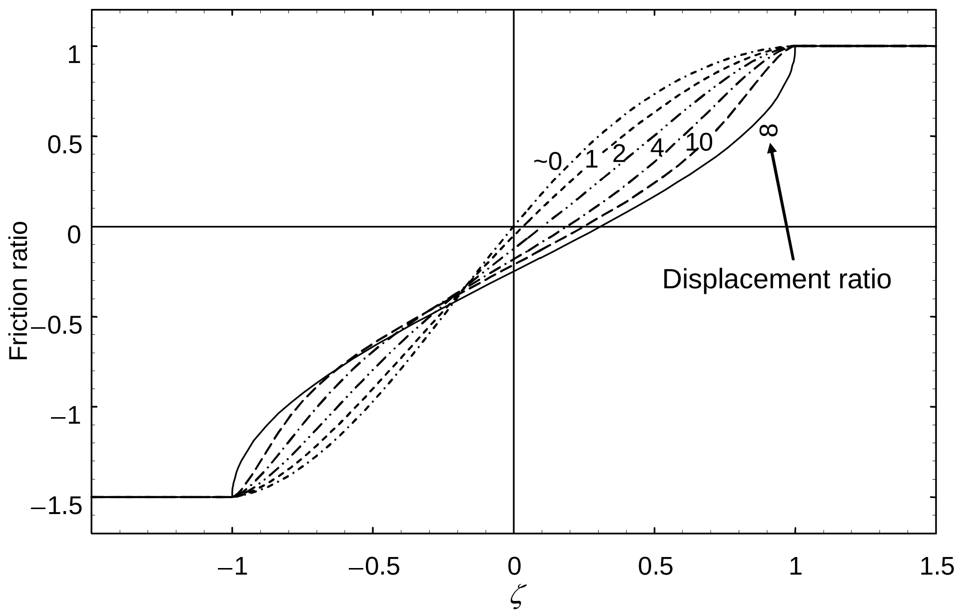

Fig. 2.19 Friction ratios for the asymmetrical Coulomb friction ($r_f = 1.5$)

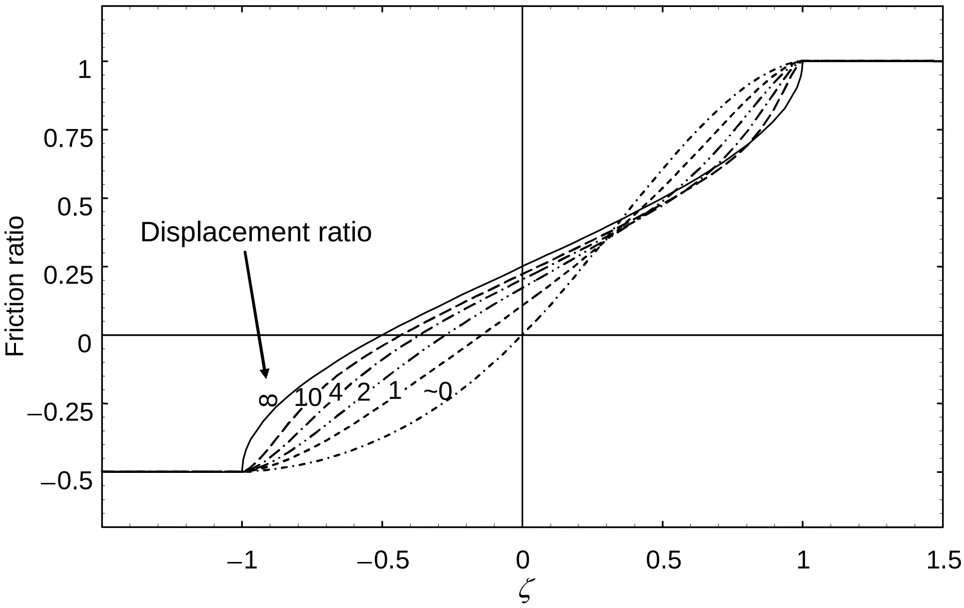

Fig. 2.20 Friction ratios for the asymmetrical Coulomb friction ($r_f = 0.5$)

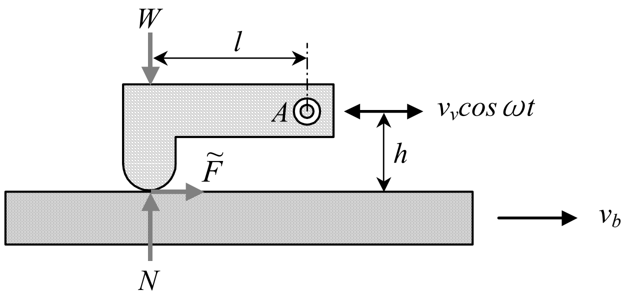

(a) Forces acting upon a hinged element

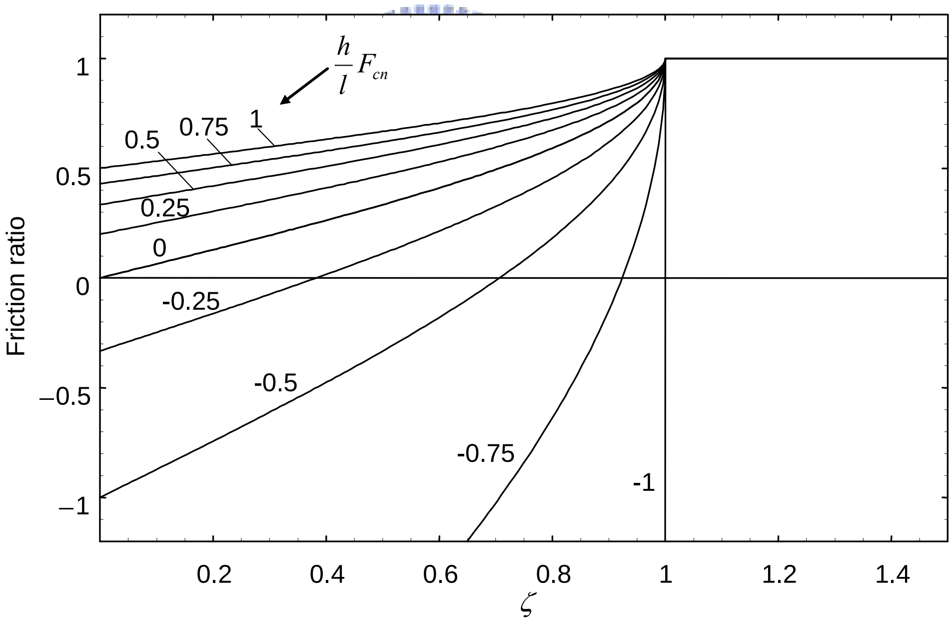

(b) $r_{\min}$ for different values of $(h/l)F_{cn}$

Fig. 2.21 Self-servo effect and its influence on the friction ratio

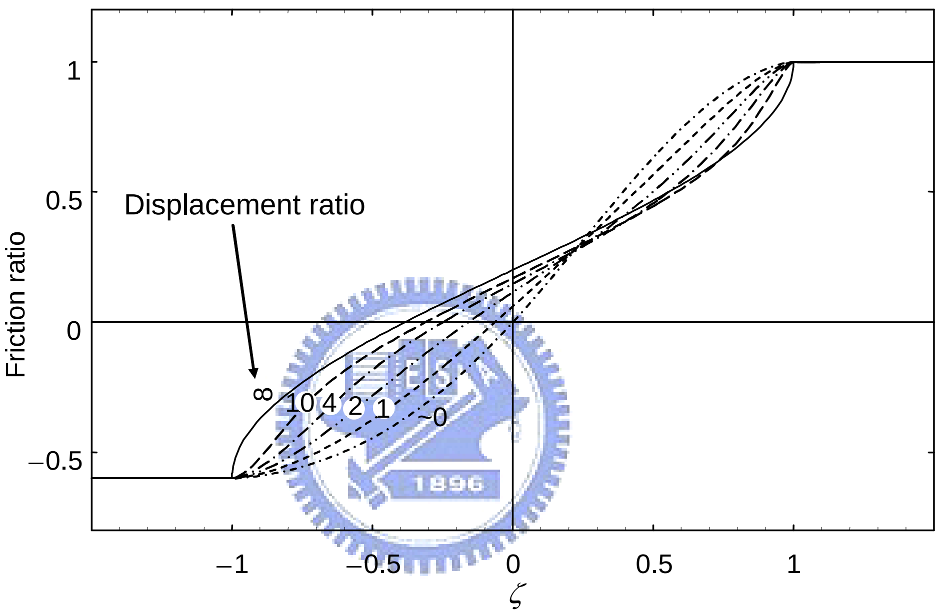

Fig. 2.22 Friction ratios with the self-servo effect $\left((h/l)F_{cn} = 0.25\right)$.

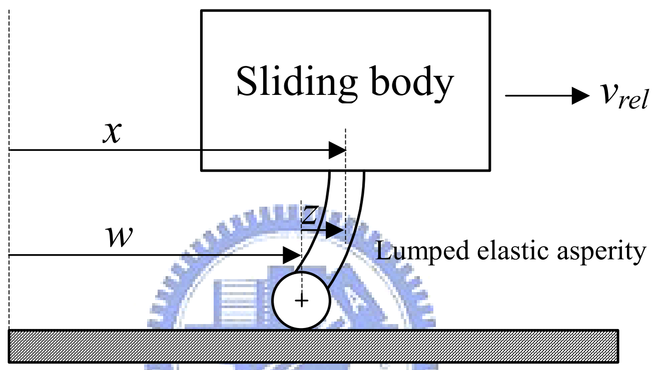

Fig. 2.23 Displacement x decomposed into elastic z and plastic (sliding) components w

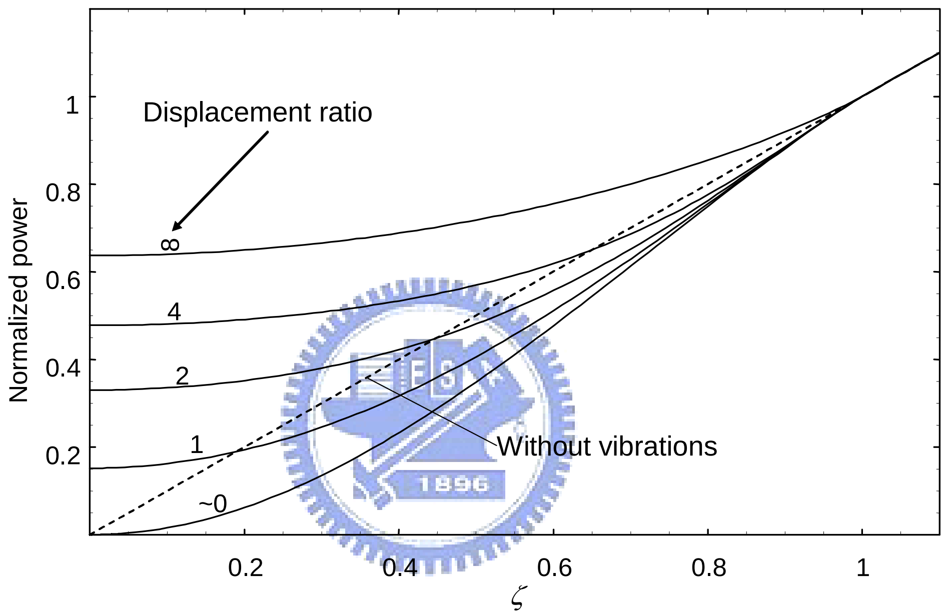

Fig. 2.24 Normalized average dissipated power $\dfrac{P_{v,Dahl}}{F_c v_v}$

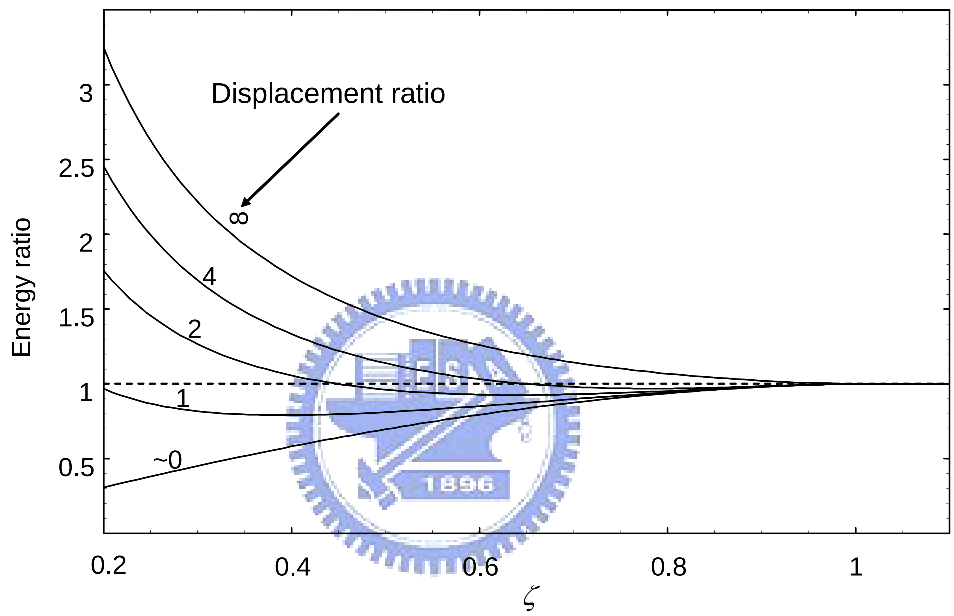

Fig. 2.25 The ratio of the dissipated energy with vibrations to that without vibrations

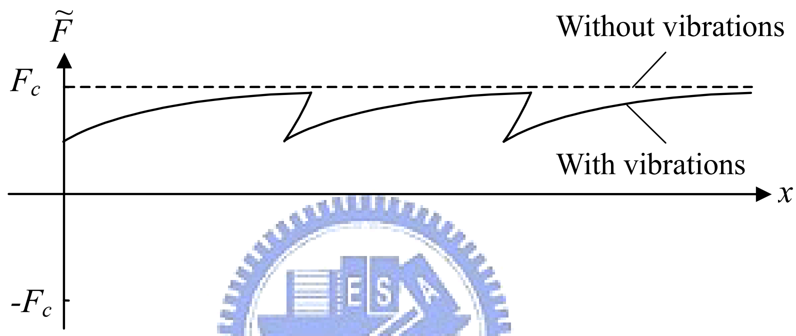

Fig. 2.26 The friction and displacement under the steady state

CHAPTER 3 FRICTION REDUCTION IN THE LUBRICATED CONTACTS

3.1 Introduction

The friction behavior in the lubricated contacts is different form that in the dry contact. For this reason, a friction model that can capture the friction behavior in the lubricated contacts is required. In this chapter, the LuGre model is applied to investigate the friction reduction observed in the lubricated contacts with the parallel vibrations.

In order to capture more frictional phenomena observed in the experiments, Canudas de Wit *et al.* (1995) proposed a new model, LuGre friction model, which is an extension of the Dahl model. They were inspired by the bristle model proposed by Haessig and Friedland (1991). The surfaces in contact are visualized as two rigid bodies that make contact through elastic bristles. When a tangential force is applied, the bristles will deflect like springs which gives rise to the friction force. If the deflection is sufficiently large, the bristles start to slip. The average bristle deflection for a steady state motion is determined by the velocity. It is lower at low velocities, which implies that the steady state deflection decreases with increasing velocity. This models the Stribeck effect that is the steady-state relationship between friction force and slip velocity. In addition, the damping effect of the bristles and viscous friction between the surfaces are also included. This dynamic model can capture most of the friction behavior. This includes the presliding displacement, Stribeck effect, hysteresis, and varying breakaway force. Further analysis of the model and its application can be found (Dupont *et al.*, 1997; Olsson *et al.*, 1998; Altpeter, 1999; Canudas de Wit and Tsiotras, 1999; Barabanov and Ortega, 2000).

A significant limitation of the Dahl and LuGre models, however, is that they exhibit drift when systems subjected to a small bias force and small vibrations. To minimize the drift, Dupont *et al.* (2000, 2002) proposed a elasto-plastic model in which presliding is elasto-plastic, *i.e.*, under loading the displacement is first purely elastic (reversible) before transitioning to plastic (irreversible).

3.2 LuGre Model

The LuGre model is an extension of Dahl's model that can provide representations of many friction behaviors, including the presliding displacement, Stribeck effect, hysteresis, and varying breakaway force. This model is given by

$$\widetilde{F} = \sigma_0 z + \sigma_1 \frac{dz}{dt} + \sigma_2 v, \tag{3.1}$$

and $$\frac{dz}{dt} = v\left(1 - \frac{\sigma_0}{F_{ss}(v)}\operatorname{sgn}(v) z\right), \tag{3.2}$$

where state variable z denotes the average deflection of the asperities, σ_0 and σ_2 are contact stiffness and viscous friction parameters, and σ_1 provides damping for the tangential compliance. The model can be represented as the analogy depicted in Fig. 3.1. The parameters σ_0, σ_1 and σ_2 are usually assumed to be constant in the applications. The function $F_{ss}(v)$ is the steady state friction force versus rigid body velocity for lubricated systems, called the Stribeck curve, and is illustrated in Fig. 3.2. The negative going portion of the curve arises from the contact riding up on a lubricant film; as the lubricant film grows thicker with increasing velocity, the friction decreases. Fig. 3.3 presents several friction-velocity curves (Armstrong *et al.*, 1994). Details of the friction-velocity curve depend on the degree of boundary lubrication and the detail of partial fluid lubrication. When lubricants that provide little or no boundary lubrication are employed, the friction decreases as the velocity increases before full fluid lubrication dominates, as curve (a). When boundary lubrication is more effective, the friction is relatively constant up to the velocity at which partial fluid lubrication begins to play a role, as curve (b). A curve of type (c) is given by way lubricants. The boundary lubrication provided by the additives to these oils reduces static friction to a level below kinetic friction. For analysis or simulation it is important to have a mathematical model of the Stribeck curve. But for the moment no predictive model of the Stribeck curve is available, an empirical model is required.

A reasonable choice of $F_{ss}(v)$ which gives a good approximation of the Stribeck effect is given by

$$F_{ss}(v) = F_c + (F_{ba} - F_c)e^{-|v/v_s|^{\alpha}}, \tag{3.3}$$

where F_c is the Coulomb friction force (minimum kinetic friction), F_{ba} is the breakaway force (static friction), v_s is the characteristic velocity of the Stribeck curve that determines how $F_{ss}(v)$ vary within its bounds $F_c < F_{ss}(v) \leq F_{ba}$, and α is a parameter that determines the shape of the Stribeck curve (an effective boundary lubricant would suggest α very large; the value $\alpha = 2$ is used by Canudas *et al.*). By appropriate choice of parameters, curves of types (a), (b) and (c) can be realized. The viscous friction is not added here; it is added to Eq. (3.1) to fully describe the Stribeck's friction. The Stribeck friction curve is sometimes plotted only in the first quadrant; here a more general form is considered in which $F_{ss}(v)$ is a signed quantity, as shown in Fig. 3.4. As the LuGre model includes the Stribeck, damping and viscous effects, it can capture more friction behaviors than the Dahl's model. The LuGre model reduces to the Dahl's model if $F_{ss}(v) = F_c$ and $\sigma_1 = \sigma_2 = 0$.

3.3 Time-averaged Friction of the LuGre Model

The friction of LuGre model, Eq. (3.1), is the sum of the three individual terms. So the influence of them on the friction reduction effect by vibrations can be analyzed individually.

The parameters σ_0, σ_1 and σ_2 are also assumed to be constant in the study. Hence the time-averaged friction of the LuGre model has the form

$$\overline{F} = \overline{F}_{\sigma_0} + \overline{F}_{\sigma_1} + \overline{F}_{\sigma_2} . \tag{3.4}$$

The system to be analyzed is the same with Fig. 2.1 where the relative sliding velocity is

$$v_{rel}(t) = v_b - v(t) = v_v(\zeta - \cos(\omega t)) . \tag{3.5}$$

The three individual terms of LuGre model over one steady state period is plotted in Fig. 3.5.

3.3.1 Damping Term

In a steady state period (periodic), the deflections in the beginning and end of the period are equal, *i.e.* $z(0) = z(T)$. $z(t)$ is a continuous function. Thus the definite integral of $\dot{z}(t)$ on the period T is

$$\int_0^T \dot{z}(t)dt = z(T) - z(0) = 0 . \tag{3.6}$$

This leads to the time average of the damping term of the LuGre model,

$$\overline{F}_{\sigma_1} = \frac{1}{T}\int_0^T \sigma_1 \frac{dz(t)}{dt} dt = \frac{\sigma_1}{T}\int_0^T \dot{z}(t)dt = 0 . \tag{3.7}$$

Fortunately, this term has no effect on the time-average friction.

3.3.2 Viscosity Term

The time average of the viscous term of the LuGre model is given by

$$\overline{F}_{\sigma_2} = \frac{1}{T}\int_0^T \sigma_2 v = \frac{\omega}{2\pi}\int_0^{\frac{2\pi}{\omega}} \sigma_2 v_v\left(\zeta - \cos(\omega t)\right) = \sigma_2 v_v \zeta = \sigma_2 v_b , \tag{3.8}$$

which is equal to the viscosity term without vibrations. In other words, the vibrations do not affect the time average of the viscous term. Substituting Eqs. (3.7) and (3.8) into Eq. (3.4) gives

$$\overline{F} = \overline{F}_{\sigma_0} + \sigma_2 v_b . \tag{3.9}$$

Equation (3.2) gives the steady state deflection,

$$z_{ss} = \frac{F_{ss}(v_b)}{\sigma_0} . \tag{3.10}$$

Without vibration (*i.e.* the constant sliding velocity), the steady state friction force is given by

$$F = \sigma_0 z_{ss} + \sigma_2 v = F_{ss}(v_b) + \sigma_2 v_b . \tag{3.11}$$

Hence, the friction ratio is

$$r = \frac{\overline{F}}{F} = \frac{\overline{F}_{\sigma_0} + \sigma_2 v_b}{F_{ss}(v_b) + \sigma_2 v_b} = \frac{r_{\sigma_0} + \dfrac{\sigma_2 v_b}{F_{ss}(v_b)}}{1 + \dfrac{\sigma_2 v_b}{F_{ss}(v_b)}} , \tag{3.12}$$

where $r_{\sigma_0} = \overline{F}_{\sigma_0} / F_{ss}(v_b)$ is the friction ratio without the viscous friction. For $r_{\sigma_0} < 1$, the friction ratio increases as the viscous friction increases. In other words, the viscous friction reduces the effect of friction reduction by vibrations. If the viscosity term dominates the friction, the friction ratio is

$$r = \frac{\overline{F}}{F} \approx \frac{\sigma_2 v_b}{\sigma_2 v_b} = 1 . \tag{3.13}$$

Thus the vibrations have little effects on the friction when the viscous effect dominates the friction, such as the contacts with the hydrodynamic lubrication that the surfaces are pushed apart by the lubricant.

Adding the viscous friction to the Dahl's model, the increase of the friction ratio (the decrease of the friction reduction effect) is shown in Fig. 3.6.

3.3.3 Elastic Term

The Stribeck effect is a friction phenomenon that arises from the use of fluid lubrication.

Thus, for dry friction, $F_{ss}(v) = F_c$ and $\sigma_2 = 0$. Besides, the time average of the damping term of the LuGre model is zero. So in the case of dry friction the friction reduction based on the LuGre model is same with that based on the Dahl model that only has the elastic term. However, in the lubricated contacts the elastic term $\sigma_0 z$ of the LuGre model is different from that of the Dahl model because it includes the Stribeck effect.

3.4 Parameter Studies

Due to the fact that the damping term has no effect on the time-averaged friction and the viscous term simply degrades the friction reduction effect (refer to Eqs. (3.7) and (3.12)) and is normally not sufficiently large to have obvious influence on the friction ratio, the following study can only focus on the elastic term, $\sigma_0 z$.

3.4.1 Influence of Stribeck Effect on the Friction Reduction Effect

The simple general solution of Eq. (3.2) was not found. So a simpler case was first studied, which the stiffness parameters σ_0 was assumed to be very large ($\sigma_0 \to \infty$), to reveal the influence of Stribeck effect on the friction reduction effect. Due to the rigid body assumption, the friction force with Stribeck effect is given by

$$\tilde{F}(t) = \operatorname{sgn}(v_{rel}(t))\left(F_c + (F_{ba} - F_c)e^{-\left|v_{rel}(t)/v_s\right|^{\alpha}}\right). \tag{3.14}$$

Instantaneous friction force and relative sliding velocity over one period is plotted in Fig. 3.7. The friction force increases when the relative sliding velocity approaches zero.

The relative sliding velocity with vibrations is defined in Eq. (3.5). The effective friction force, which is observed macroscopically, is the time-averaged mean friction force over one period of vibration:

$$\overline{F} = \frac{\omega}{2\pi}\int_0^{\frac{2\pi}{\varpi}} \operatorname{sgn}(v_v(\zeta - \cos(\omega t)))\left(F_c + (F_{ba} - F_c)e^{-|v_v(\zeta - \cos(\omega t))/v_s|^{\alpha}}\right)dt$$
$$= \frac{1}{2\pi}\int_0^{2\pi} \operatorname{sgn}(v_v(\zeta - \cos(\tau)))\left(F_c + (F_{ba} - F_c)e^{-|v_v(\zeta - \cos(\tau))/v_s|^{\alpha}}\right)d\tau \quad , \tag{3.15}$$

where $\tau = \omega t$. Without vibrations, the steady state friction force is

$$F = F_c + (F_{ba} - F_c)e^{-|v_v\zeta/v_s|^{\alpha}} . \tag{3.16}$$

The effect of friction reduction by superposed vibrations can be described quantitatively by the friction ratio

$$r = \frac{\overline{F}}{F} . \tag{3.17}$$

Introducing $r_{sf} = F_{ba}/F_c$ and $r_{sv} = v_v/v_s$, and substituting $\overline{F}$ from Eq. (3.15) and F from Eq. (3.16) give

$$r = \frac{\frac{1}{2\pi}\int_0^{2\pi} \operatorname{sgn}(\zeta - \cos(\tau))\left(1 + (r_{sf} - 1)e^{-|r_{sv}(\zeta - \cos(\tau))|^{\alpha}}\right)d\tau}{1 + (r_{sf} - 1)e^{-|r_{sv}\zeta|^{\alpha}}} . \tag{3.18}$$

The above integral can be calculated explicitly if $r_{sf} = 1$ or $\alpha = 0$, which represents the case without the Stribeck effect, as follows:

$$r_{r_{sf}=1} = \begin{cases} \frac{2}{\pi}\sin^{-1}\zeta & -1 \le \zeta \le 1 \\ 1 & \zeta > 1 \end{cases} . \tag{3.19}$$

This is the same with the friction ratio based on the Coulomb friction model whose friction only depends on the direction of the relative sliding velocity (refer to Sec. 2.1).

In the literature surveyed, α ranges from 0.5 to a large value. The more effective boundary lubrication would suggest a larger α. The LuGre model adopted $\alpha = 2$. So a reasonable basic set of the parameters of Eq. (3.18) is $(r_{sf}, r_{sv}, \alpha) = (1.8, 2, 2)$. The calculations for friction ratio were performed for varying parameters. The results are shown in Table 3.1 and Fig. 3.8.

When r_{sv} is small or large enough, the influence of the Stribeck effect on the friction ratio is small. It has the maximum influence when r_{sv} is in the range of 1~2. For a small velocity ratio ζ (about 0~1), the friction ratio decreases as r_{sf} or α increases. For a larger velocity ratio ζ (about > 1), the friction ratio increases as r_{sf} or α increases. The normalized Stribeck curves with varying parameters are plotted in Fig. 3.9. The higher r_{sf} represents the greater Stribeck effect, and the larger α represents that the friction variation is larger when the sliding velocity is close to the Stribeck velocity v_s.

The Stribeck friction under vibrations is plotted in Fig. 3.10. When r_{sv} is small (the amplitude of the vibrating velocity v_v is small compared to the Stribeck velocity v_s), the change of the Stribeck friction in quantity over one vibration period is small. So the friction ratio is close to that of $r_{sv}=0$ where the value of friction force is constant within a cycle. When r_{sv} is large enough, the larger Stribeck frictions near low velocities only occupy a small part of time over one period. So the friction ratio is also close to that of $r_{sv}=0$. The greatest effect of the Stribeck friction on the friction ratio occurs when r_{sv} is close to 1~2. When the velocity ratio ζ is large enough to keep high sliding velocities, there would be no friction rise over one period. The lowest sliding velocity within one cycle is $v_v(\zeta-1)$. Supposing the threshold of the friction rise is $(1+1\%)F_c$ (refer to Fig. 3.9.), the maximum velocity ratio ζ where the Stribeck friction can raise within one cycle can be derived from Eq. (3.14) and expressed as follows:

$$\begin{aligned}\zeta &= 1+\frac{v_s}{v_v}\log^{\frac{1}{\alpha}}[100(\frac{F_{ba}}{F_c}-1)] \\ &= 1+\frac{1}{r_{sv}}\log^{\frac{1}{\alpha}}[100(r_{sf}-1)].\end{aligned} \tag{3.20}$$

Taking parameters $(r_{sf}, r_{sv}, \alpha) = (1.8,4,2)$ as an example, the maximum velocity ratio ζ is 1.5 (as shown in Table 3.1). When the velocity ratio ζ is larger than 1.5, the friction ratio is not affected by the Stribeck effect, approaching to the curve of $r_{sf} = 1$. Note that the viscous friction is not included in the above calculations. To add this term to the calculated friction ratio, refer to Eq. (3.12).

3.4.2 Lubricated Contacts with Tangential Compliance

The rigid body assumption simplifies the calculations. In the condition with high frequency vibrations, however, the vibrating displacement is usually very small (some μms), and the tangential compliance can be comparable to the vibrating displacement. In this condition, the tangential compliance should be included in the calculations, which were presented in the following study.

It is worthy to mention that the LuGre model captures the friction lag phenomenon by the elastic term. If $\sigma_0 \to \infty$ (rigid body), there is no friction lag. Hence, if the friction behavior of the contacts with vibrations does shows the friction lag phenomenon, the rigid body assumption is not suitable for that condition.

In order to investigate the influence of the Stribeck effect on the friction reduction by vibrations, an initial set of parameter values in Table 3.2 have been used. The parameters are varied individually, one at a time. The stiffness σ_0 was chosen to give a presliding displacement of the same magnitude as reported in various experiments (about 0.3~10 μm). The Coulomb friction level F_c corresponds to a friction coefficient $\mu \approx 0.1$ for a unit mass, and F_{ba} gives a higher friction for very low velocities. The Stribeck velocity v_s is the same order of magnitude as given in (Hess and Soom, 1990). The LuGre model adopted $\alpha = 2$. The vibrating velocity v_v and frequency ω of the system are also the same with that of the experiment by Littmann *et al.* (2001a, 2001b, 2002). The damping term and the viscous term were not included here.

The influence of the contact stiffness σ_0 on the friction reduction effect was studied first. The results are shown in Fig. 3.11, where the solid line indicates the parameter configuration corresponding to Table 3.2. For a small velocity ratio ζ (about < 1), the friction ratio decreases (*i.e.* the amount of the friction reduction increases) as the contact stiffness σ_0 increases. In other words, the tangential compliance reduces the friction reduction effect. This is very similar to the results based on the Dahl model as shown in Fig. 2.6, where the friction ratio is a function of the displacement ratio and the velocity ratio ζ, and decreases as the displacement ratio increases for $\zeta < 1$. The displacement ratio in the study based on the Dahl model is defined as

$$r_{disp} = \frac{v_v \sigma_0}{\omega F_c} = \frac{v_v / \omega}{F_c / \sigma_0} = \frac{x_v}{z_{ss}}. \tag{3.21}$$

It is a ratio of the displacement amplitude of the vibration to the steady state deflection of the asperities. The displacement ratio indicates how close the instantaneous friction approaches the "saturated" friction (F_c in the Dahl model) before the reverse of the sliding direction. A larger displacement ratio represents that the instantaneous friction is closer to the saturated friction during the unidirectional sliding. As the friction of the Dahl model is a function of displacement (refer to Fig. 2.4), the response of the instantaneous friction depends on the displacement but not time. The LuGre model is the extension of the Dahl model. So the behaviors of the asperities are similar to that of the Dahl model. One of the differences between these two models is that the LuGre model includes the Stribeck effect that describes the steady-state behavior of the lubricated contacts. The underlying assumption of the LuGre model is that the fluid layer develops its thickness instantaneously in response to the input sliding velocity and the slower asperity dynamics control the evolution to the steady sliding friction force associated with the sliding velocity. Hence, the "saturated" friction will change with the sliding velocity, which is formulated by the Stribeck curve. The displacement ratio may vary between $(v_v\sigma_0)/(\omega F_{ba})$ to $(v_v\sigma_0)/(\omega F_c)$, depending on the sliding velocity (refer to Eq. (3.3)). The lowest one of the two ratios can be used as a rough indication of the influence of the tangential compliance on the friction ratio. The lowest displacement ratios of the curves in Fig. 3.11 are 0.3 for $\sigma_0 = 5\times10^5$, 3.4 for $\sigma_0 = 5\times10^6$ and ∞ for $\sigma_0 = \infty$. A small displacement ratio represents that the friction response is not fast enough to approach the "saturated" friction, as shown in Fig. 3.12 where the curve of $\sigma_0 = 5\times10^5$ is always lower than the curve of $\sigma_0 = \infty$ (representing the saturated friction). If the Stribeck effect is not effective ($r_{sf} = F_{ba}/F_c$ or $r_{sv} = v_v/v_s$ is small), it is reasonable to take $(v_v\sigma_0)/(\omega F_c)$ as the indication.

For $\zeta > 1$, the friction ratio with the Stribeck effect can be larger than 1, which represents that the time-averaged friction is larger than the steady friction without vibrations, as shown in Fig. 3.13. When $\zeta > 1$, the relative sliding velocity only changes its magnitude but not direction, so does the instantaneous friction. As the sliding velocity decreases in its magnitude, the instantaneous friction increases due to the Stribeck effect. Thus, if the steady velocity v_b is large enough to produce a small steady friction, the friction ratio can be larger than 1. However, as the steady velocity v_b increases, the influence of the Stribeck effect on the instantaneous friction decreases. Then the friction ratio approaches 1 (refer to Fig. 3.11). It is worthy to mention that the instantaneous friction lags behind the sliding velocity during dynamic sliding speed variations. As was previously stated, the LuGre model captures the friction lag phenomenon by the elastic term. The friction lag decreases as the contact stiffness σ_0 increases. Note that the damping term and the viscous term are not included here. If these two terms are included, the maximum of instantaneous friction depends on the summation of the three terms in the LuGre model as shown in Fig. 3.5.

The friction ratios for varied breakaway force F_{ba} and for varied Stribeck velocity v_s are plotted in Fig. 3.14 and Fig. 3.15. The influence of the Stribeck parameters on the friction ratio is similar to that with the rigid body assumption. The major difference between the two cases is that the tangential compliance smoothes the curves around $\zeta = 1$.

The viscous friction, which is normally not sufficiently large to have obvious influence on the friction ratio, was not included in the above calculations. If it is included, the friction reduction effect will be degraded (refer to Eq. (3.12)). For example, let $\sigma_2 = 0.5$, the calculated friction ratios are plotted in Fig. 3.16. When the friction ratio without the viscous friction is lower than 1, the increase of the viscous friction increases the friction ratio, degrading the friction reduction effect. When the friction ratio without the viscous friction is larger than 1, which is due to the Stribeck effect, the increase of the viscous friction reduces the friction ratio. The instantaneous friction force with the viscous friction at $\zeta = 0.5$ is plotted in Fig. 3.17. Note the influence of the viscous friction on the maximum of instantaneous friction.

The damping term of the LuGre model was not included in the above calculations because it doesn't have influence on the friction ratio (Eq. (3.7)). However, if it is included, it has influence on the instantaneous friction force. It is worth pointing out that the elastic damping combined with the Stribeck effect can cause some non-physical conditions. One of them is the "Stribeck slingshot effect" (Dupont *et al.*, 2000,2002). The Stribeck curve indicates that the steady-state friction force is a decreasing function of velocity magnitude. As the sliding velocity increases, the elastic deflection of the asperities must decrease to produce the smaller steady-state friction force. The inequality

$$\operatorname{sgn}(v) \neq \operatorname{sgn}(\dot{z}), \tag{3.22}$$

will hold during the elastic relaxation. The elastic damping can reverse the direction of the friction force during relaxation, rendering the model non-dissipative, as shown in Fig. 3.18. This is a non-physical modeling artifact because the modeled friction force actually accelerates the mass forward. This effect can be avoided by proper choice of model parameters (Barabanov and Ortega, 2000).

3.5 Influence of the Normal Force on the Stribeck Curve

In order to include the normal force in the LuGre model, the author of the LuGre model suggested this form (Canudas de Wit, C and Tsiotras, 1999):

$$\tilde{F} = N\left(\sigma_0 z + \sigma_1 \frac{dz}{dt} + \sigma_2 v\right), \tag{3.23}$$

$$\frac{dz}{dt} = v\left(1 - \frac{\sigma_0}{\mu_{ss}(v)}\operatorname{sgn}(v) z\right), \tag{3.24}$$

and $\mu_{ss}(v) = \mu_c + (\mu_{ba} - \mu_c)e^{-|v/v_s|^\alpha}$, (3.25)

where N is the normal force, $\mu_{ss}(v)$ the normalized friction force, μ_c the normalized Coulomb friction, and μ_{ba} the normalized static friction. This form was also used by Dupont *et al.* (1997). This form implies that the normalized Stribeck curve, Eq. (3.25), is independent of the normal force. However, the experimental results presented by Hess and Soom showed that the normalized Stribeck curve influenced by not only the normal force but also the viscosity of the lubricant, as shown in Fig. 3.19 for different normal loads. A better-normalized Stribeck curve is given by an equation of the form:

$$\mu_{ss}(v) = \mu_c + (\mu_{ba} - \mu_c)e^{-\left|C_v \frac{\eta v}{N}\right|^\alpha}, \tag{3.26}$$

where η is the viscosity, W the normal force, and C_v the empirical parameter. Replacing

Eq. (3.25) with this equation, a simulation of different normal loads is plotted in Fig. 3.20, which shows the same tendency as the experimental data in Fig. 3.19. Comparing Eq. (3.25) with Eq. (3.26), it implies that the Stribeck velocity v_s depends on the viscosity and the normal force.

3.6 Identification of the Model Parameters

The parameters of the LuGre model can be identified by the use of model properties, as shown in Fig. 3.21 and Fig. 3.22. The parameters, F_{ba} and σ_0, can be obtained by the experiments that produce the Dahl curve. The parameters, F_c, σ_2 and v_s, can be obtained by the experiments that produce the Stribeck curve. The damping coefficient σ_1 can be obtained by identifying the system dynamics within small displacements (stiction regime). Considering a mass m in contact with a fixed horizontal surface, the equation of motion is

$$m\frac{d^2x}{dt^2} = -F = -\sigma_0 z - \sigma_1\frac{dz}{dt} - \sigma_2\frac{dx}{dt}. \tag{3.27}$$

The stiction condition is analogous to the existence of an elastic region on the stress-strain curve of a material, where the displacement is very small and the deflection of the asperity is equal to the displacement of the mass. Thus,

$$\frac{dz}{dt} = \frac{dx}{dt}. \tag{3.28}$$

Inserting Eq. (3.28) into Eq. (3.27) gives

$$m\frac{d^2x}{dt^2} + (\sigma_1 + \sigma_2)\frac{dx}{dt} + \sigma_0 x = 0. \tag{3.29}$$

This shows that the contact with small displacements behaves like a damped second-order system.

3.7 Concluding Remarks

A theoretical approach based on the LuGre friction model is presented that describes the friction reduction observed in the lubricated contacts with the parallel vibrations. It is showed that the linear damping of the asperities has no effect on the friction reduction, and the linear viscosity of the contacts, whose time-averaged value is not affected by the vibrations, degrades the effect of friction reduction by vibrations. The tangential compliance of the contacts also reduces the effect of friction reduction by vibrations, and its influence on the friction reduction can be represented roughly by the displacement ratio of the displacement amplitude of the vibration to the steady state deflection of the asperities.

The influence of Stribeck effect on the friction reduction effect is presented. Comparing with the sliding without Stribeck effect, the presence of the Stribeck effect leads to a lower friction ratio for a small velocity ratio (about 0~1) and a larger friction ratio for a larger velocity ratio. The tangential compliance reduces the Stribeck effect on the friction reduction.

An approach to include the normal force in the LuGre model is proposed, which shows a better agreement with the experimental results in the literatures.

Table 3.1 Friction ratio with the Stribeck effect for varied parameters. (The basic set of parameters for these curves are $(r_{sf}, r_{sv}, \alpha) = (1.8, 2, 2)$; gray line for $r_{sf} = 1$; short dashed line for $r_{sf} = 1.2$; solid line for $r_{sf} = 1.8$; long dashed line for $r_{sf} = 2.4$)

r_{sv} \ α	1	2	4
0.5	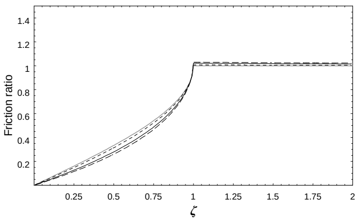	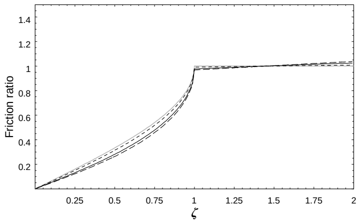	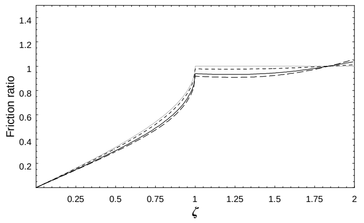
1	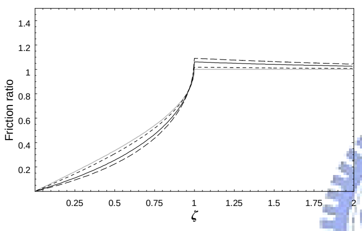	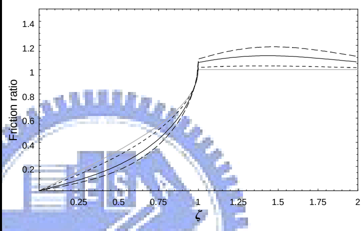	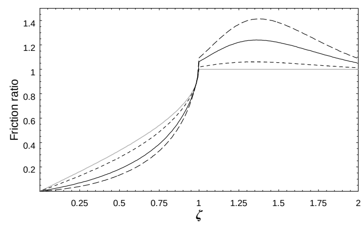
2	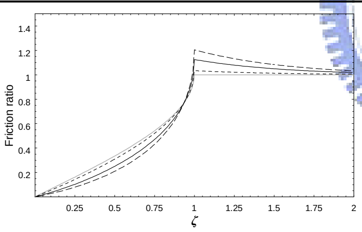	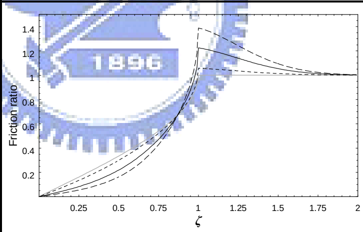	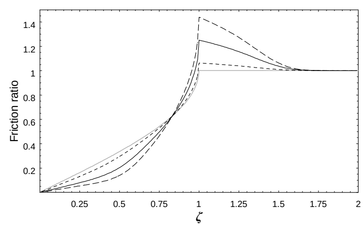
4	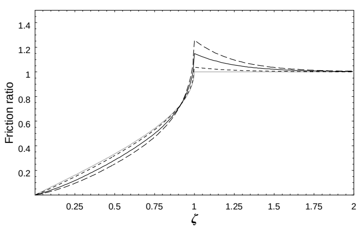	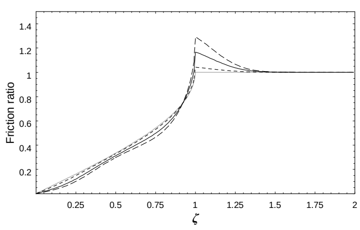	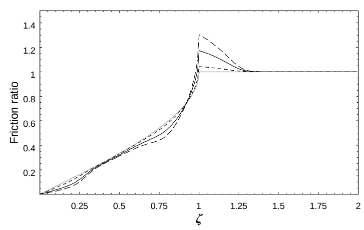

Table 3.2 Basic set of parameters used in the simulation

Parameter	*Value*	*Unit*
σ_0	5000000	N/m
σ_1	0	Ns/m
σ_2	0	Ns/m
F_c	1	N
F_{ba}	1.8	N
v_s	0.1	m/s
α	2	
v_v	0.26	m/s
ω	120000π	rad/s

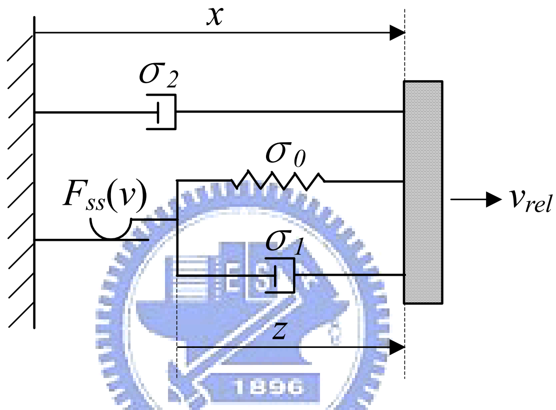

Fig. 3.1 Analogy of the LuGre model

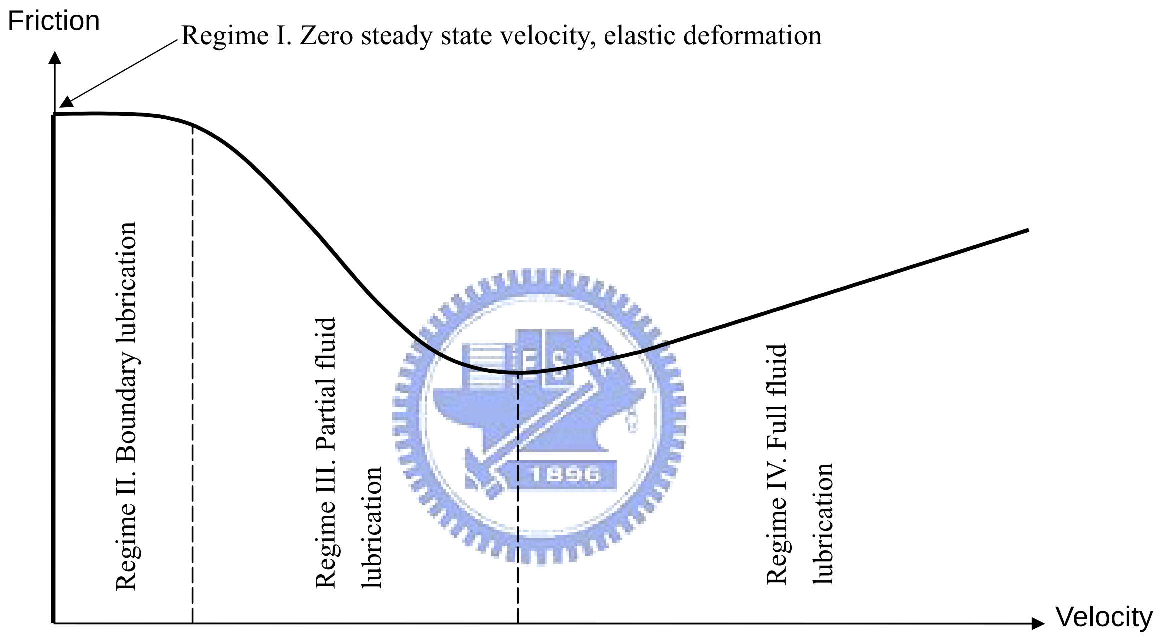

Fig. 3.2 The generalized Stribeck curve, showing friction as a function of velocity for low velocities

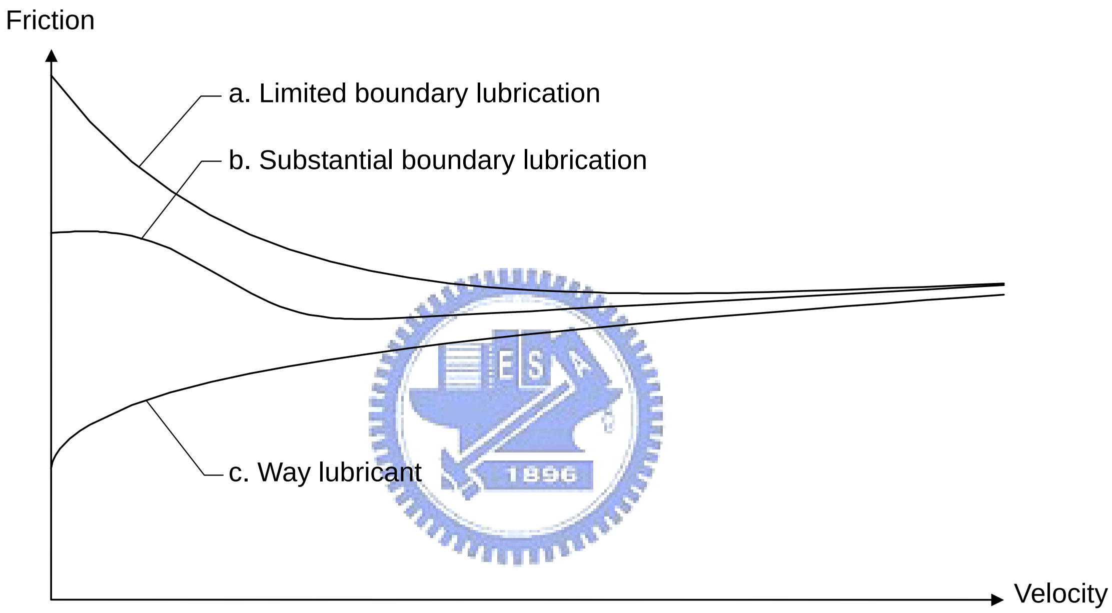

Fig. 3.3 Friction as a function of steady state velocity for various lubricants; the Stribeck curve

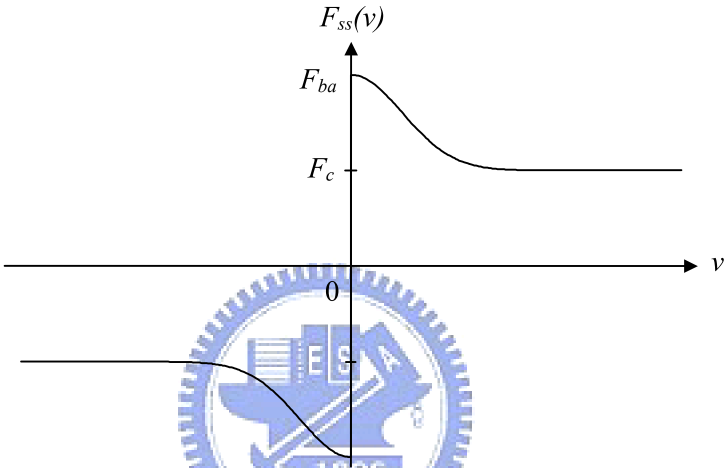

Fig. 3.4 Stribeck curve of steady-state friction force versus sliding velocity v

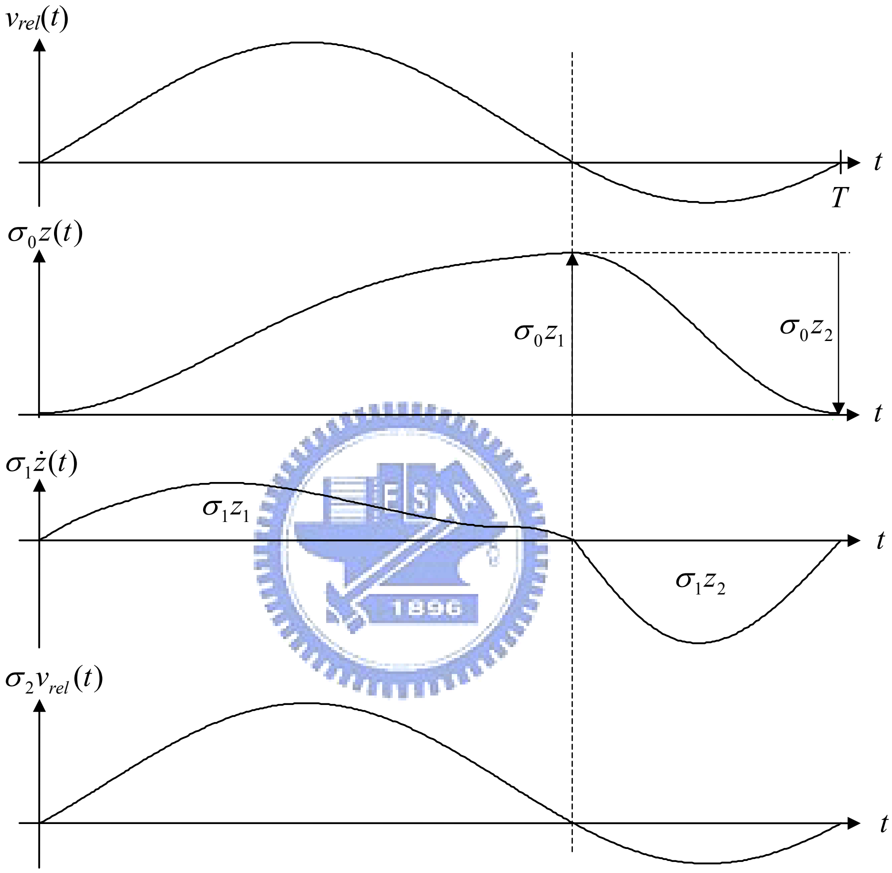

Fig. 3.5 Friction components of LuGre model over one steady state period

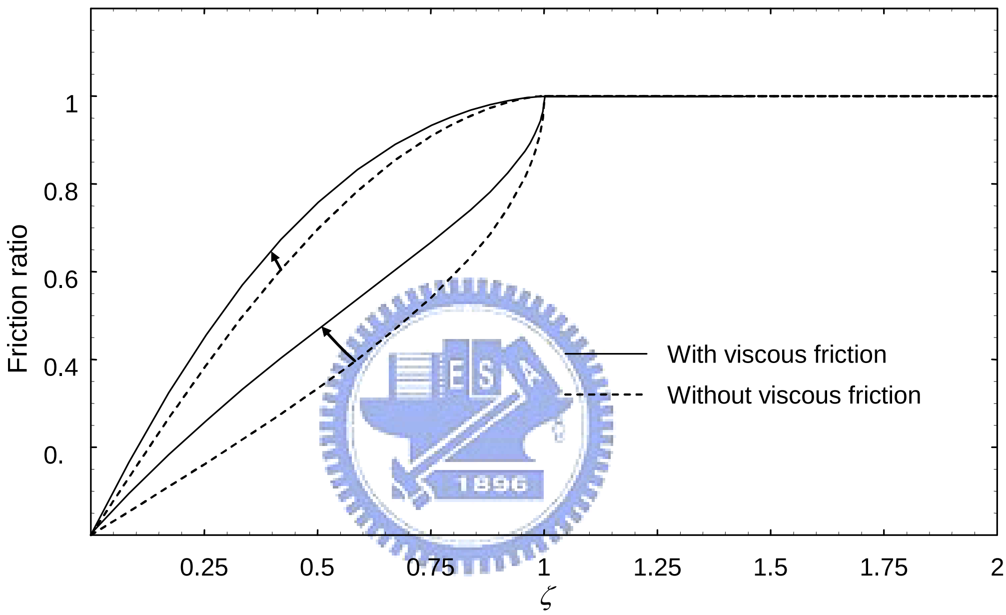

Fig. 3.6 Friction ratios based on Dahl's model with viscous friction

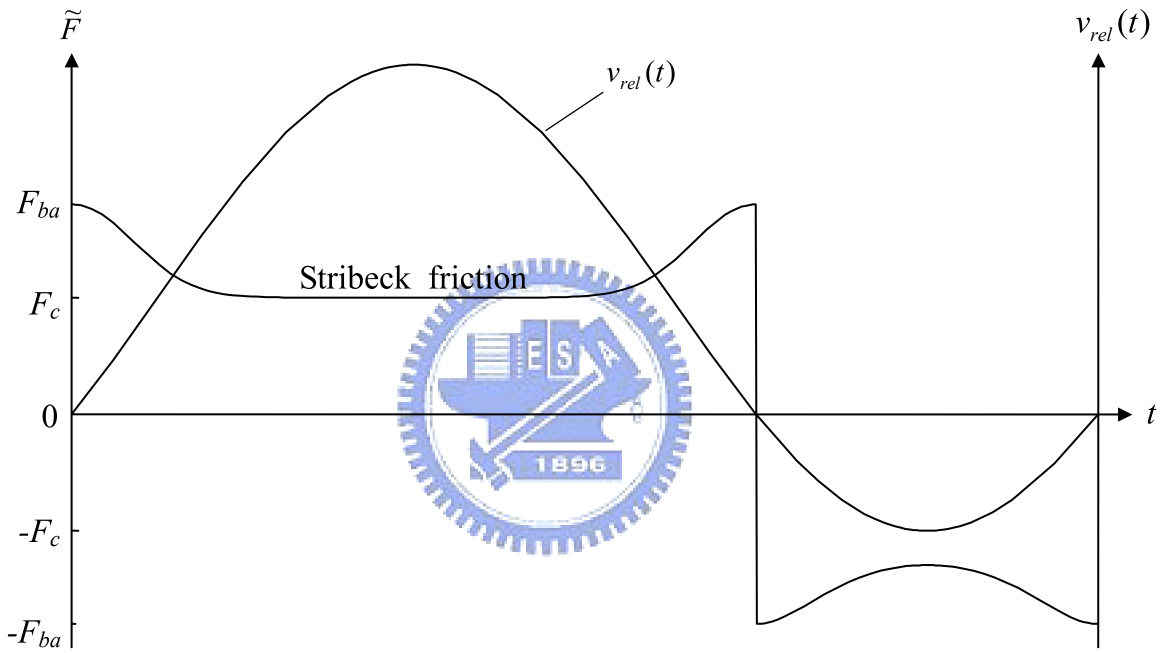

Fig. 3.7 Instantaneous friction force and relative sliding velocity over one period

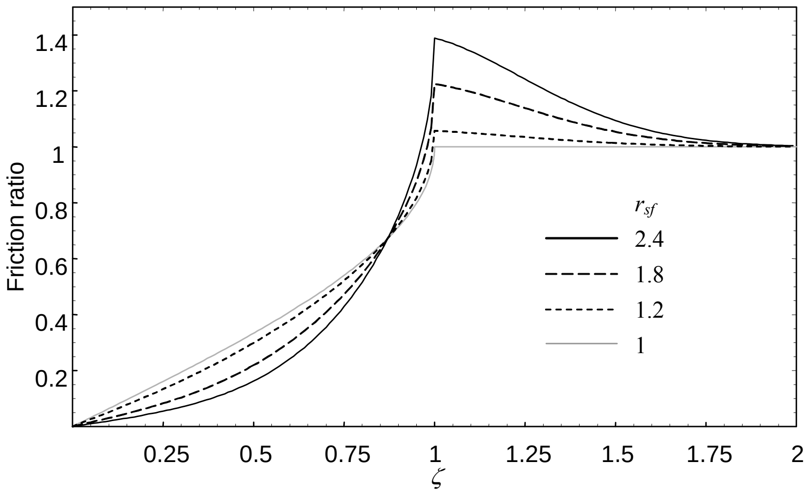

(a) Varied r_{sf}

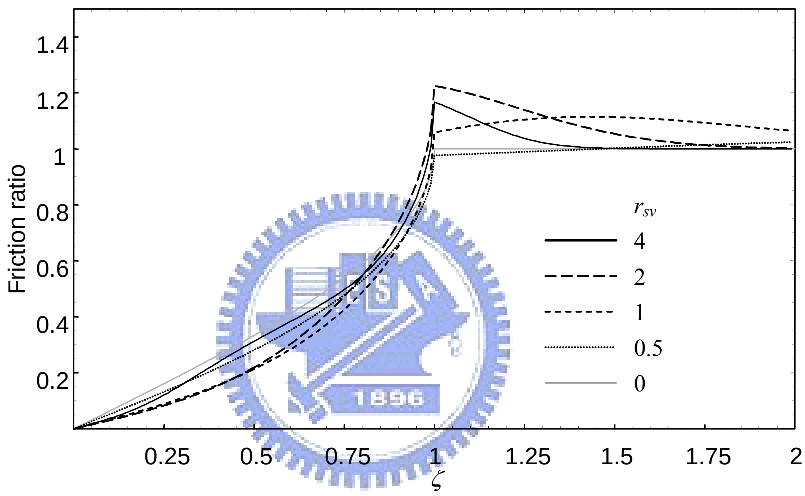

(b) Varied r_{sv}

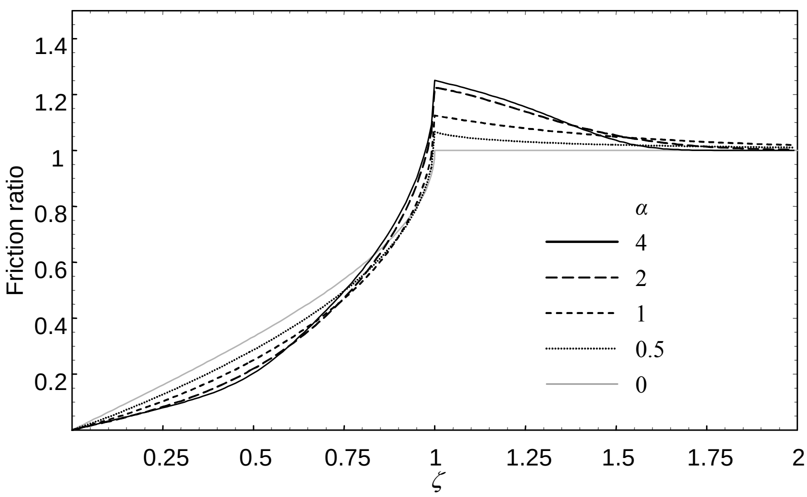

(c) Varied α

Fig. 3.8 Friction ratios with the stribeck effect

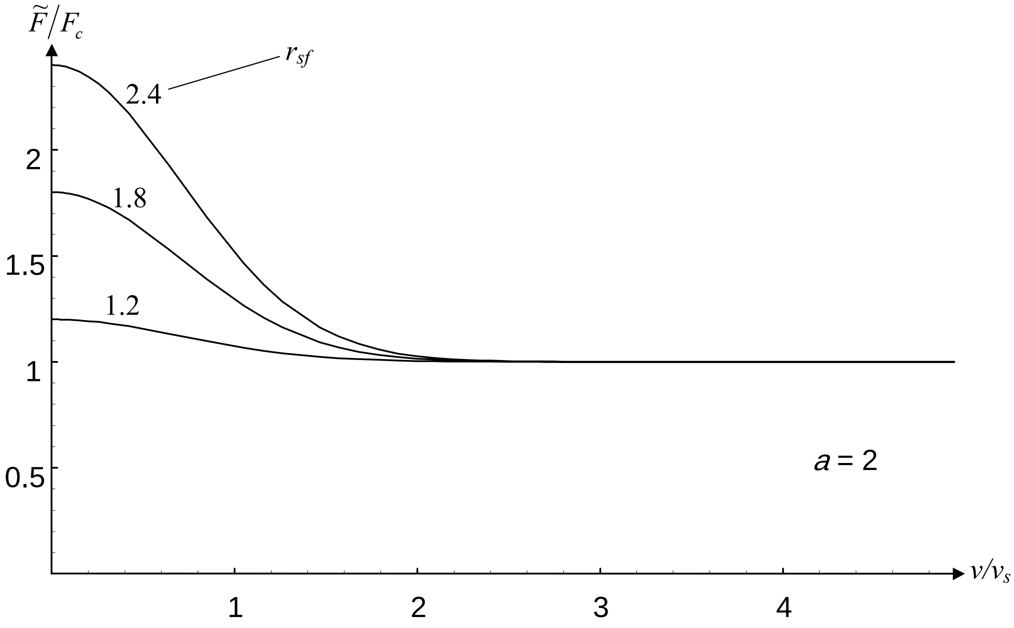

(a) Varied r_{sf}

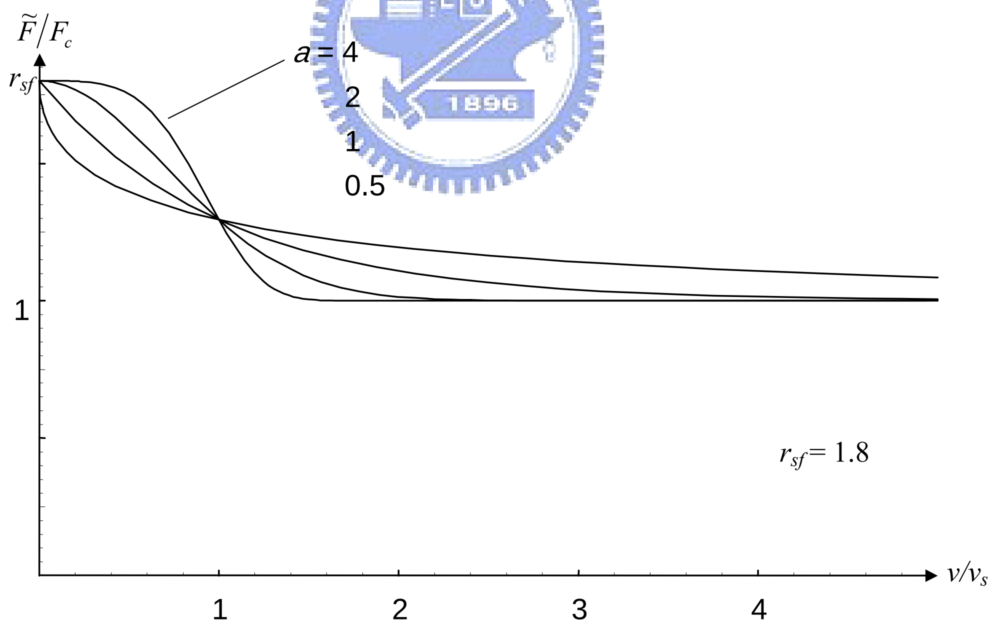

(b) Varied α

Fig. 3.9 Normalized Stribeck curves

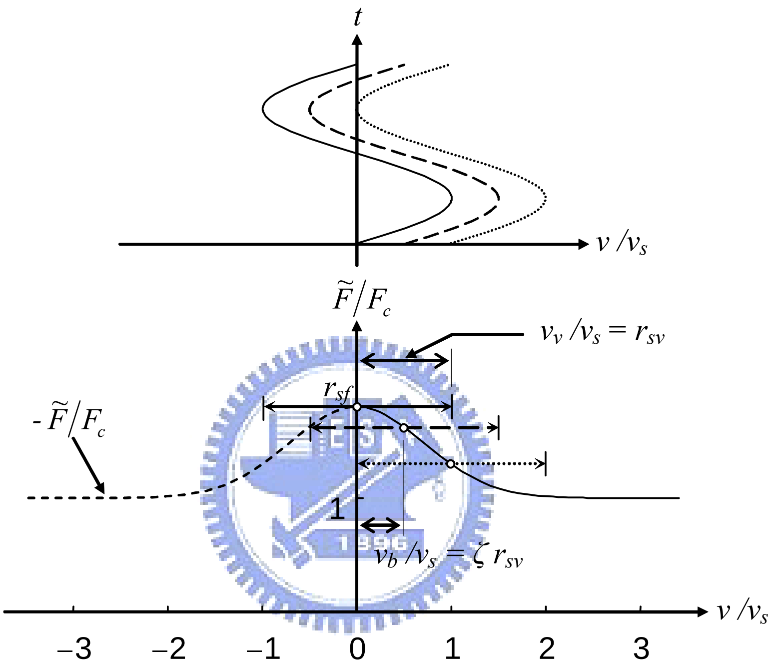

Fig. 3.10 Stribeck friction under vibrations

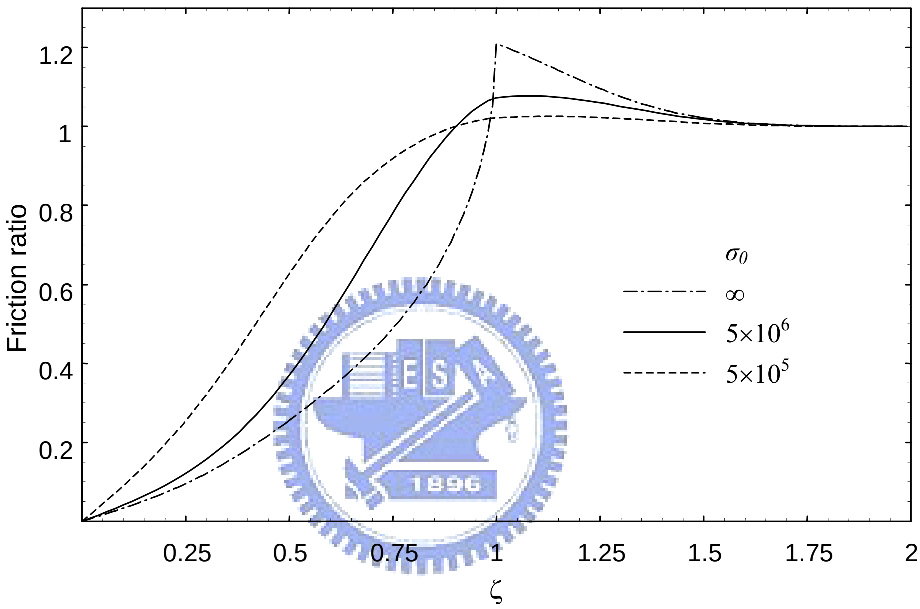

Fig. 3.11 Friction ratios with the stribeck effect for varied contact stiffness σ_0

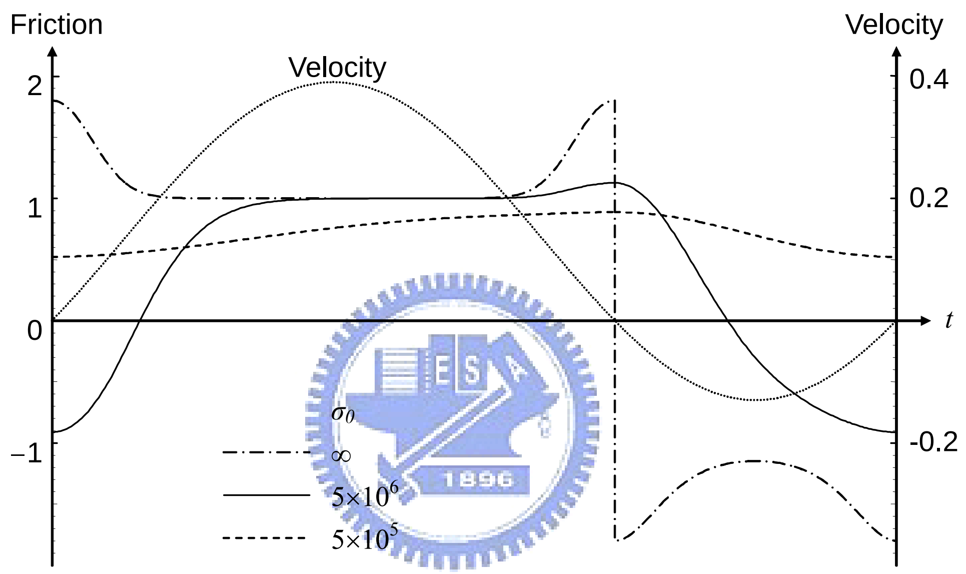

Fig. 3.12 Instantaneous friction force for varied stiffness σ_0 and relative sliding velocity over one period, $\zeta = 0.5$

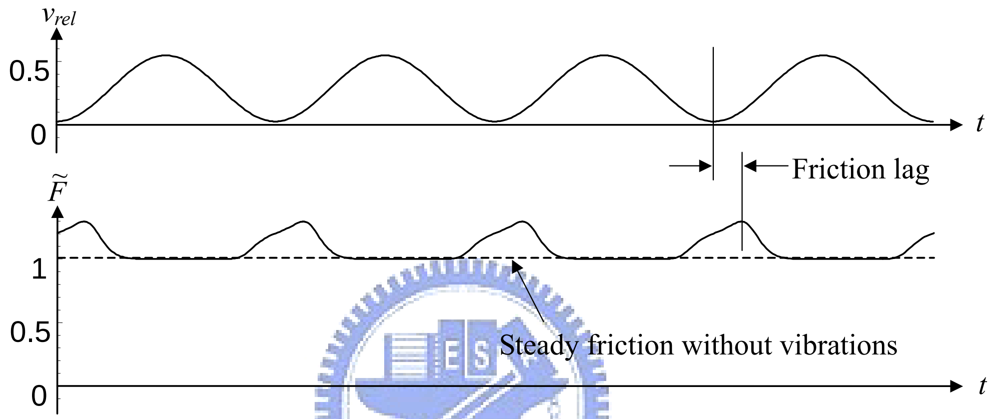

Fig. 3.13 Instantaneous friction force and relative sliding velocity for $\zeta = 1.1$

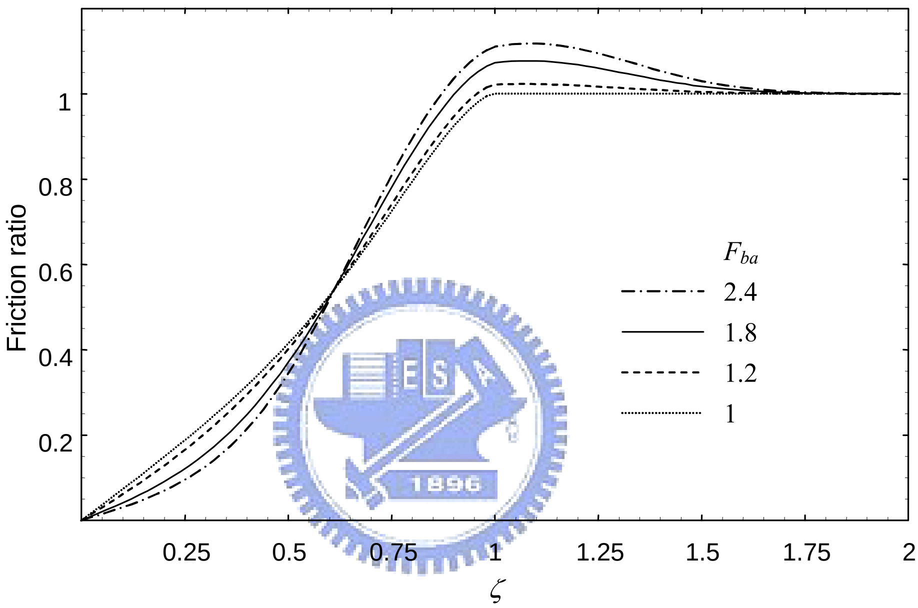

Fig. 3.14 Friction ratios with the stribeck effect for varied breakaway force F_{ba}

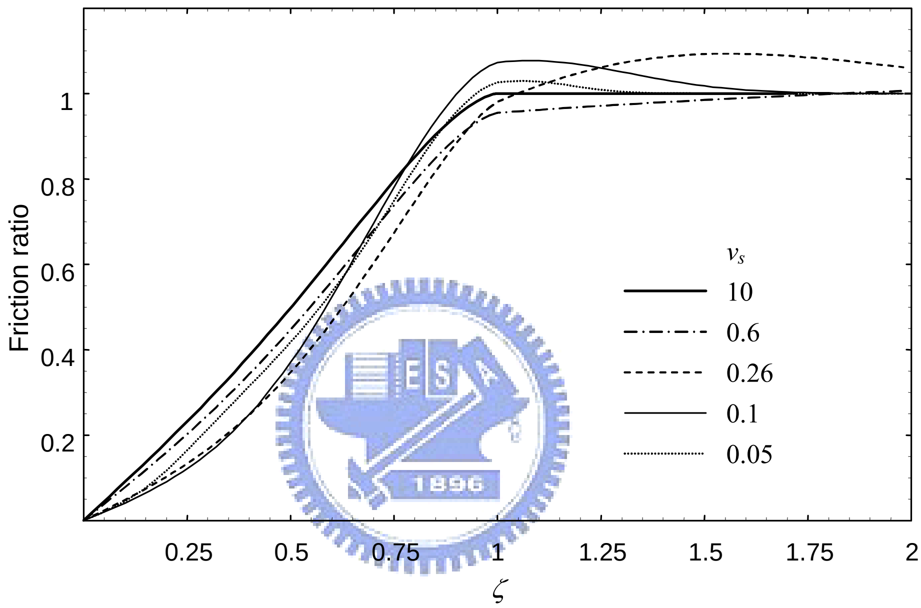

Fig. 3.15 Friction ratios with the stribeck effect for varied Stribeck velocity v_s

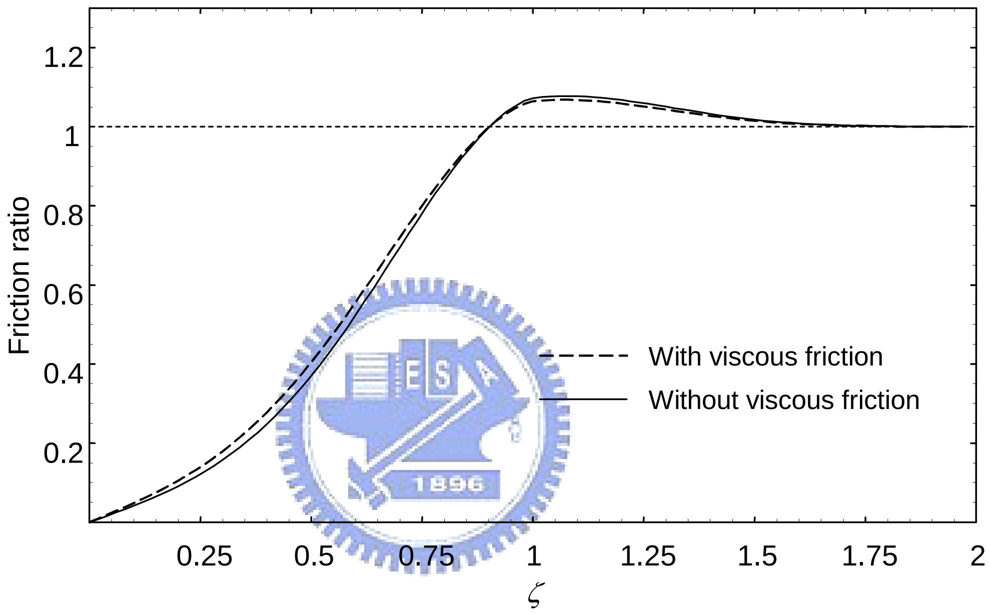

Fig. 3.16 Friction ratios with the Stribeck effect and the viscous friction under $\sigma_2 = 0.5$

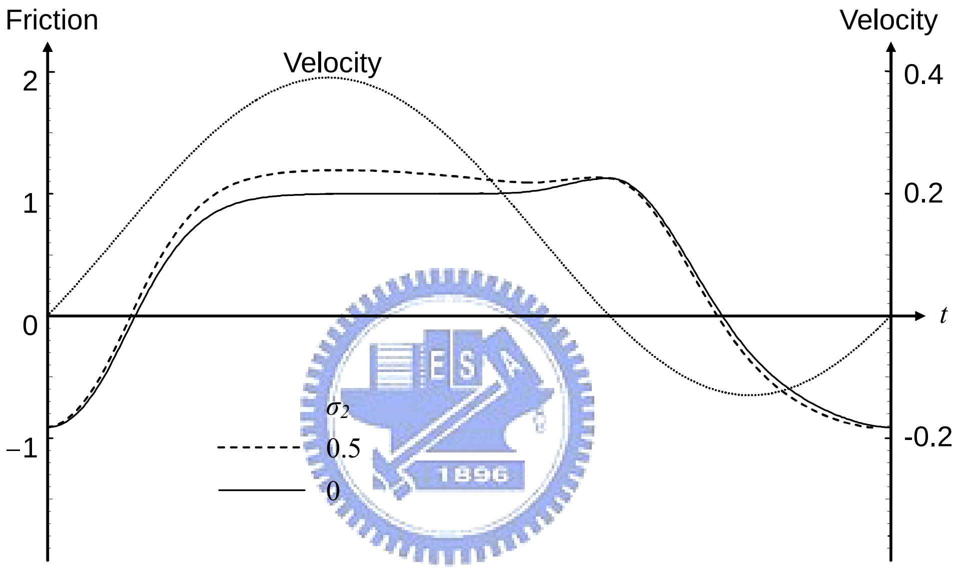

Fig. 3.17 Instantaneous friction force for varied viscous friction parameter σ_2 at $\zeta = 0.5$

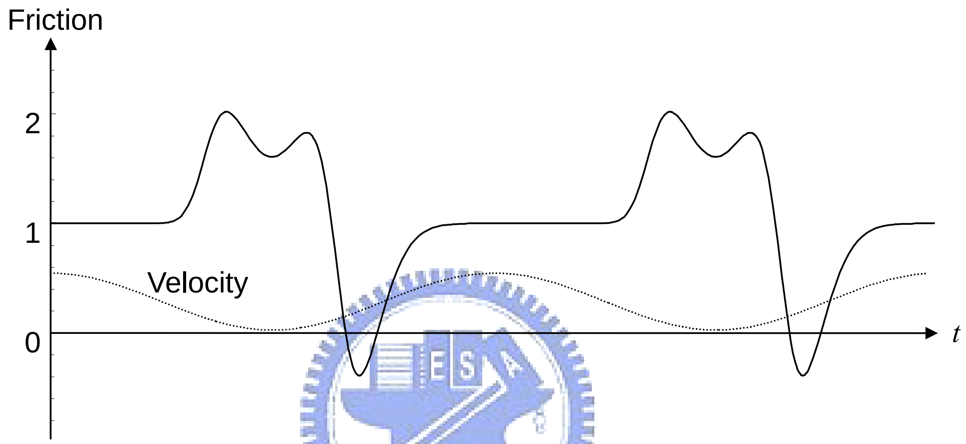

Fig. 3.18 Friction reversal arising with elastic damping and Stribeck friction for $\sigma_1 = 200$ at $\zeta = 1.1$

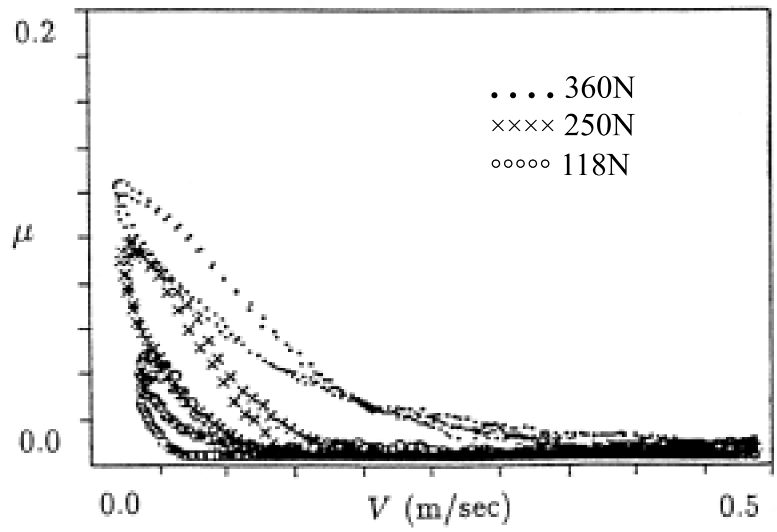

Fig. 3.19 Friction-velocity data for different normal loads (Hess and Soom, 1990)

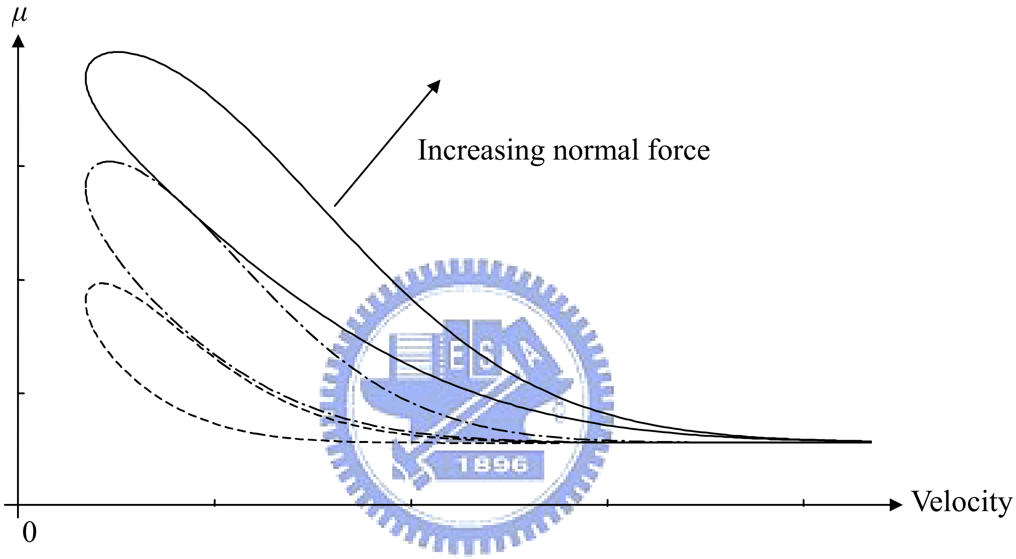

Fig. 3.20 Simulation of different normal loads

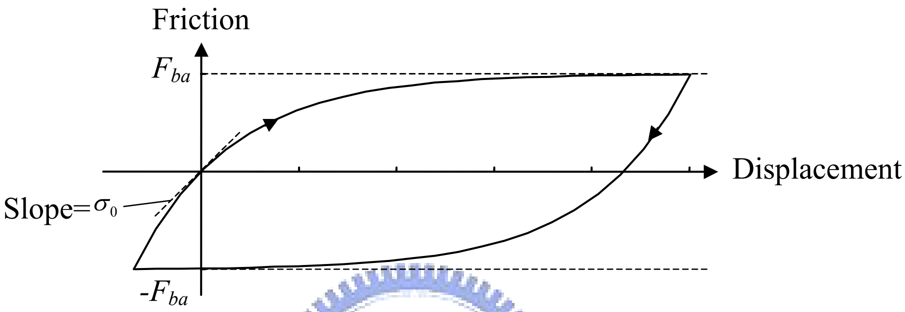

Fig. 3.21 Dahl curve

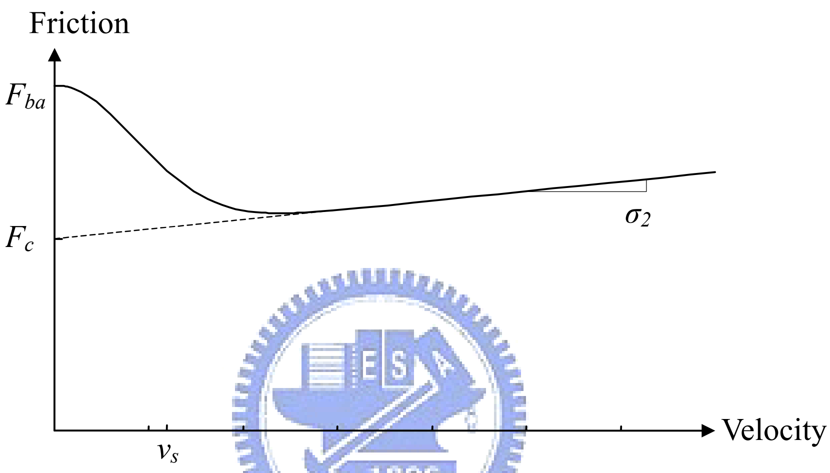

Fig. 3.22 Stribeck curve

CHAPTER 4 FRICTION REDUCTION BY TANGENTIAL VIBRATIONS

4.1 Introduction

The angle of the tangential vibrations with the direction of the macroscopic velocity is influential to the friction reduction. The friction reduction by the parallel vibrations has been presented in Chapter 2 and 3. In this chapter, the friction reduction by tangential vibrations at any angle, particularly perpendicular vibrations, is investigated.

4.2 Sliding of Rigid Body

The friction system under investigation comprises a rigid body sliding over a rigid and flat plane at a prescribed velocity under constant normal force, as shown in Fig. 4.1. The prescribed velocity consists of two components. The first component is a macroscopic constant velocity v_b, and the second is a harmonic velocity $(v_v \cos \omega t)$ representing the vibration.

Let θ denote the angle of the harmonic velocity $(v_v \cos \omega t)$ with the constant velocity v_b that is parallel with the x-axis. The velocity of the rigid body can be expressed as the vector

$$\vec{v} = (v_b + v_v \cos(\omega t) \cos\theta)\vec{i} + v_v \cos(\omega t) \sin\theta \, \vec{j} \, . \tag{4.1}$$

Since the Coulomb friction works on the body in the opposite direction to the relative sliding velocity, the instantaneous Coulomb friction becomes

$$\vec{F} = -\mu N \frac{\vec{v}}{|\vec{v}|} = \widetilde{F}_x \vec{i} + \widetilde{F}_y \vec{j} \, , \tag{4.2}$$

where N represents the normal force, as shown in Fig. 4.2. The components of the friction are given by

$$\tilde{F}_x(\tau) = \frac{-\zeta - \cos\theta\cos\tau}{\sqrt{\zeta^2 + 2\zeta\cos\theta\cos\tau + \cos^2\tau}}\mu N , \tag{4.3}$$

and $$\tilde{F}_y(\tau) = \frac{-\sin\theta\cos\tau}{\sqrt{\zeta^2 + 2\zeta\cos\theta\cos\tau + \cos^2\tau}}\mu N , \tag{4.4}$$

where τ is the normalized time defined as

$$\tau = \omega t , \tag{4.5}$$

and ζ denotes the velocity ratio which is defined in Section 2.1.

The mechanism of friction reduction by tangential vibrations is illustrated in Fig. 4.3. The velocity of the sliding body frequently changes its direction in accordance with the vibration component, and the direction of Coulomb friction also changes. Because the amplitude of instantaneous Coulomb friction remains constant, the friction force in the direction of v_b reduces on time-average. It is important to recognize that the superposed vibrations reduce the time-average friction force, not the real (instantaneous) friction.

The effective friction force that is observed macroscopically is the time-averaged friction force. The time-averaged friction force in the directions of x (*i.e.* the direction of the macroscopic velocity v_b) and y are defined as

$$\overline{F}_x = \frac{1}{2\pi}\int_0^{2\pi} \tilde{F}_x(\tau)d\tau , \tag{4.6}$$

and $$\overline{F}_y = \frac{1}{2\pi}\int_0^{2\pi} \tilde{F}_y(\tau)d\tau . \tag{4.7}$$

The effect of friction reduction by superposed vibrations can be described quantitatively by the ratio of the time-averaged friction force $\overline{F}$ to the friction force $F = -\mu N$ observed in the absence of vibrations. The friction ratio in the directions of x and y become

$$r_x(\zeta,\theta)=\frac{1}{2\pi}\int_0^{2\pi}\frac{\zeta+\cos\theta\cos\tau}{\sqrt{\zeta^2+2\zeta\cos\theta\cos\tau+\cos^2\tau}}d\tau\,, \tag{4.8}$$

and $$r_y(\zeta,\theta)=\frac{1}{2\pi}\int_0^{2\pi}\frac{\sin\theta\cos\tau}{\sqrt{\zeta^2+2\zeta\cos\theta\cos\tau+\cos^2\tau}}d\tau\,. \tag{4.9}$$

The friction ratio in the direction of x (the direction of the macroscopic constant velocity v_b) is of most interest. It can be calculated explicitly if $\theta=0$ and $\theta=\pi/2$ respectively as follows:

$$r_x(\zeta,0)=\begin{cases}\dfrac{2}{\pi}\sin^{-1}\zeta & 0\le\zeta\le1\\ 1 & \zeta>1\end{cases}, \tag{4.10}$$

and $$r_x(\zeta,\frac{\pi}{2})=\frac{2}{\pi}\frac{\zeta}{\sqrt{1+\zeta^2}}K(\frac{1}{1+\zeta^2}), \tag{4.11}$$

where $K(m)$ is the complete elliptic integral of the first kind. The friction ratio r_x for different angles is plotted in Fig. 4.4. The friction ratio decreases with decreasing velocity ratio ζ. A significant friction reduction effect is observed whenever the macroscopic velocity is smaller than the velocity amplitude of the vibration component. For velocity ratio $\zeta<0.95$, the vibration parallel to the direction of the macroscopic velocity ($\theta=0$) exerts the greatest effect on the friction reduction. For velocity ratio $\zeta>1$, the vibration perpendicular to the direction of the macroscopic velocity ($\theta=\pi/2$) has a larger effect on the friction reduction, but the amount of the friction reduction is limited.

4.3 Sliding with Tangential Compliance

Surfaces are very irregular at the microscopic level. Therefore two surfaces contact at a number of asperities. When a tangential force is applied, the asperities will deflect like springs giving rise to the friction force. If the force is sufficiently large, some of the asperities deflect so much that they will slip. The average behavior of the asperities can be represented by the physical analogy depicted in Fig. 4.5. Here, the sliding body experiences a friction force due to the deformation of a single lumped asperity contact.

The deflection z of the lumped asperity is defined as the horizontal distance between points P and T. The deflection z can be modeled by the extension of Dahl model. The Dahl model has the general form

$$\frac{dF}{dx} = \sigma_0 \left(1 - \frac{F}{F_c}\operatorname{sgn}(v)\right)^i , \tag{4.12}$$

where F denotes the friction force, x represents the displacement of the sliding body, σ_0 is the stiffness of the asperity, F_c denotes the Coulomb friction force and i represents a parameter that determines the shape of the friction-displacement curve. The value $i = 1$ is most commonly used. Higher values will gives a friction-displacement curve with a sharper bend, as shown in Fig. 4.6. Notably, in this model the friction force is only a function of the displacement and the sign of the velocity. This so-called rate independence is an important property of the model.

To introduce the deflection z into the model, the friction force is defined as

$$\widetilde{F} = \sigma_0 z , \tag{4.13}$$

then the model can be written as

$$\frac{dz}{dt} = v\left(1 - \frac{\sigma_0}{F_c}\operatorname{sgn}(v) z\right)^i , \tag{4.14}$$

Equation (4.14) claims that during the unidirectional sliding the deflection z approaches the magnitude

$$z_{ss} = \frac{F_c}{\sigma_0}, \tag{4.15}$$

which is the steady state deflection of the asperity. Thus Eq. (4.14) can be written as

$$\frac{dz}{dt} = v\left(1 - \frac{z}{z_{ss}}\text{sgn}(v)\right)^i. \tag{4.16}$$

The hypothesis of Dahl model, including most friction models, is that the friction force is parallel to the velocity of the sliding body. Some difficulties arise in modeling the behavior of the asperity in the friction system shown in Fig. 4.1, where the instantaneous friction force may not be parallel to the velocity of the sliding body. In this friction system, the velocity of the sliding body frequently changes direction in accordance with the vibrations. The vibration direction must be parallel to the direction of the macroscopic velocity (*i.e.* $\theta = 0$) for the instantaneous friction force to parallel to the velocity of the sliding body, and the Dahl model can be applied without difficulty. However, the behavior of the lumped asperity becomes more complicated when the direction of vibrations is not parallel to the direction of the macroscopic velocity (*i.e.* $\theta \neq 0$).

Figure. Fig. 4.7 shows the behavior of the lumped asperity when the sliding body moves along a curve. This figure is the top view of Fig. 4.5 and only the points P and T are shown. The trajectory of point P of the sliding body is known and the trace of the point T of the asperity needs to be determined to calculate the friction force. The trace of the point T can be approximated by the following procedure. At time t, point P of the sliding body is in position $P(t)$ and point T of the asperity is in position $T(t)$. At time $(t+\Delta t)$, point P moves to the position $P(t+\Delta t)$. If the time increment Δt is small, the asperity is pulled approximately along line $\overline{T(t)P(t+\Delta t)}$ to a new position $T(t+\Delta t)$. The length of line $\overline{T(t+\Delta t)P(t+\Delta t)}$, namely the new deflection of the asperity, depends on the friction force and the elasticity of the asperity, which are discussed below. Following this scheme and using a small time change Δt can obtain the trace of the point T, as shown in Fig. 4.8.

4.3.1 Asperity Slip without a Stiction Phase (Dahl Model with $i=1$)

Referring to Dahl model to Eq. (4.14), the deflection change after a small time increase Δt can be expressed as

$$\Delta z \approx v(t)\left(1-\frac{\sigma_0}{F_c}\operatorname{sgn}(v(t))z(t)\right)\Delta t\,, \tag{4.17}$$

where the value $i=1$ is used. Obviously Δz approaches zero as the deflection $z(t)$ approaches the steady state deflection $(z_{ss}=\sigma_0/F_c)$. The deflection of the asperity at time t is given by

$$z(t)=\overline{T(t)P(t)}=\sqrt{(P_x(t)-T_x(t))^2+(P_y(t)-T_y(t))^2}\,, \tag{4.18}$$

where $P(t)=(P_x(t),P_y(t))$ and $T(t)=(T_x(t),T_y(t))$. The velocity $v(t)$ in Eq. (4.17) can be approximated by the mean velocity of the point P along line $\overline{T(t)P(t+\Delta t)}$, *i.e.*

$$\begin{aligned} v(t) &\approx \frac{\overline{T(t)P(t+\Delta t)}-\overline{T(t)P(t)}}{\Delta t} \\ &= \frac{\sqrt{(P_x(t+\Delta t)-T_x(t))^2+(P_y(t+\Delta t)-T_y(t))^2}-z(t)}{\Delta t} \end{aligned}. \tag{4.19}$$

According to Eq. (4.17), the deflection of the asperity at time $(t+\Delta t)$ is written as

$$z(t+\Delta t)=z(t)+\Delta z \approx z(t)+v(t)\left(1-\frac{\sigma_0}{F_c}\operatorname{sgn}(v(t))z(t)\right)\Delta t\,, \tag{4.20}$$

which can be obtained by inserting Eqs. (4.18) and (4.19). Once the new deflection of the asperity at time $(t+\Delta t)$ is obtained, the new position of point T, $T(t+\Delta t)$, is given by

$$T_x(t+\Delta t)=P_x(t+\Delta t)-\frac{z(t+\Delta t)}{\overline{T(t)P(t+\Delta t)}}(P_x(t+\Delta t)-T_x(t))\,, \tag{4.21}$$

and $T_y(t+\Delta t) = P_y(t+\Delta t) - \dfrac{z(t+\Delta t)}{T(t)P(t+\Delta t)}(P_y(t+\Delta t) - T_y(t))$. (4.22)

The friction force depends on the deflection and the direction of the asperity. The friction force at time (t+Δt) therefore can be expressed as (refer to Eq. (4.13))

$$\widetilde{F}_x(t+\Delta t) = \sigma_0(P_x(t+\Delta t) - T_x(t+\Delta t)), \tag{4.23}$$

and $\widetilde{F}_y(t+\Delta t) = \sigma_0(P_y(t+\Delta t) - T_y(t+\Delta t))$, (4.24)

which is the component form of the friction force. Following Eqs. (4.18)~(4.24), the friction force at time (t+2Δt) can be obtained. Continuing this process can obtain the friction force during sliding with tangential vibrations.

4.3.2 Asperity Slip with a Stiction Phase (Dahl Model with $i = 0$)

Equation (4.14) shows that in the Dahl model with $i \neq 0$ the asperity can slip (*i.e.* $dz \neq v(t)dt$) even when the deflection is very small. Thus, when an oscillatory applied force that is far smaller than the Coulomb friction F_c applies to the sliding body, the position of the sliding body drifts. To minimize the drift, Dupont *et al.* (2000, 2002) proposed an elasto-plastic friction model that possesses a stiction phase. The asperity sticks (*i.e.* $dz = v(t)dt$) when its deflection is smaller than a breakaway deflection. Consequently, it is reasonable to assume that the asperity as shown in Fig. 4.7 sticks when its deflection is smaller than the steady state deflection. Here, the value $i = 0$ is used in the Dahl model to render stiction. The Dahl model then reduces to

$$\frac{dz}{dt} = \begin{cases} v(t) & z < z_{ss} \\ 0 & z \geq z_{ss} \end{cases}, \tag{4.25}$$

and $\widetilde{F} = \sigma_0 z$, (4.26) which is essentially an elastic Coulomb friction model. The asperity is modeled as a linear spring. When an increasing tangential force is applied, the asperity does not slip until the force increases to the size of the Coulomb friction F_c. Before slippage, the deflection of the asperity equals the displacement of the sliding body. Thus, the deflection of the asperity at time (t+ Δt) in Fig. 4.7 can be written as

$$z(t+\Delta t)=\begin{cases}\overline{T(t)P(t+\Delta t)} & \text{if} \quad \overline{T(t)P(t+\Delta t)}<z_{ss} \\ z_{ss} & \text{if} \quad \overline{T(t)P(t+\Delta t)}\geq z_{ss}\ .\end{cases} \tag{4.27}$$

Replacing Eq. (4.20) with Eq. (4.27) and following Eqs. (4.18)~(4.24) can yield the friction force during sliding with tangential vibrations.

4.4 Friction Ratio

In the friction system shown in Fig. 4.1, the trajectory of point P of the sliding body is given by

$$P_x(t)=\zeta v_v t+\frac{v_v}{\omega}\sin(\omega t)\cos\theta\,, \tag{4.28}$$

and $$P_y(t)=\frac{v_v}{\omega}\sin(\omega t)\sin\theta\,. \tag{4.29}$$

In steady state, the time-averaged friction force in the directions of x and y are defined as

$$\overline{F}_x=\frac{\omega}{2\pi}\sum_{k=1}^{n}F_x(t+k\Delta t)\Delta t\,, \tag{4.30}$$

and $$\overline{F}_y=\frac{\omega}{2\pi}\sum_{k=1}^{n}F_y(t+k\Delta t)\Delta t\,, \tag{4.31}$$

where

$$n=\frac{2\pi}{\omega\Delta t}\,. \tag{4.32}$$

The effect of friction reduction by superposed vibrations can be described quantitatively by the friction ratio in the direction of x, *i.e*. the direction of the macroscopic velocity, which is given by

$$r_x = \frac{\overline{F}_x}{F_c} = \frac{\omega}{2\pi F_c}\sum_{k=1}^{n} F_x(t + k\Delta t)\Delta t \,. \tag{4.33}$$

As stated, in the Dahl model the friction force is only a function of the displacement and the sign of the velocity. In other words, the friction force depends on the trajectory of point P, which depends on $(\zeta, \theta, v/\omega)$. For the value $i=1$ or $i=0$, this property leads to the relation in which the time-averaged friction force is a function of the displacement ratio

$$r_{disp} = \frac{v_v \sigma_0}{\omega F_c} = \frac{v_v/\omega}{F_c/\sigma_0} = \frac{x_v}{z_{ss}} \,, \tag{4.34}$$

which is a ratio of the displacement amplitude of the vibration component to the steady state deflection of the asperity. The displacement ratio can be seen as an index of the influence of the tangential compliance on the friction reduction.

Equations (4.18)~(4.24) can yield the friction force over one steady state period. The friction ratios r_x with the value $i=1$ (without a stiction phase) and $i=0$ (with a stiction phase) for $\theta = \pi/2$ (perpendicular vibrations) are plotted in Fig. 4.9 and Fig. 4.10 respectively. The friction ratios for $\theta = \pi/6$ are plotted in Fig. 4.11 and Fig. 4.12. These figures show that a larger displacement ratio leads to a lower friction ratio. With increasing displacement ratio, the friction ratio approaches to that based on rigid Coulomb friction model (refer to Fig. 4.4). Comparing the curves for $i=1$ with the curves for $i=0$ clearly shows that for larger velocity ratios the friction ratios are equal, while for smaller velocity ratios the former drops faster than the latter with decreasing velocity ratio. This result can be explained by the asperity behaviors.

As the velocity ratio ζ decreases, the trajectory of point P of the sliding body is squeezed in the x-axis direction, as shown in Fig. 4.13. When the sliding body travels along the trajectory with large curvature, the asperity may relax due to the decrease in the horizontal distance between points P and T. Equation (4.14) shows that during asperity relaxation and the stretching, the Dahl model with $i=1$ has a larger relaxing rate (where $\mathrm{sgn}(v)=-1$) and a lower stretching rate (where $\mathrm{sgn}(v)=1$) than the Dahl model with $i=0$, for which $dz/dt=v(t)$. Consequently, over one steady state period, the friction magnitude of the Dahl model with $i=1$ is lower than that of the Dahl model with $i=0$, leading to a lower friction ratio (refer to Fig. 4.14).

As the velocity ratio ζ increases, the trajectory of point P of the sliding body is lengthened in the direction of x-axis, as shown in Fig. 4.15(a). If the velocity ratio is sufficiently large, the curvature of the trajectory of point P will be too small to cause a relaxation of asperity. In steady state, the deflection of the asperity reaches the steady state deflection z_{ss}, namely the magnitude of the friction force keeps constant (F_c), as shown in Fig. 4.15(b). Hence, Dahl model predicts the same friction ratio in this condition whether $i=1$ or $i=0$.

The comparison of friction ratio between calculated values and experimental results by Littmann *et al*. (2002) is shown in Fig. 4.16. The results based on Dahl model clearly display better agreement with the experimental results than those based on the rigid Coulomb friction model. Additionally, for lower velocity ratios, the results based on the Dahl model with a stiction phase exhibit closer agreement with the experimental results than those without a stiction phase. It is worthy to point out that the displacement ratios matching the experimental results by Littmann *et al.* are equal for the perpendicular and the parallel vibrations (where the displacement ratio = 2).

Comparing the experimental data with the calculated results has shown that the tangential compliance should be considered in modeling the effect of friction reduction by vibrations. Although the tangential compliance of the Dahl model results from the small-scale asperities, the tangential compliance of the bulk material exerts a similar influence on the friction reduction.

4.5 Concluding Remarks

This study presents a theoretical approach based on the Dahl friction model that describes the friction reduction observed in the presence of the tangential vibrations at an arbitrary angle. The analysis results demonstrate that the vibrations parallel to the macroscopic velocity most effectively reduce the friction. The friction reduction effect is significant whenever the magnitude of macroscopic velocity is smaller than the velocity amplitude of vibration. However, when the magnitude of macroscopic velocity is larger than the velocity amplitude of vibration, the vibrations perpendicular to the macroscopic velocity still take effect and are most effective but the friction reduction is not significant. At any vibration angle, the tangential compliance of the contacts reduces the friction reduction effect. The results obtained using the proposed approach exhibit better agreement with the experimental data than those based on the rigid Coulomb friction model.

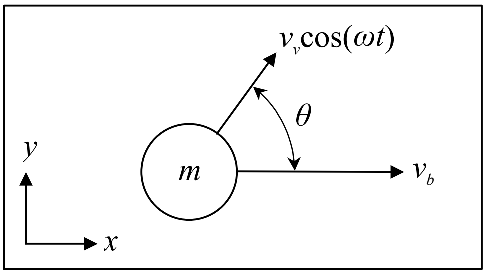

Fig. 4.1 An analytical model for sliding with tangential vibrations

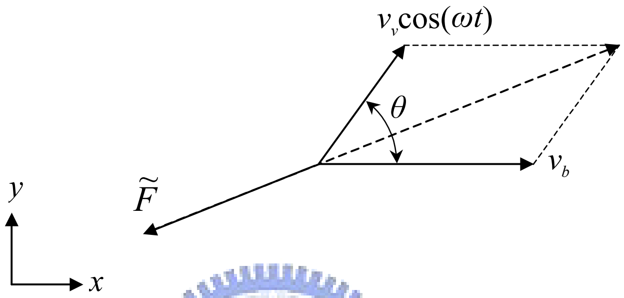

Fig. 4.2 Friction and velocities

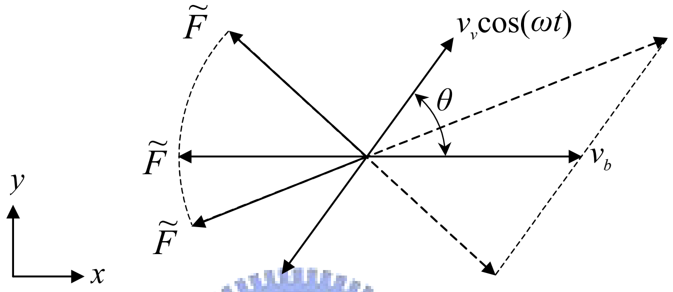

Fig. 4.3 Mechanism of time-average friction reduction

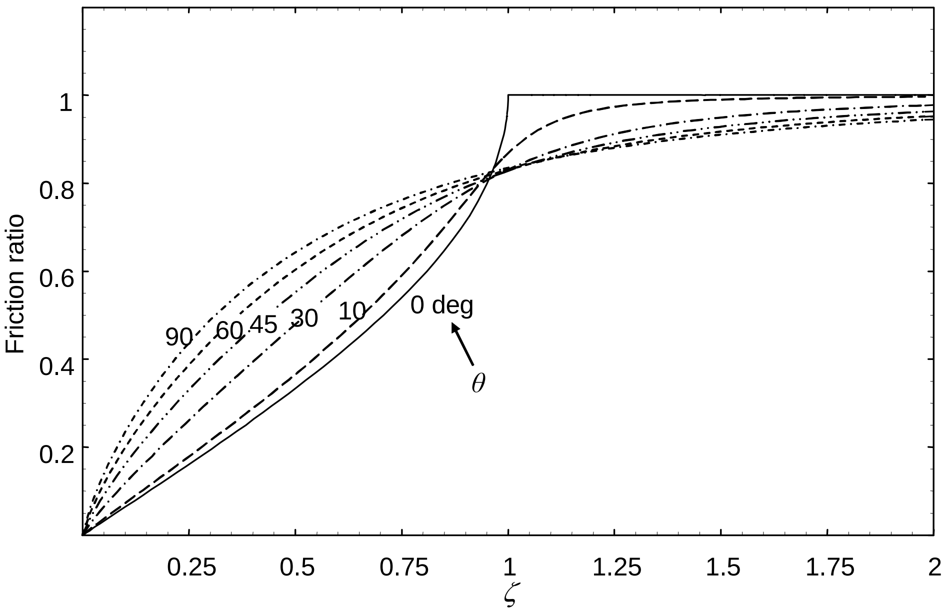

Fig. 4.4 Friction ratios r_x for different angles

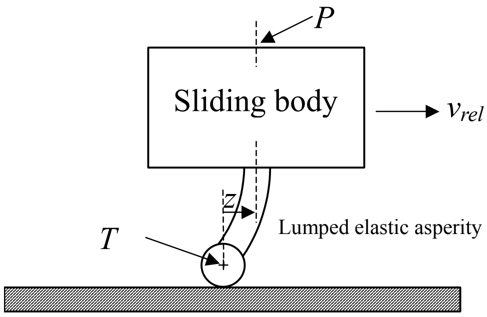

(a) Side view

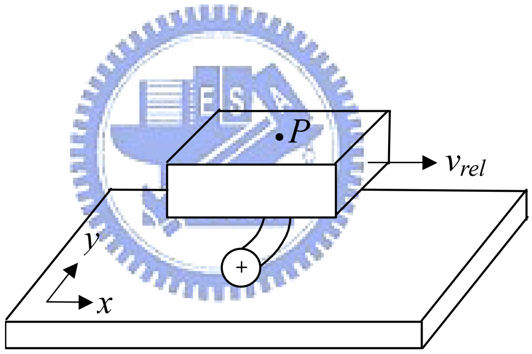

(b) Perspective view

Fig. 4.5 The friction interface between two surfaces is thought of as a lumped elastic asperity

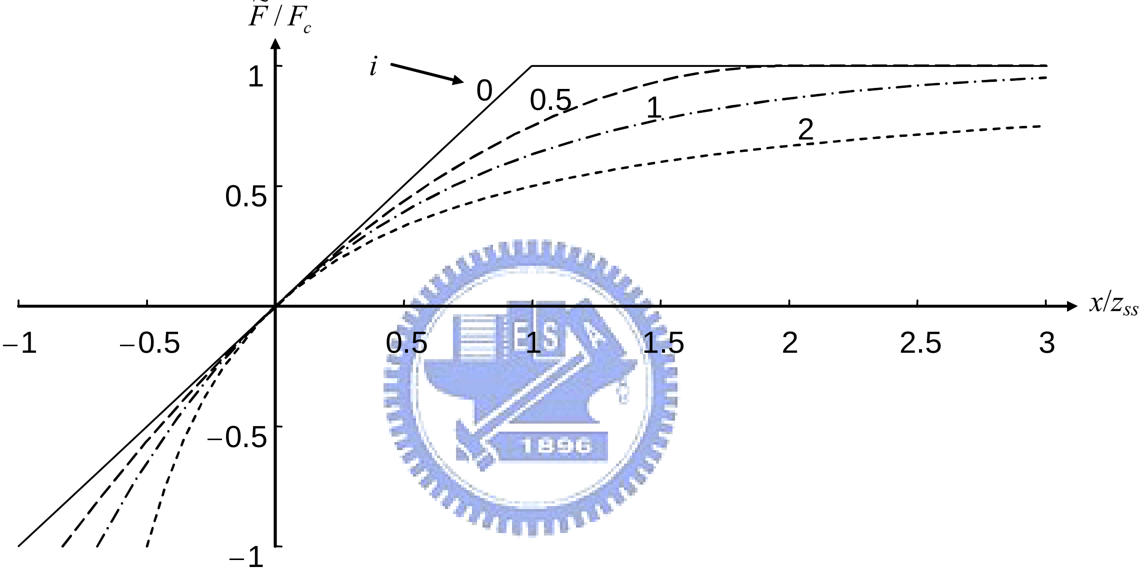

Fig. 4.6 Friction-displacement curves for $v > 0$

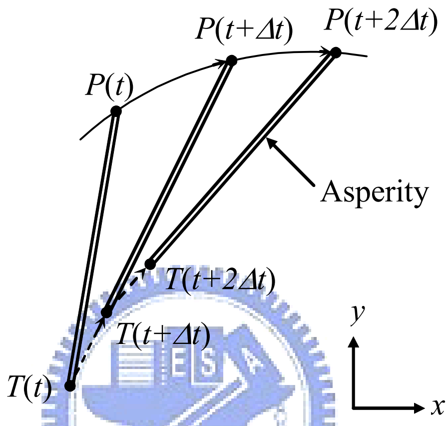

Fig. 4.7 Behavior of the lumped asperity (top view)

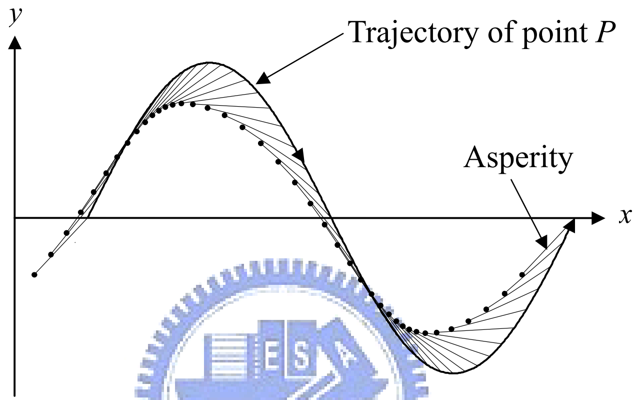

Fig. 4.8 Behavior of the lumped asperity over one steady state period.

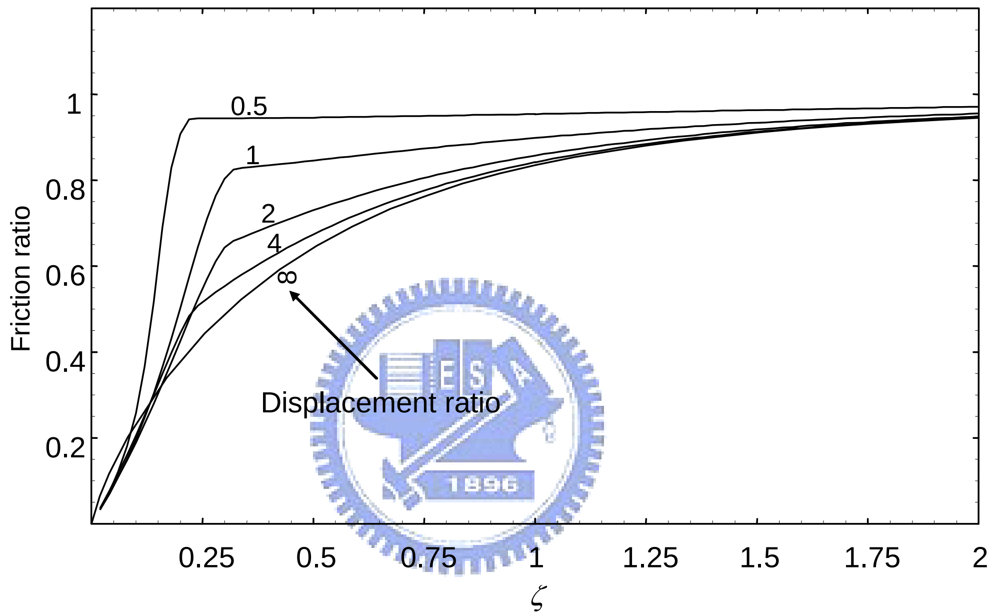

Fig. 4.9 Friction ratios with $i = 1$; $\theta = \pi / 2$

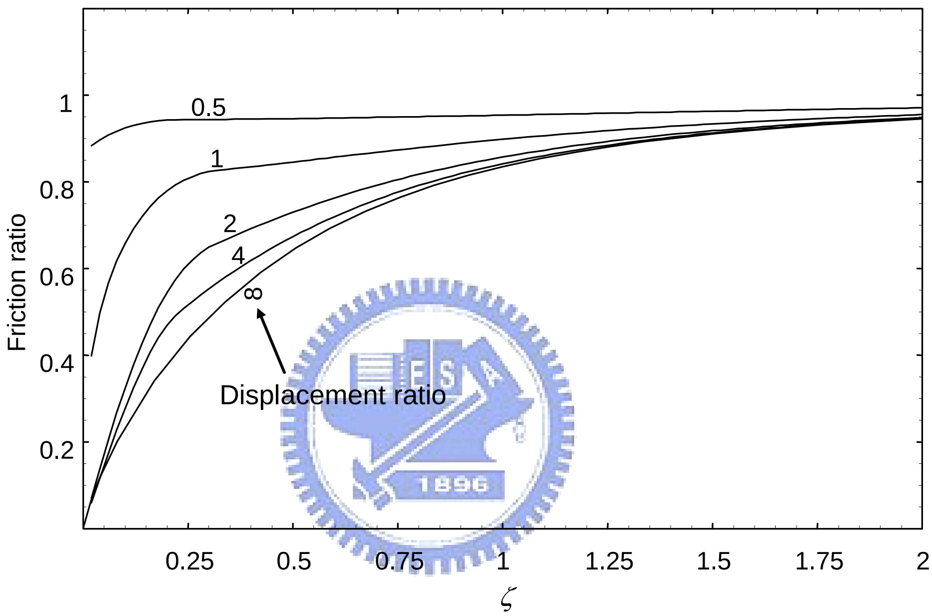

Fig. 4.10 Friction ratios with $i = 0$; $\theta = \pi / 2$

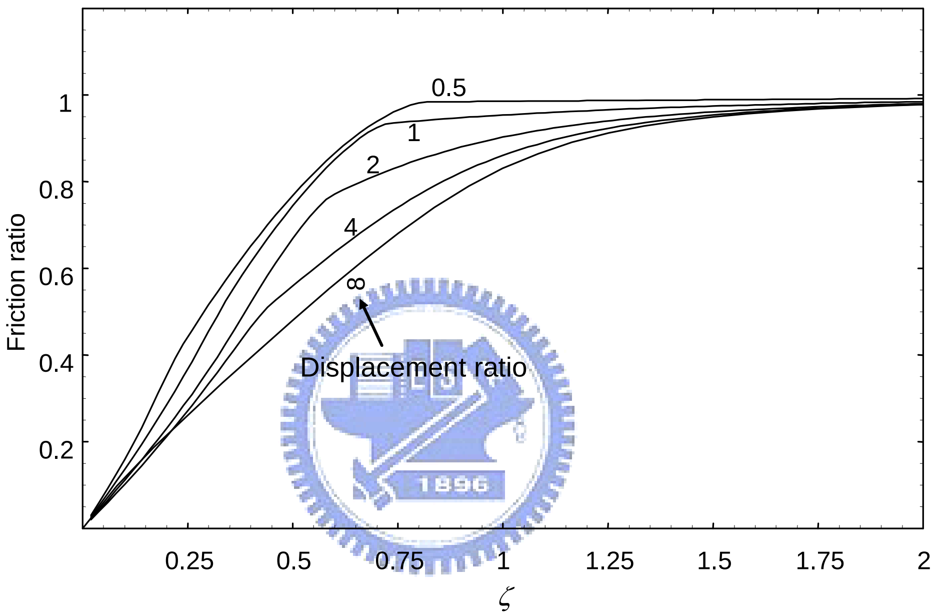

Fig. 4.11 Friction ratios with $i = 1$; $\theta = \pi / 6$

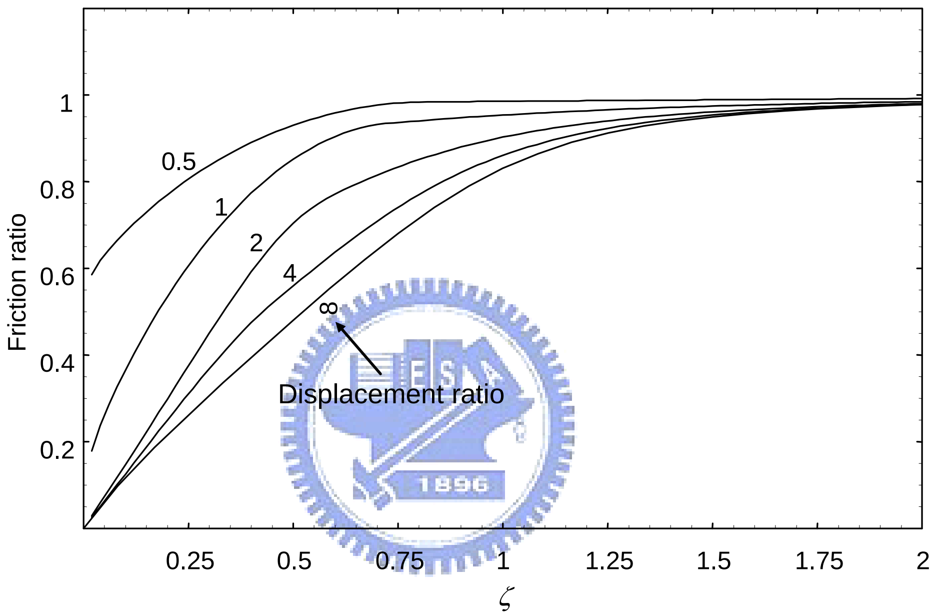

Fig. 4.12 Friction ratios with $i = 0$; $\theta = \pi / 6$

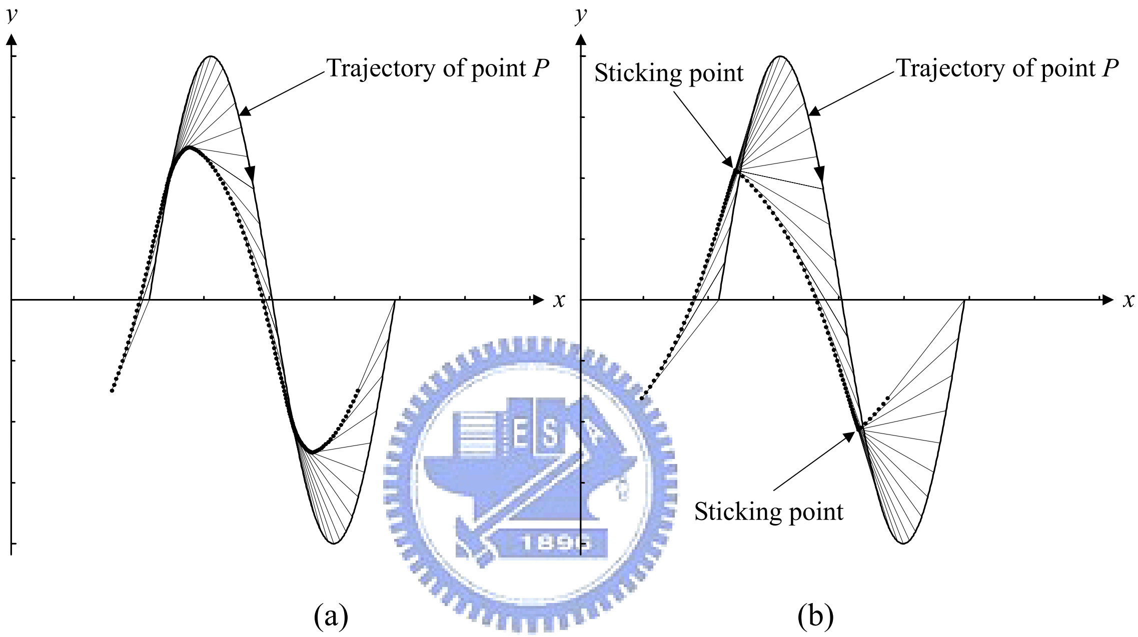

Fig. 4.13 Comparison of the behaviors of asperity over one steady state period ($r_{disp} = 2$, $\zeta = 0.15$, $\theta = \pi / 2$): (a) Dahl model without a stiction phase ($i = 1$); (b) Dahl model with a stiction phase ($i = 0$)

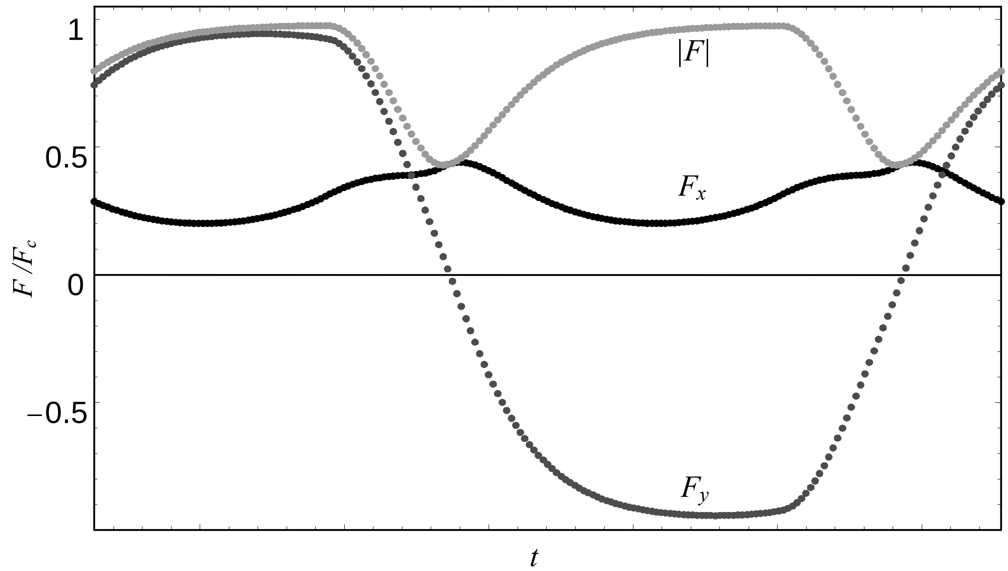

(a) For Fig. 4.13(a)

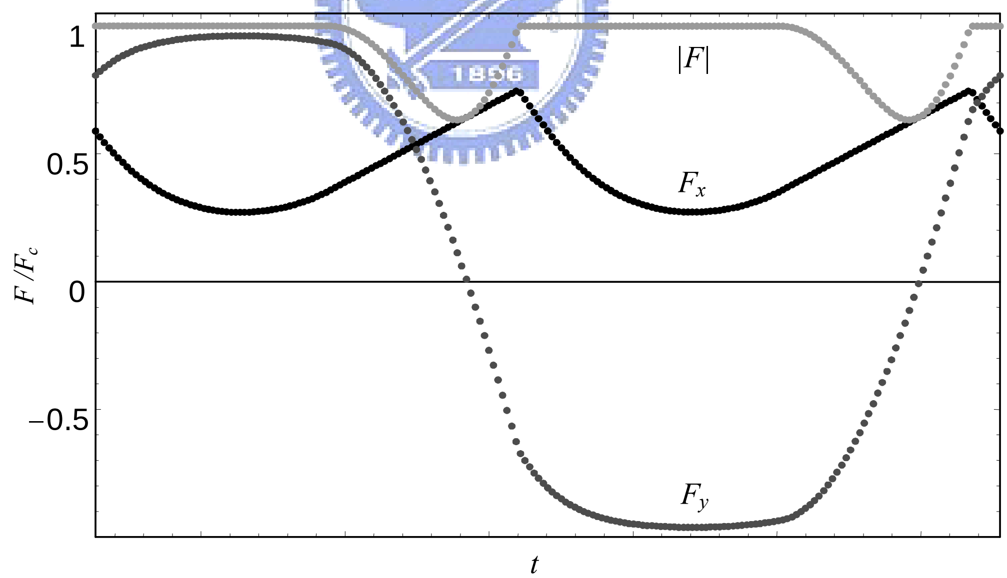

(b) For Fig. 4.13(b)

Fig. 4.14 Friction forces over one steady state period

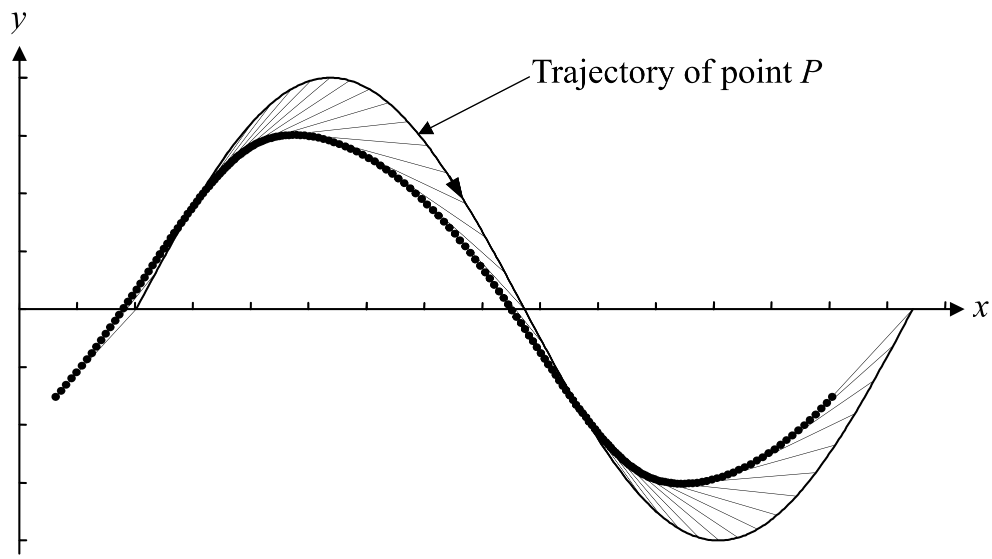

(a) Behavior of asperity

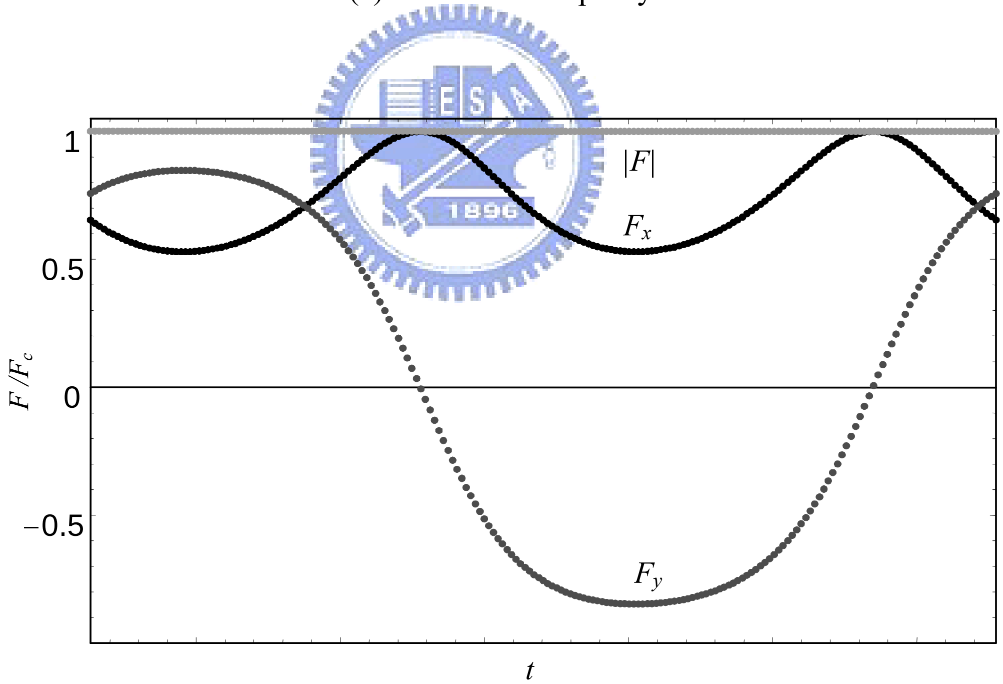

(b) Friction forces

Fig. 4.15 Behavior of asperity over one steady state period ($r_{disp} = 2$, $\zeta = 0.5$, $\theta = \pi / 2$)

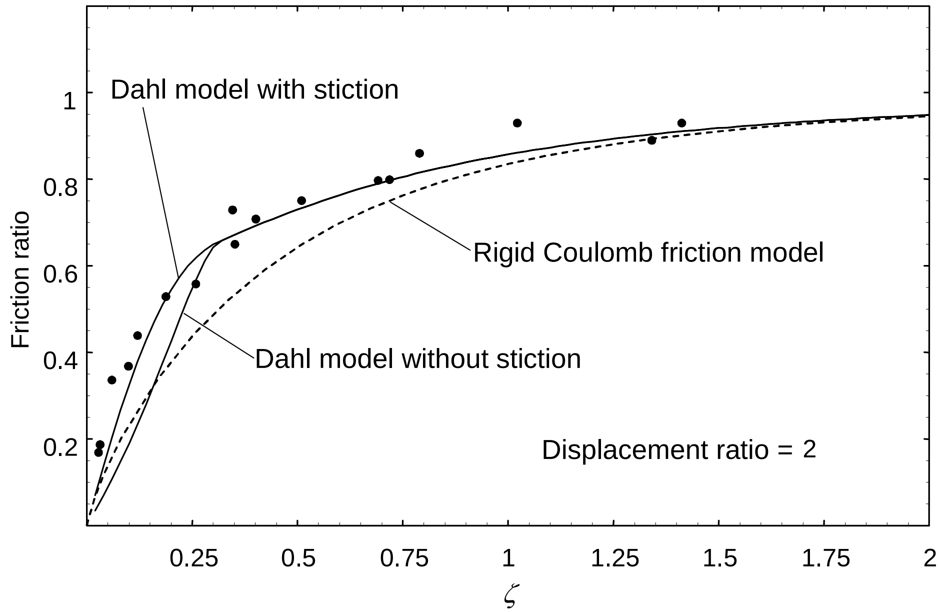

(a) Perpendicular vibrations; $\theta = \pi / 2$

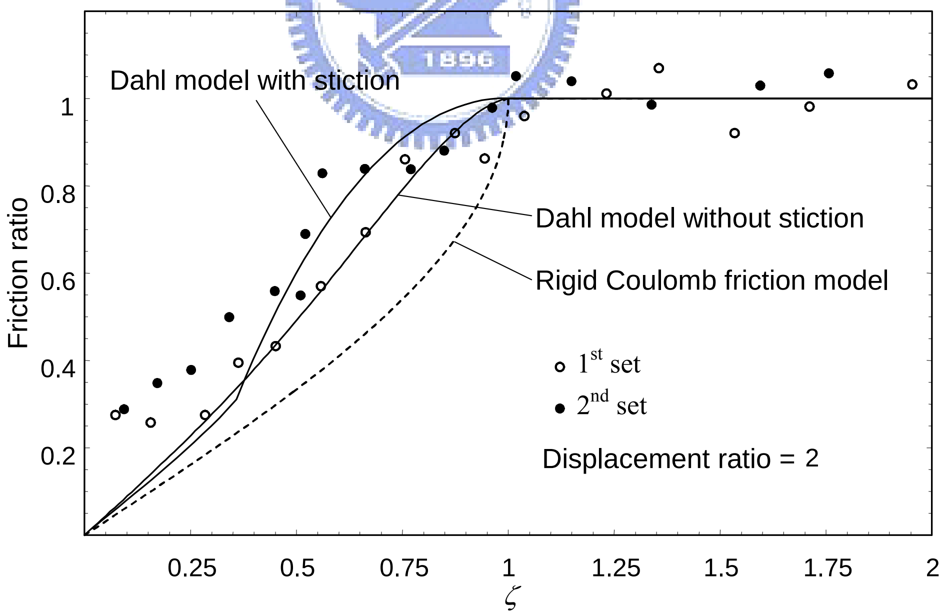

(b) Parallel vibrations; $\theta = 0$

Fig. 4.16 Comparison of friction ratios between calculated values and experimental results (dot) by Littmann *et al*. (2001, 2002)

CHAPTER 5 FRICTION REDUCTION BY NORMAL VIBRATIONS

5.1 Introduction

In this chapter Dahl model was applied to analysis the friction reduction phenomenon in the presence of the normal vibrations. The friction reduction when the contact is broken for part of the normal vibration cycle was also studied.

In the first part of this chapter, a simple analysis is performed for a contact that is modeled simply as a nonlinear spring without the tangential compliance. While not many practical contacts can be modeled as this, this analysis provides physical insight into friction force during normal vibrations.

5.2 Friction Based on Adhesion Theory

In the presence of the normal vibration, the dynamic normal force changes the true area of contact. Based on the adhesion theory of friction, the instantaneous friction force can be assumed to be proportional to the area of the contact. Therefore, the friction under dynamic normal forces can be obtained by this load-area-friction relation.

5.2.1 True Area of Contact

When two surfaces contact with each other, the surfaces asperities are themselves deformed elastically, plastically, viscoelastically or brittly. The area of contact is determined by the deformation properties of the materials and the detailed topography of the surfaces. Several models of the contact were presented (Tabor, 1981). They are summarized in Table 5.1. If the number of asperity contacts remains constant and the load N is increased, the area of contact in the range where the asperities deform elastically will be proportional to $N^{2/3}$. If the number of asperity contacts increase with the load such that the average size of each asperity contact remains constant the area of contact in the elastic region will be proportional to *N*. If the asperities are conical or pyramidal the area will always be proportional to *N*. Finally if plastic deformation takes place, the area of contact will be roughly proportional to *N* whatever the asperity distribution since the yield pressure for each asperity contact will be a material constant. There are many variations on this theme which yield slightly different conclusions but the broad picture remains the same however much the details may vary.

5.2.2 Maximum Friction Reduction without Loss of Contact

Based on the adhesion theory of friction, the instantaneous friction is assumed to be proportional to the area of the contact. To obtain the maximum friction reduction without loss of contact, a simple analysis can be performed for a contact that is modeled simply as a nonlinear spring, without any system dynamics. The maximum friction reduction occurs when the dynamic load is high enough to cause the onset of contact loss. At loss of contact, the mean and applied harmonic loads are

$$N = N_0(1+\cos\omega t)\,. \tag{5.1}$$

Based on the adhesion theory of friction, the relation of average friction during steady-state vibration is

$$\frac{F_{av}}{F_0} = \frac{A_{av}}{A_0}, \tag{5.2}$$

where A_0 and N_0 correspond to the static values. If the relation between the area of contact *A* and the normal load *N* is (Table 5.1)

$$A \propto N^{2/3}, \tag{5.3}$$

the average value of the friction at the onset of contact loss is

$$\frac{F_{av}}{F_0}=\frac{A_{av}}{A_0}=\frac{\dfrac{\omega}{2\pi}\int_0^{\frac{2\pi}{\omega}}[N_0(1+\cos\omega t)]^{2/3}dt}{N_0^{2/3}}=\frac{\omega}{2\pi}\int_0^{\frac{2\pi}{\omega}}(1+\cos\omega t)^{2/3}dt=0.92\,. \tag{5.4}$$

However, when the relation between the area of contact A and the normal load N is

$$A\propto N\,, \tag{5.5}$$

the value is

$$\frac{F_{av}}{F_0}=\frac{A_{av}}{A_0}=\frac{\omega}{2\pi}\int_0^{\frac{2\pi}{\omega}}(1+\cos\omega t)dt=1\,, \tag{5.6}$$

which means that the average friction is not reduced. Therefore, before loss of contact, there is no friction reduction in those cases that area of contact is linearly proportional to the normal contact force.

Similar studies (Hess and soom, 1991) that model the contact region as a nonlinear spring in parallel with a viscous damping element got the similar results. Their results showed that the maximum reduction in average friction for Hertzian contacts ($A\propto N^{2/3}$) at primary resonance under dynamic loading without any loss of contact is approximately ten percent, and for rough planar contacts ($A\propto N$) is approximately zero.

5.3 Influence of the Tangential Compliance

The tangential compliance of the contacts has obvious influence on the instantaneous friction force that in turn changes the average friction under dynamic loading. In this section, both normal vibrations with and without loss of contacts are considered.

5.3.1 System Model

The analytical model for normal vibrations is shown in Fig. 5.1. The dynamic normal load is given as follows:

$$N(t) = N_0 + A_N \cos \omega t\ , \tag{5.7}$$

where N_0 is the static load, and A_N is the amplitude of the harmonic load with a frequency ω. However, in the case of $N_0 < A_N$, the value of the normal load can becomes negative. This means that the contact is broken for part of the vibration cycle. Therefore, when $N_0 < A_N$, the dynamic normal load in a period is given as follows:

$$N(t) = \begin{cases} N_0 + A_N \cos \omega t & t_1 \le t \le t_2 \\ 0 & 0 \le t \le t_1, t_2 \le t \le \dfrac{2\pi}{\omega} \end{cases}, \tag{5.8}$$

where t_1 and t_2 represent the starting and the finishing time of contact respectively in a period. t_1 and t_2 are given as follows:

$$t_1 = \frac{1}{\omega} \cos^{-1}\left(\frac{N_0}{A_N}\right), \tag{5.9}$$

and $t_2 = \dfrac{2\pi}{\omega} - t_1$. $$\tag{5.10}$$

The typical dynamic normal loads in a cycle of contact are shown in Fig. 5.2.

When two surfaces contact with each other and have a relative motion, the asperities on the surfaces will deform like springs which gives rise to the friction force. When the strain of any particular asperity exceeds a certain level, the bond is broken and a new bond having a smaller strain is established. Dahl (1976) modeled the average stress-strain curve by a differential equation. Here, the Dahl model can be written as follows:

$$\frac{dz}{dt} = v\left(1 - \frac{\sigma_0 z}{\mu_c} \operatorname{sgn}(v)\right)^i, \tag{5.11}$$

and $F = N\sigma_0 z$, $$\tag{5.12}$$

where σ_0 is the normalized contact stiffness, μ_c is the normalized Coulomb friction, v is the relative velocity, N is the normal force, z is the internal friction state, and i is a parameter that determines the shape of the stress-strain curve. Applications of this model commonly employ the value i=1.

5.3.2 Sliding without Loss of Contact

In the system of Fig. 5.1, the relative velocity v_b is assumed to be constant. Thus, if there is no loss of contact during sliding, the internal friction state z of the Dahl model approaches to the steady state z_{ss}

$$z_{ss} = \frac{\mu_c}{\sigma_0}, \tag{5.13}$$

leading to the instantaneous friction force

$$\tilde{F}(t) = N(t)\mu_c . \tag{5.14}$$

The effective friction force that is observed macroscopically in the presence of normal vibrations is the time-averaged friction force that is given by

$$\overline{F} = \frac{\omega}{2\pi}\int_0^{\frac{2\pi}{\omega}} \tilde{F}(t)dt . \tag{5.15}$$

Then the time-averaged friction force without loss of contact is obtained by inserting Eqs. (5.7) and (5.14) into Eq. (5.15), leading to

$$\overline{F} = N_0\mu_c . \tag{5.16}$$

This value is equal to the friction force without normal vibrations. Hence, there is no friction reduction in the condition without loss of contact.

It is worthy to point out that the static friction is reduced in the presence of the normal vibrations without loss of contact due to the oscillations of the frictional resistance of the contacts (Tworzydlo and Beckker, 1991), as shown in Fig. 5.3. In addition, the normal vibrations may induce a stick-slip sliding (Martins, 1990).

5.3.3 Sliding with Loss of Contact

If the contact is broken for part of the normal vibration cycle, the asperities deform during the contact and relax after the loss of contact. The instantaneous friction force during contact can be obtained by solving Eqs. (5.11) (with i=1) and (5.12) with the initial condition $z(0)=0$, as follows:

$$\widetilde{F}(t) = N(t)\mu_c\left(1 - e^{-\frac{\sigma_0 v_b t}{\mu_c}}\right), \qquad 0 < t < t_2 - t_1. \tag{5.17}$$

The dynamic normal load during contact is given as follows:

$$N(t) = N_0 + A_N \cos\omega(t + t_1), \qquad 0 < t < t_2 - t_1. \tag{5.18}$$

The instantaneous friction force during contact is plotted in Fig. 5.4. A larger velocity v_b or contact stiffness σ_0 lead to the faster response of the instantaneous friction force to the dynamic normal load.

The time-averaged friction force is given by

$$\overline{F} = \frac{\omega}{2\pi}\int_0^{t_2 - t_1} \widetilde{F}(t)dt. \tag{5.19}$$

The effect of friction reduction by superposed normal vibrations can be described quantitatively by the ratio of the time-averaged friction force to the friction force without vibrations, as follows:

$$r = \frac{\overline{F}}{N\mu_c}. \tag{5.20}$$

After some calculations, the friction ratio for the condition that the contact is broken for part of the normal vibration cycle can be obtained, as follows:

$$
\begin{aligned}
r = \frac{E_1}{2\pi r_{load} r_d \left(1 + r_d^{\,2}\right)} \Big(& r_{load} + \sqrt{1 - r_{load}^{\,2}} \left(E_1 \left(2 r_d^{\,3} + r_d \right) - r_d \right) + \\
& E_1 r_{load} \left(2 \sin^{-1}\left(r_{load} \right) \left(r_d^{\,3} + r_d \right) + \pi r_d^{\,3} + \pi r_d - 1 \right) \Big), \quad N_0 \le A_N \,,
\end{aligned}
\tag{5.21}
$$

where

$$E_1 = e^{-r_d \left(\pi + 2 \sin^{-1}\left(r_{load} \right) \right)},$$

$$r_{load} = \frac{N_0}{A_N},$$

and $r_d = \dfrac{v_b \sigma_0}{\omega \mu_c}$.

The friction ratio is an increasing function of r_d whose property is similar to the displacement ratio proposed in Chapter 2. When $N_0 = A_N$ (the onset of contact loss), Eq. (5.21) reduces to

$$r = \frac{e^{-2\pi r_d} + 2\pi \left(r_d^{\,3} + r_d \right) - 1}{2\pi \left(r_d^{\,3} + r_d \right)}, \tag{5.22}$$

which approaches 1 as r_d increases.

The friction ratios are plotted in Fig. 5.5. The friction ratio decreases for each of the following change in parameters: decrease of sliding velocity v_b, decrease of contact stiffness σ_0, increase of vibrating frequency ω, and increase of normalized Coulomb friction μ_c.

The system dynamics is not included here for simplification. If it is included, only the normal contact force (Eq. (5.7) and Eq. (5.8)) is changed and the above approach still can be applied.

5.4 Concluding Remarks

In this chapter, theoretical approaches based on the adhesion theory of friction and the Dahl friction model is presented that describes the friction reduction observed in the presence of the normal vibrations. It is showed that under the normal vibrations without loss of contact the reduction of the time-averaged friction is not significant. Under the normal vibrations with loss of contact, the tangential compliance reduces the instantaneous friction force, leading to the reduction in the time-averaged friction. The friction reduction increases as the tangential stiffness or the sliding velocity decreases, or as the vibrating frequency increases.

Table 5.1 Area of contact between surfaces in terms of asperity deformation

Elastic	$A \propto N^{2/3}$	Constant number of asperity contacts
	$A \propto N$	Constant size of asperity contacts
Plastic	$A \propto N$	

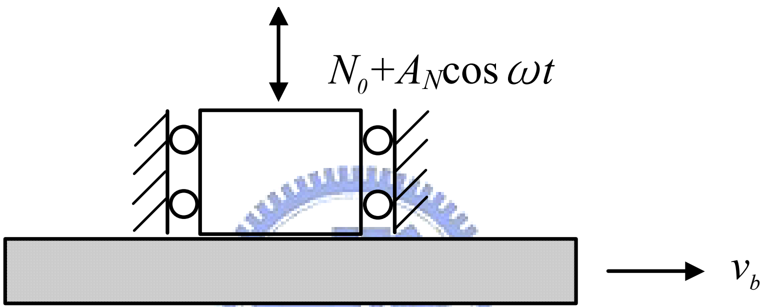

Fig. 5.1. An analytical model for normal vibrations

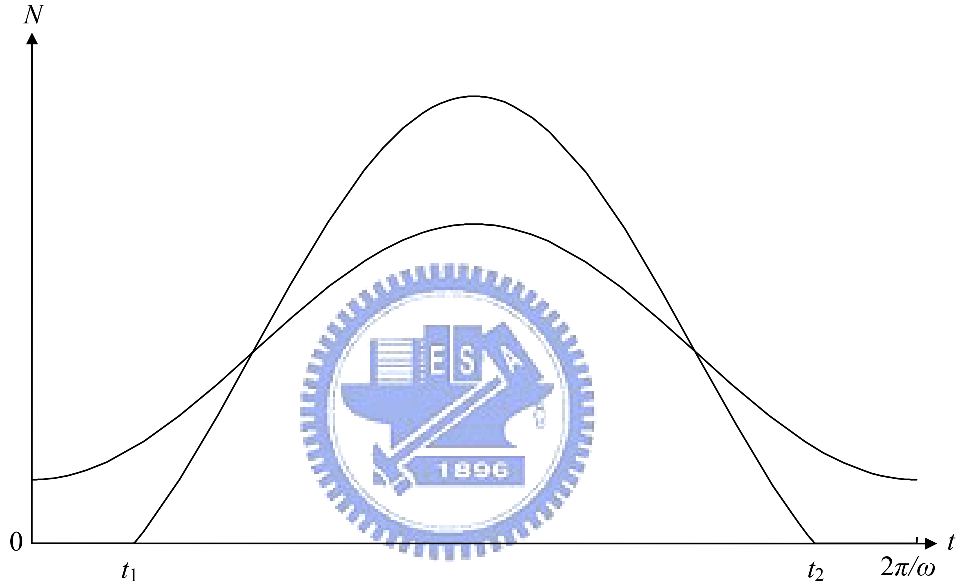

Fig. 5.2. Dynamic normal loads in a cycle of contact

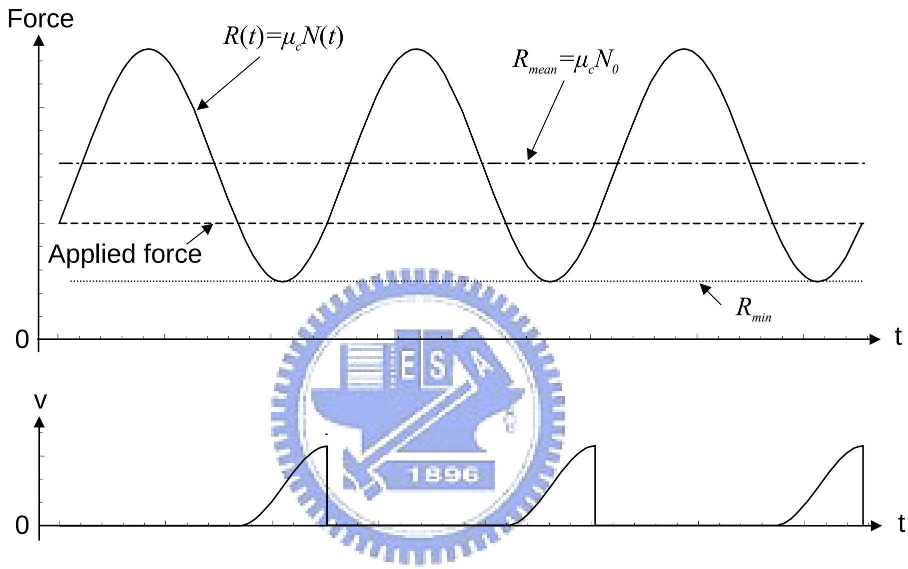

Fig. 5.3 Oscillations of the frictional resistance of the contacts and corresponding tangential velocity of the slider

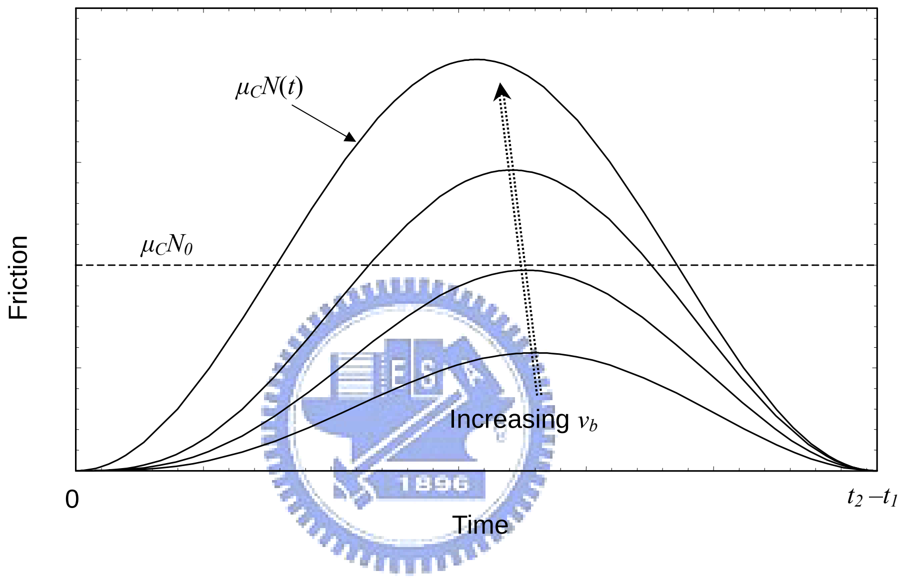

Fig. 5.4. Instantaneous friction forces during contact

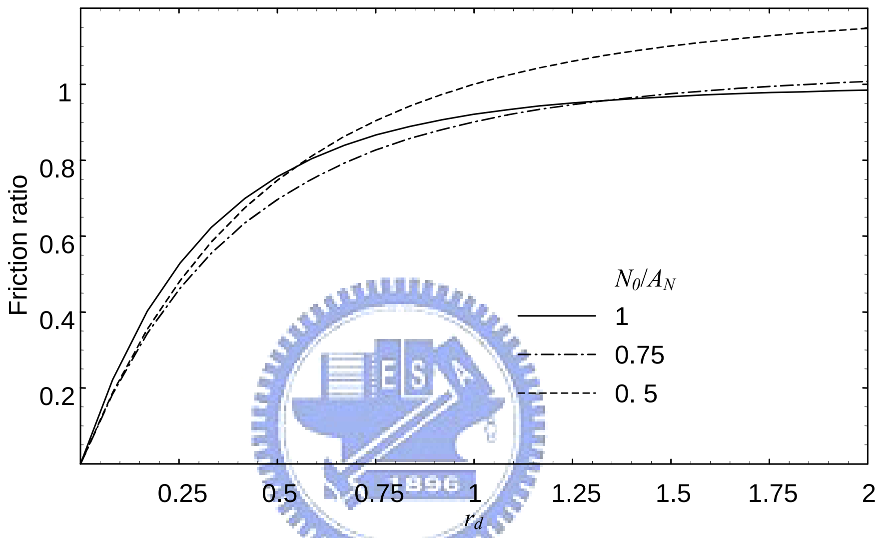

Fig. 5.5. Friction ratios for conditions with loss of contact

CHAPTER 6 CONCLUSIONS AND FUTURE WORKS

6.1 Conclusions

Theoretical approaches based on the Dahl friction model are presented that describe the time-averaged friction reduction observed in the presence of the vibrations that can be either normal or tangential to the contact surface. The underlying assumption in this study is that the friction force is not influenced by the wear and heat of the contact surfaces. The comparison between the friction reduction based on the rigid Coulomb friction model and the experimental data in the literatures shows that the tangential compliance of the contacts should be taken into consideration in the analysis of the friction reduction by vibrations. A displacement ratio of the displacement amplitude of the vibrations to the steady-state compliance of the asperity is proposed to describe the influence of the tangential compliance. For tangential vibrations, the tangential compliance degrades the effect of friction reduction. However, for normal vibrations, the tangential compliance enhances the effect of friction reduction. For any type of vibrations, the friction reduction effect is more significant when the magnitude of macroscopic velocity is smaller than the velocity amplitude of vibration.

For tangential vibrations, it is showed that the vibrations parallel to the macroscopic velocity are most effective to reduce the friction. However, when the magnitude of macroscopic velocity is larger than the velocity amplitude of vibration, the vibrations perpendicular to the macroscopic velocity still take effect and are most effective comparing to non-perpendicular vibrations but the amount of the friction reduction is limited. Comparing with the experimental data in the literatures, the results based on the proposed approach have a better agreement than that based on the rigid Coulomb friction model, and the Dahl model with a stiction phase provides a better description of the friction reduction by perpendicular vibrations.

A theoretical approach based on the LuGre friction model is presented that describes the friction reduction observed in the lubricated contacts with the parallel vibrations. It is showed that the linear damping of the asperities has no effect on the friction reduction, and the linear viscosity of the contacts, whose time-averaged value is not affected by the vibrations, degrades the effect of friction reduction by vibrations. The influence of Stribeck effect on the friction reduction effect is also presented. Comparing with the sliding without Stribeck effect, the presence of the Stribeck effect leads to a lower friction ratio for a small velocity ratio (about 0~1) and a larger friction ratio for a larger velocity ratio. The tangential compliance reduces the influence of the Stribeck effect on the friction reduction.

For normal vibrations, it is showed that under the normal vibrations without loss of contact the reduction of the time-averaged friction is not significant. Under the normal vibrations with loss of contact, the tangential compliance reduces the instantaneous friction force, leading to the reduction in the time-averaged friction. The friction reduction increases as the tangential stiffness or the sliding velocity decreases, or as the vibrating frequency increases. Due to that the dynamics of the normal vibrations with loss of contact is very complex, the system dynamics is not included here for simplification.

Other factors that also have influences on the friction reduction are proposed and investigated individually, including the waveform of the oscillation, asymmetric Coulomb friction and self-servo effect. By choosing suitable waveform of the oscillation, direction of the asymmetric Coulomb friction or self-servo structure, the friction reduction can be enhanced or suppressed depending on the applications. The energy dissipated during sliding with vibrations is also studied. As the displacement ratio decreases, the average dissipated energy with vibrations decreases and may be lower than that without vibrations. If the damping at contacts is low, quite small dynamic loads with frequency near the contact resonance frequency can lead to large normal contact motions (loss of contact is possible). Hence, from the viewpoint of energy saving, the normal vibrations may be better than the tangential vibration for friction reduction at contacts with low damping.

6.2 Future Works

The nature of the friction is fairly complex. The full description and analysis of the dynamic friction phenomena actually pose severe practical and computational difficulties. Therefore, the LuGre friction model that can capture most of the friction behavior observed experimentally still produces non-physical behaviors. There is still plenty of room for further study about the effect of friction reduction by vibrations.

In the future, this study can be extended to the topics as follows:

- This study focused on the theoretical analysis, the experimental data is needed to confirm the theoretical results and, if necessary, to modify the theoretical model (including the friction model).
- This study can be extended to multi-directional vibrations, such as circular vibrations.
- In the case of the normal vibrations, the damping of the asperities and the fluid effect between the contacts can be included in the theoretical analysis. The damping is of extreme importance since it strongly affects the actual amplitudes of normal vibrations, but it is very complex in nature.
- If the wear or heat plays an importance role and affects the friction during the sliding, other friction models will be needed, such as the brake system where the friction force depends on the growing and destruction of hard patches (Ostermeyer, 2001).
- Optimizations for specified applications can be performed.

REFERENCES

Adachi, K., Kato, K. and Sasatani, Y., "Micro-mechanism of Friction Drive with Ultrasonic Wave," Wear, Vol. 194, No. 1-2, pp. 137-142, 1996.

Altpeter, F., "Friction Modeling, Identification and Compensation," PhD thesis, Ecole Polytechnique Federale de Lausanne, 1999.

Argentieri M. and Andresen J., "Means for Avoiding Static Friction," United States Patent, Patent Number: 3,831,451, 1974.

Armour J. S., "Friction Controllers," United States Patent, Patent Number: 4,318,459, 1982.

Armour J. S. and Watson P. M. F., "Friction Controller," United States Patent, Patent Number: 4,334,602, 1982.

Armstrong, B., Control of Machines with Friction, Boston, Kluwer Academic Publishers, pp. 78-80, 1991.

Armstrong, B., Dupont P. and Canudas de Wit, C., "A Survey of Models, Analysis Tools and Compensation Methods for the Control of Machines with Friction," Automatica, Vo. 30, No. 7, pp. 1083-1138, 1994

Barabanov, N. and Ortega, R., "Necessary and Sufficient Conditions for Passivity of the LuGre Friction Model," IEEE Transactions on Automatic Control, Vol. 45, No. 4, pp. 830-832, 2000.

Bliman, P.-A. J., "Mathematical Study of the Dahl's Friction Model," European Journal of Mechanics, A/Solids, Vol. 11, No. 6, pp. 835-848, 1992.

Broeze J. E. and Laubendorfer W. J., "Low Friction Bearing," United States Patent, Patent Number: 3,239,283, 1966.

Broniec, Z. and Lenkiewicz, W., "Static Friction Processes under Dynamic Loads and Vibration," Wear, Vol. 80, pp. 261-271, 1982.

Canudas de Wit, C., Olsson, H., Astrom, K. J. and Lischinsky, P., "A New Model for Control of Systems with Friction," IEEE Transactions on Automatic Control, Vol. 40, No. 3, pp. 419-425, 1995.

Canudas de Wit, C. and Tsiotras, P., "Dynamic tire friction models for vehicle traction control," Proceedings of the IEEE Conference on Decision and Control, Vol. 4, pp. 3746-3751, 1999.

Dahl, P. R., "Solid Friction Damping of Mechanical Vibrations," AIAA Journal, Vol. 14, No. 12, pp. 1675-1682, 1976.

Dinelli, F., Biswas, S. K., Briggs, G. A. D. and Kolosov, O. V., "Ultrasound Induced Lubricity in Microscopic Contact," Applied Physics Letters, Vol. 71, No. 91, pp. 1177-1179, 1997.

Dupont, P., Kasturi, P. and Stokes, A., "Semi-active Control of Friction Dampers," Journal of Sound and Vibration, Vol. 202, No. 2, pp. 203-218, 1997.

Dupont, P., Armstrong, B. and Hayward, V., "Elasto-plastic Friction Model: Contact Compliance and Stiction," Proceedings of the American Control Conference, Vol. 2, pp. 1072-1077, 2000.

Dupont, P., Hayward, V., Armstrong, B. and Altpeter, F., "Single State Elasto-Plastic Friction Models," IEEE Transactions on Automatic Control, Vol. 47, No. 5, pp. 787-792, 2002.

Hagman, L. A. and Olofsson, U., "Model for Micro-slip Between Flat Surfaces Based on Deformation of Ellipsoidal Elastic Asperities — Parametric Study and Experimental Investigation," Tribology International, Vol. 31, No. 4, pp. 209-217, 1998.

Haessig, D. A. Jr. and Friedland, B., “On the Modeling and Simulation of Friction,” Journal of Dynamic Systems, Measurement and Control, Transactions of the ASME, Vol. 113, No. 3, pp. 354-362, 1991.

Hayashi, M., Jin, M., Thipprakmas, S., Murakawa, M., Hung, J. C., Tsai, Y. C. and Hung, C. H., “Simulation of Ultrasonic-vibration Drawing Using the Finite Element Method (FEM),” Journal of Materials Processing Technology, Vol. 140, pp. 30-35, 2003.

Hesjedal, T. and Behme, G., “The Origin of Ultrasound-induced Friction Reduction in Microscopic Mechanical Contacts,” IEEE Transactions on Ultrasonics, Ferroelectrics, and Frequency Control, Vol. 49, No. 3, pp. 356-364, 2002.

Hess, D. P. and Soom, A., “Friction at a Lubricated Line Contact Operating as Oscillating Sliding Velocities,” Journal of tribology, Vol. 112, pp. 147-152, 1990.

Hess, D. P. and Soom, A., “Normal Vibrations and Friction under Harmonic Loads: Part 1. Hertzian Contacts,” Transactions of the ASME. Journal of tribology, Vol. 113, pp. 80-86, 1991.

Hess, D. P. and Soom, A., “Normal Vibrations and Friction under Harmonic Loads: Part 2. Rough Planar Contacts,” Transactions of the ASME. Journal of tribology, Vol. 113, pp. 87-92, 1991.

Hess, D. P., Soom, A. and Kim, C.H., “Normal Vibrations and Friction at a Hertzian Contact Under Random Excitation: Theory and Experiments,” Journal of Sound and Vibration, Vol. 153, No. 3, pp. 491-508, 1992.

Hess, D. P. and Soom, A., “Normal Vibrations and Friction at A Hertzian Contact Under Random Excitation: Perturbation Solution,” Journal of Sound and Vibration, Vol. 164, No. 2, pp. 317-326, 1993.

Kramer D. A., “Device for Reducing Friction on Sliding Glass,” United States Patent, Patent Number: 6,125,589, 2000.

Kuribayashi, K., Shimizu, S., Yuasa, K., Taniguchi, T. and Ikeda, Y., "Friction force reduction of conduit guided wire by vibration," Proceedings of the International Symposium on Micro Machine and Human Science, pp. 185-189, Oct. 2-4, 1994.

Lehtovaara, A., "Influence of Vibration on the Kinetic Friction Between Plastics and Ice," Wear, Vol. 115, No. 1-2, pp. 131-138, 1987.

Littmann, W., Storck, H. and Wallaschek, J., "Reduction of Friction Using Piezoelectrically Excited Ultrasonic Vibrations," Proceedings of SPIE - The International Society for Optical Engineering, Vol. 4331, pp. 302-311, 2001.

Littmann, W., Storck, H. and Wallaschek, J., "Sliding Friction in the Presence of Ultrasonic Oscillations: Superposition of Longitudinal Oscillations," Archive of Applied Mechanics, Vol. 71, No. 8, pp. 549-554, 2001.

Littmann, W., Wallaschek, J., Mracek, M. and Storck, H., "The Effect of Friction Reduction in Presence of Ultrasonic Vibrations and Its Relevance to Travelling Wave Ultrasonic Motors," Ultrasonics, Vol. 40, No. 1-8, pp. 379-383, 2002.

Matunaga, S. and Onoda, J., "A Novel Method of Friction Force Reduction by Vibration and Its Application to Gravity Compensation," Proceedings of the AIAA/ASME/ASCE/AHS/ASC Structures, Structural Dynamics, and Materials Conference, pp. 1531-1537, Apr. 13-15, 1992.

Martins, J. A. C., Oden, J. T. and Simões, F. M. F., "A Study of Static and Kinetic Friction," International Journal of Engineering Science, Vol. 28, No. 1, pp. 29-92, 1990.

Olofsson, U., "Cyclic Micro-slip under Unlubricated Conditions," Tribology International, Vol. 28, No. 4, pp. 207-217, 1995.

Olsson, H., Astrom, K. J., Canudas de Wit, C., Gafvert, M. and Lischinsky, P., "Friction Models and Friction Compensation" European Journal of Control, Vol. 4, No. 3, pp. 176-195, 1998.

Ostermeyer, G. P., “Friction and Wear of Brake Systems,” Forschung im Ingenieurwesen/Engineering Research, Vol. 66, No. 6, pp. 267-272, 2001.

Saito N. and Mohri N., “Fitting Method Utilizing Both Continuous and Intermittent Ultrasonic Vibration,” United States Patent, Patent Number: 5,121,533, 1992.

Tabor, D., “Friction – The Present State of Our Understanding,” Journal of Lubrication Technology, Vol. 103, pp. 169-179, 1981.

Tani, K., “Friction Models for a Mobile Machine Using Piezo Vibration,” International Workshop on Advanced Motion Control, AMC, Vol. 2, pp. 717-722, 1996.

Tolstoi, D. M., Borisova, G. A. and Grigorova, S. R., “Friction Reduction by Perpendicular Oscillation,” Soviet physics-doklady, Vol. 17, No. 9, pp. 907-909, 1973.

Tworzydlo, W. W. and Becker, E., “Influence of Forced Vibrations on the Static Coefficient of Friction - Numerical Modeling,” Wear, Vol. 143, No. 1, pp. 175-196, 1991.

Zeng, P., Li, J., Cheng, G. and Yang, Z., “The Study of Rotary Ultrasonic Vibration Anti-friction Experimental Mechanism,” Piezoelectrics and Acoustooptics, Vol. 20, No. 6, pp. 393-396, 1998.

PUBLICATION LIST

I. REFERRED PAPERS

1. Tsai, C. C. and Tseng, C. H., “Using TRIZ for an Engineering Design Methodology Course at NCTU in Taiwan,” TRIZ Journal, 2000.

2. Tsai, C. C., Chang, C. Y., and Tseng, C. H., “Optimal Design of Metal Seated Ball Valve Mechanism,” Journal of the International Society for Structural and Multidisciplinary Optimization, Vol. 26, No. 3-4, pp. 249-255, 2004.

3. Tsai, C. C. and Tseng, C. H., “Friction Reduction in the Presence of Parallel Vibrations,” Submitted to Tribology International, 2004.

4. Tsai, C. C. and Tseng, C. H., “The Effect of Friction Reduction in the Presence of In-plane Vibrations,” Submitted to Archive of Applied Mechanics, 2004.

II. CONFERENCE PAPERS

1. Tsai, C. C., Chang, C. Y., and Tseng, C. H., “Optimal design of metal seated ball valve mechanism,” USNCCM-VI Design Optimization Symposium, Dearborn, MI, USA, Aug. 1-4, 2001.

III. OTHERS

1. 蔡鎮竹與曾錦煥，壓電煞車之專利介紹，機械月刊，2002。

VITA

姓　名　：蔡鎮竹

生　日　：民國 62 年 10 月 1 日

地　址　：台中縣大甲鎮興安路 231 號

E-mail　：bamboo.me85g@nctu.edu.tw

學　歷　：省立台中第二高級中學
（民國 78 年 9 月至 81 年 6 月）

國立交通大學機械工程學系
（民國 81 年 9 月至 85 年 6 月）

國立交通大學機械工程學系碩士班
（民國 85 年 9 月至 86 年 6 月）

國立交通大學機械工程學系博士班
（民國 86 年 9 月至 93 年 6 月）